SYNTHESIS AND CHARACTERIZATION OF S-LAYER PROTEIN BIOCONJUGATES: A Route to Biologically-Based Self-Assembled Monolayers

By

PARTHASARATHY SAMPATHKUMAR

A dissertation submitted to the Graduate Faculty in Engineering in partial fulfillment of the requirements for the degree of Doctor of Philosophy, The City University of New York

2004

This manuscript has been read and accepted by the Graduate Faculty in Engineering in satisfaction of the dissertation requirement for the degree of Doctor of Philosophy

8/27/04 — Date

M. Lane Gilchrist — Dr. M. Lane Gilchrist

Chair of Examining Committee

8/27/2004 — Date

Mumtaz K. Kassir — Dr. Mumtaz Kassir

Executive Officer

_____ Dr. Alexander Couzis

_____ Dr. Charles Maldarelli

_____ Dr. John Tarbell

_____ Dr. Rastislav Levitky

Supervisory Committee

THE CITY UNIVERSITY OF NEW YORK

ABSTRACT

SYNTHESIS AND CHARACTERIZATION OF S-LAYER PROTEIN BIOCONJUGATES: A Route to Biologically-Based Self-Assembled Monolayers

By

Parthasarathy Sampathkumar

Advisor: Dr. M. Lane Gilchrist

Numerous bacterial species possess nanostructured monolayers of self-assembled proteins on their surfaces called the crystalline surface layer (S-layer) that efficiently display molecules. We utilize these protein-based molecular display systems to develop novel, multicomponent bioactive nanostructured surfaces. Essentially, S-layer proteins were conjugated with specific tethered molecules and subsequently self-assembled on surfaces using combinations of bioconjugated protein monomer "modules". The bioconjugate modules are similar in function to the alkanethiols and silanes that form self-

assembled monolayers (SAMs) on respectively gold and silicon surfaces. The S-layer proteins in comparison, serve as the "headgroups" or molecular carriers and the driving force for the formation of SAMs positioning the tethered "endgroups" on the surface. The inherent nanostructure of the S-layer crystal lattice dictates the endgroup orientation and spacing.

We have isolated and purified the S-layer proteins from microbial cultures of *Lactobacillus brevis* and *Bacillus sphaericus*. S-layer protein bioconjugate modules have been built with small molecule probes and polyethylene glycol (PEG) tethered ligands using amine-based reactions. The conjugations were performed at pH 6.5 to limit multiple labeling of protein amine groups. The modules have been characterized using HPLC, mass spectrometry and SDS-PAGE. Yields of singly N-terminus labeled proteins were 24-39%. To reduce the percentage of unlabeled S-layer proteins and further purify these modules, we have developed a protocol employing monomeric avidin affinity chromatography. We have assembled our bioconjugate modules onto polymer microspheres, silicon chips, positively charged glass slides and cationic liposomes. The distribution of modules in the assembled surfaces was followed using fluorescence spectroscopy and confocal microscopy. The surface-assembled structures were also examined with TEM, SEM, FT-IR and AFM. The surfaces obtained exhibited

homogeneous distributions of tethered molecules and had no evidence for phase separation when modules with dissimilar endgroups were self-assembled to form "mixed monolayers". Our studies indicate that we can control the surface composition and density of displayed bioactive molecules by manipulating the bulk concentrations of the functionalized modules at the start of the self-assembly experiment. These molecularly engineered self-assembling protein surfaces provide a novel route for the display of large functionalized molecules, e.g. growth factors, at interfaces presenting notable innovation in SAM technology.

ACKNOWLEDGEMENTS

I would like to take this opportunity to thank Dr. Gilchrist for his excellent advice, training, motivation and assistance in performing this research project. Dr. Gilchrist is also greatly appreciated for his tolerance and patience. Prof. David Calhoun is gratefully acknowledged for teaching me various laboratory skills.

I also express my sincere gratitude to Prof. Alexander Couzis and Prof. Charles Maldarelli for their timely guidance and support and to Distinguished Prof. John Tarbell, Prof. David Rumschitzki and Prof. Rastislav Levitky, Columbia University for accepting to review my thesis.

I would like to thank Dr. Cliff Soll at Hunter College for helping in performing Mass spectrometry, Mr. Ronald Goldman at Mount Sinai School of Medicine for TEM and Hongjie Liu, PhD student, Chemical Engineering, CUNY for helping in the investigation of surfaces with AFM. Last but not least, it is my duty to thank my family, colleagues and department staff for their continued cooperation and encouragement.

Additionally, Mount Sinai School of Medicine Confocal Microscopy Shared Research Facility, supported, in part, with funding from NIH-NCI shared resources grant (1 R24 CA095823-01) and funding agency DoD / Army Research Office (grant 45349-LS-HSI) are enthusiastically thanked.

TABLE OF CONTENTS

TABLES AND FIGURES

Chapter 1: INTRODUCTION

1.1 Motivation

Biomaterials are designed to replicate, mimic or extend functions performed by biological systems. To obtain design criteria to create such biomaterials, it is important to gain an understanding of how cells respond to molecular signals in the cellular microenvironment.[1] In plants and animals, extracellular signaling molecules control metabolic processes within cells, the growth of tissues, the synthesis and secretion of proteins, and the composition of intracellular and extracellular fluids. The signaling molecule can either be a hormone, a growth factor, a neurotransmitter or just an adhesion peptide. The cellular response to a particular extracellular signaling molecule is generated by a set of successive events. First, the signaling molecule or "ligand" binds to a specific "receptor", usually a membrane protein, located on the surface of a target cell (fig. 1.1). Binding of this ligand generally causes a conformational change in the receptor. This change then initiates a chain of reactions leading to a specific cellular response. The response can range from adhesion/spreading, migration,

differentiation, proliferation and tissue construction to apoptosis or programmed cell death.

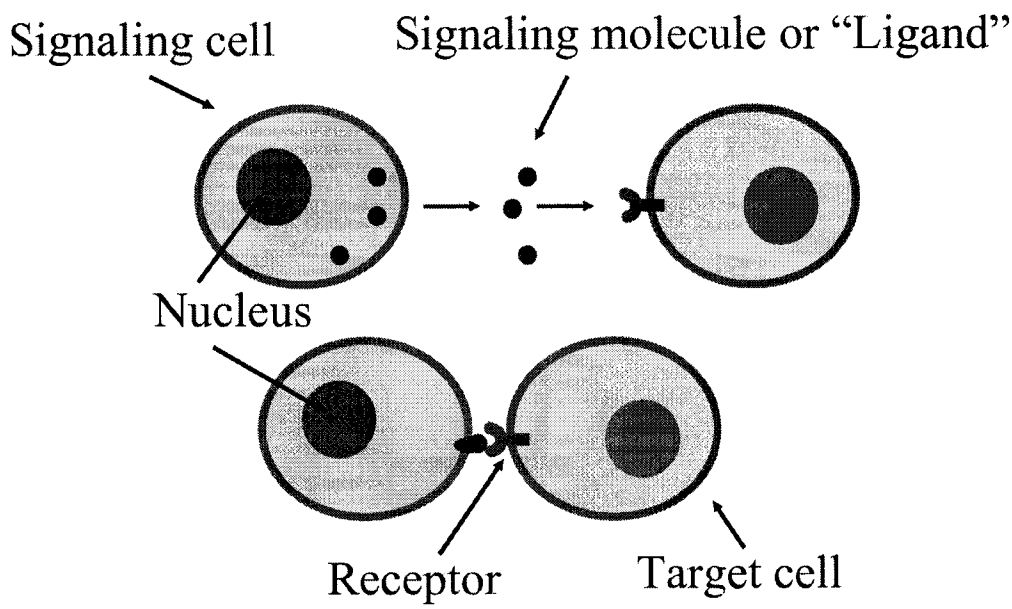

Figure 1.1: Extracellular Signaling

Different types of cells may have varying receptor subtypes for the same ligand, each influencing the cell response in a different way. The most important example of this is the integrin receptor family of cell adhesion, known to contain over 20 distinct subtypes.[2] Moreover, various types of cells can possess the same receptor, and the binding of a given ligand can trigger different responses in each cell type. [3, 4] In the extracellular environment, as shown in the schematic in fig. 1.2, the cell detects a multitude of molecular signals simultaneously.

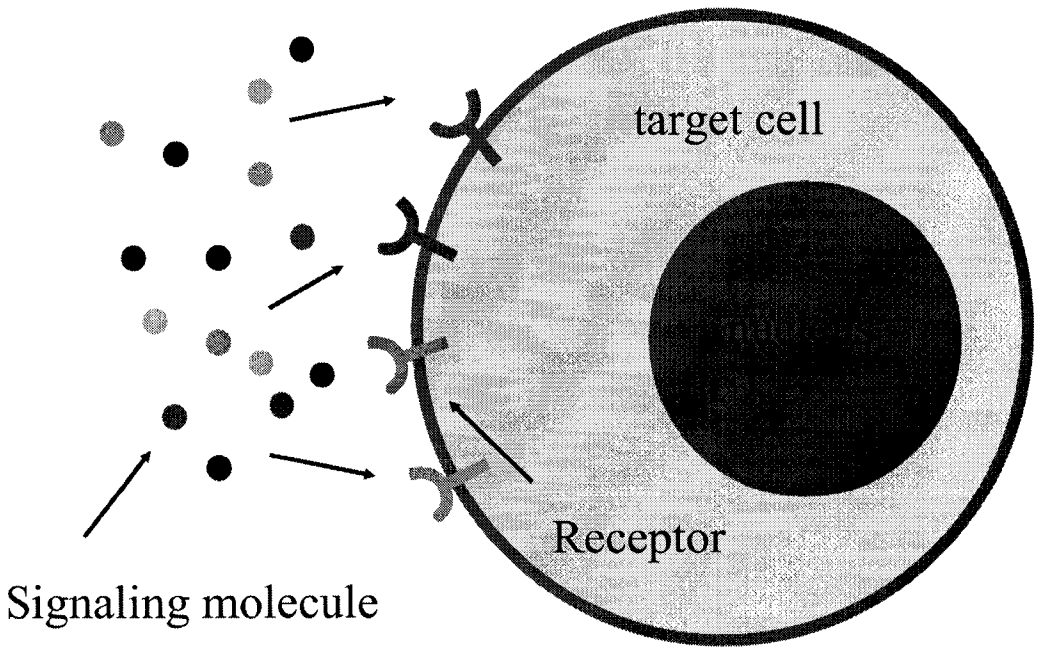

Figure 1.2: Extracellular Environment

For quantitative studies of such cell response, new materials that present controlled display of bioactive ligands (e.g., cell adhesion peptides and growth factors) are needed.[5, 6] Ideally, to really simulate the cellular microenvironment where one can test cell responses, we need a surface that presents multiple (one, two, three or probably ten) ligands. In the field of bioactive biomaterials, one of the main objectives is to confer controlled bioactivity to polymers and surfaces such that the cell response can be studied. [7, 8] Previously, this has been accomplished mainly by surface tethering of adhesion peptides or growth factors to a surface or polymer. The response of a cell or tissue

to such adhesion peptides is dependent on the particular adhesion peptide receptors the cell possesses and also by the intracellular reactions initiated by the binding of any single adhesion peptide to its receptor. A more detailed survey of previous research work by others in this area has been given in section 1.6. In most of these cases, only a single bioactive molecule or at the most two have been displayed. An efficient method for the controlled and reproducible display of combinations of many bioactive ligands on surfaces has not yet been developed. One needs a model system that can vary surface concentrations of each of the many ligands; estimate their concentration thresholds and study its effect on cell response. We are developing such model systems with potential for precise control of multiple bioactive ligand display by engineering surface self-assembling proteins (S-layer proteins).

1.2 Additional Motivations for S-layer Research

These S-layers have numerous applications. [9] Phospholipid bilayers or tetraether lipid films incorporating functional molecules represent key elements in the development of S-layer supported biomimetic membranes and act as carriers for Langmuir-Blodgett films.[10, 11, 12]

Losche and coworkers have reconstituted S-layers on phospholipids monolayers and shown reciprocal influence between protein and lipid components using FT-IR techniques.[13, 14] It appears evident that the protein crystallization drives the fluid lipid into a state of higher order. We foresee using these nanostructured S-layers with tethered lipids that in addition to stabilizing the bilayer membranes, would also dictate protein-protein interactions. Tethered lipid bilayers have been made using lipopolymer silanes, metal-affinity ligand-receptor pairs, peptide or protein coupling layers, but without any control on tether spacing.[15, 16, 17] In another related research, Frank and coworkers have reported stabilized phospholipid bilayers on lipopolymer molecules tethered to glass substrates.[18] They have shown capability to control tethering density between the polymer and the phospholipid bilayer. Recent progress in the field of tethered supported lipid bilayers has also been reviewed.[19] In contrast, in our work, as shown in the schematic in fig. 1.3, the nanostructure of the S-layers beneath the supported lipid bilayers would control the tether spacing of attached molecules and present an inherent order. S-layers on solid supports can act as the substrate (in place of just functionalized glass) that is tethered through lipopolymers for anchoring lipid bilayers. The S-layers would drive the

self-assembly and also control the orientation of the tethered molecules with its inherent structure. Apparently, there is potential for studying interactions between reconstituted membrane proteins and S-layer tethered proteins within the polymer tether "cushion". This function would be a potential development to the S-layer supported lipid bilayer model that has been well characterized by other groups as stated above.

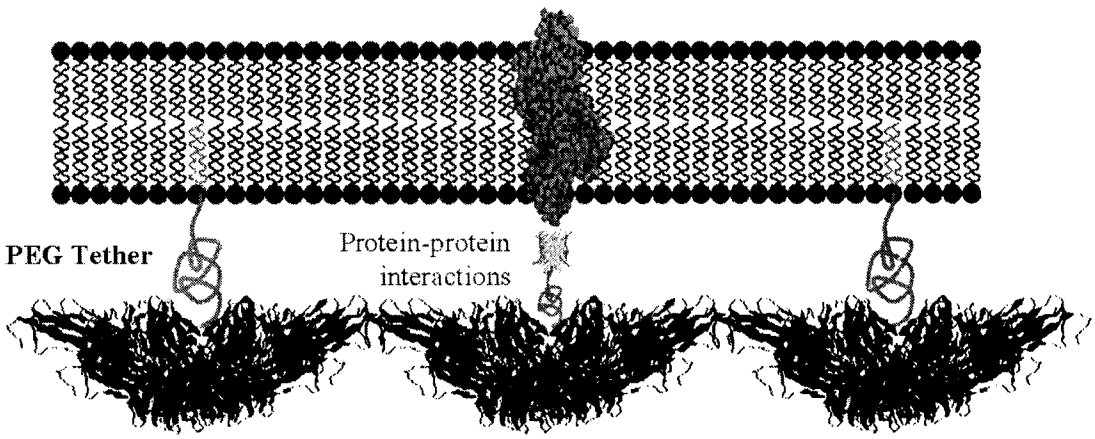

Figure 1.3: Supported Lipid Bilayers with S-layers

Various biotechnological and biomimetic applications of these S-layers have been reviewed by Sara and Sleytr.[20, 21] Solid (silicon wafer) supported S-layers have been used as patterning elements in the fields of molecular nanotechnology; micro- and nano-lithography. [22, 23] S-layer protein monolayers have been patterned using deep ultraviolet laser

radiation.[24] Upon irradiation with laser pulses the protein layer has been completely removed in the exposed regions while retaining its structural and functional integrity in the unexposed regions. Breitwieser and co-workers have used the S-layers as matrices for controlled immobilization of functional molecules for diagnostic systems (dipsticks) and solid phase immunoassays.[25] Sara and co-workers have made micron length cup shaped "microparticles" that are covered with identically oriented S-layer on both surfaces of the peptidoglycan-containing layer.[26] They have shown its use for quantifying the amount of immobilized macromolecules and for calculating the binding capacity of the lattices. S-layers have also been used to functionalize surfaces and as base structures for fiber-optic biosensors.[27] Sleytr and co-workers have designed conjugated vaccines by covalent coupling of antigens and/or weakly immunogenic substances to the S-layers.[28] Also recently, functional S-layer fusion proteins containing streptavidin monomers,[29] antibody fragments[30] and pollen allergen[31] have been created. The proteins with fused allergen have been shown to retain their ability to self-assemble, displaying the allergen molecules in a defined orientation.[32] Utilizing these capabilities, and the approach detailed in section 1.7, we visualize patterning S-layers on solid

supports for developing functionalized surfaces to create "Protein Chips".

1.3 The S-layers: An Introduction

Nature's wonderful creations, the S-layers, represent a unique set of biological structures. The S-layers assemble in a two-dimensional array on the cell surface covering the cell completely and adding stability to other structures of the cell envelope. They occur in over 500 species of bacteria. They are known to protect the cell from larger protein complexes like lytic enzymes or even from predator attack.[33] Particularly, the S-layers of *Bacillus sphaericus* act as specific receptors for bacteriophages.[34] The S-layers are also known to function as adhesion sites for high-molecular-weight exozymes and further trigger their releases too. [35, 36] Various other functions of these proteins that border between the cells and its environment have been reviewed and reported.[37] Most S-layers are 5 to 15 nm thick and possess pores of identical size and morphology in the range of 2 to 6 nm. These properties have been exploited for the manufacture of ultrafiltration membranes.[38] Those membranes having definite pore sizes have also been utilized as molecular sieves to separate particles of molecular

size.[39] Due to their crystalline character, attached functional groups have well-defined positions and orientations. But with respect to their inner and outer faces, they are highly anisotropic structures with different topography and physicochemical properties. Besides, anchoring of these proteins through hydrophobic interactions into membranes has effect on the membrane properties and their constituents.[40] S-layers are associated through the cytoplasmic membrane in Archaea; with the peptidoglycan surface in gram positive bacteria; and via the outer membrane in gram negative bacteria. They also possess structural linkages with both the cell envelope and extracellular components.

1.4 Composition and Structure of S-layer proteins

S-layers are composed of a single protein or glycoprotein species of molecular weight 40-200 kDa. They exhibit oblique, square or hexagonal lattice symmetry with unit cell dimensions in the range of 3 to 30 nm. [41, 42] Depending on the lattice symmetry, one morphological unit consists of up to six identical subunits. Lysine is the predominant amino acid while arginine, histidine and methionine contents are low.[43, 44, 45] Cysteine has been detected only in few S-layers. While glycosylation is

a common and diverse covalent modification of proteins, glycosylated S-layer proteins have been established as constituents of archaeal and bacterial cell envelopes. The glycan chains are polymers of 2 to 6 monosaccharide units. A special sequence motif, the SLH (S-layer homology) domain has been detected among some S-layer proteins, extracellular enzymes and special outer membrane proteins.[46] Baumeister and coworkers have proposed that this motif functions as a peptidoglycan binding structure.[47] More than 40 proteins present in various bacteria have been identified to possess these SLH motifs that consist of a conserved sequence of about 55 amino acids.

The three-dimensional structures of some surface layer proteins have been reported using reconstituted multiple tilted angle TEM images. [48, 49, 50] In their native assembled states, the S-layer proteins are incompatible with the classical structural methods (e.g. X-ray crystallography and solution Nuclear Magnetic Resonance techniques) that are used for obtaining the three-dimensional structures of proteins. This is most probably due to the inherent two-dimensional crystalline structure of the S-layers and their size. Recently, Springer and coworkers have deduced beta propeller structures of an archeal surface layer protein with 2.4 Å resolution using X-ray Diffraction techniques.[51]

Besides, Engel's group has reported 3D structure of surface layer of *Corynebacterium glutamicum* by unzipping double layers with the Atomic Force Microscope stylus.[52] These studies should further enable 3D structural studies on more of these proteins.

1.5 Nanotechnology: In *vitro* Self-assembly of S-layer Proteins

These crystalline bacterial cell surface layer proteins are also fascinating self-assembly systems. The replication of a single constituent subunit defines the properties of a whole self-assembled array. This has been shown to offer striking advantages in achieving perfect positional control at the molecular level.[53] Extraction of these S-layer proteins from bacterial cells can be achieved by disrupting their lattices using high concentrations of agents like lithium chloride (LiCl), guanidine hydrochloride (GHCl), sodium dodecyl sulfate (SDS) and urea or by altering the pH. It has been shown that ~80% of the cells were viable after LiCl treatment.[54] The S-layer proteins do not denature during this treatment. In fact, some S-layers are highly stable even under extreme conditions.[55] Many S-layers are also known to be incredibly protease-resistant.[56] Interestingly, when the disrupting agent used in the dissolution procedure is removed, the S-layer proteins (with

unit cell dimensions of 3 to 30 nm) reassemble into flat sheets, open ended cylinders or closed vesicles. [57, 58] Isolated S-layer proteins can be recrystallized into innate two-dimensional arrays on various surfaces (e.g., silicon wafers, metals and polymers) and at interfaces. S-layer lattices allow binding of molecules and particles in regular arrays since they have a well-defined arrangement of functional groups.[42]

Adding to the utility of these S-layer proteins as described in the previous sections, the *in-vitro* self-assembly property would enable development of novel modular bioactive surfaces and patterned protein chips for nanotechnological applications.

1.6 Development of Bioactive Surfaces and Measurement of Cellular Response: Existing Methods

Coating of surfaces and cell culture beads with extracellular matrix proteins such as collagen and fibronectin to enhance cell growth have been used since the 1980s.[59, 60] In addition, the extracellular matrix proteins have also been extensively used to probe cell response.[61, 62] Immobilization or cross-linking of molecules containing RGD, the adhesion domain of fibronectin, onto surfaces has been performed by various methods. Other oligopeptides like the REDV of fibronectin,

heparin binding YKKIIKKL,[63] integrin receptor ligand YIGSR[64] and IKVAV of laminin[65] have also been used for constructing bioactive surfaces. Chemical ligation, simple adsorption or more advanced methods like surface deposition utilizing self-assembled monolayers, peptide amphiphiles and cross-linked polyethylene oxide (PEO) tethers[66] have been used. Substrates used for these creations include modified glass slides, silane wafers, other polymers, hydrogels and also functionalized biological materials like collagen and silk.[67] Zhang and co-workers have demonstrated the formation of bioactive adhesion surfaces using self-assembling oligopeptides covalently attached to gold-coated surfaces.[68] Also, peptide amphiphiles or lipophilic moieties attached to peptide chains (triple helical, alpha-helical structures and RGD) have been aligned at the lipid-solvent interface to form bioactive surfaces. [69, 70]

The effect of bioactive ligand clustering in biomaterials has also been addressed, though, limited to materials based on one type of bioactive ligand. Studies done by Griffith and coworkers using galactose ligands tethered to branched polyethylene oxide (PEO)-based hydrogels, has shown that the cellular response does not simply depend upon the density of spatially constrained, substratum-bound

ligands.[71] They have assayed for the hepatocytes (liver cells) spreading mediated by the asialoglycoprotein receptor. Here, they have reported that the favorable cell spreading response occur when the tethered ligands possessed sufficient mobility to cluster and form multivalent bonds with the receptor. In subsequent work with human fibroblasts and tethered RGD (integrin receptor) ligands, they have used cell migration as the response indicator.[66] It has been shown that ligand clustering led to a reduced, average ligand density that was needed to support migration. The pronounced effects of clustered ligand displays represent an important step in the direction of a more accurate simulation of the extracellular environment.

Cellular response to tethered, immobilized growth factors,[72, 73] to controlled release growth factors[74, 75] and to controlled release proteins[76] have been extensively investigated. West and co-workers have studied the synergistic effects of adhesion peptides and growth factors on extracellular matrix production. In all, the research done so far describes the spatially controlled display or controlled release of peptides and single growth factors to the cells and their subsequent consequences like cell differentiation and multiplication. One needs a model system that can: 1. control and reproducibly display

combinations of many bioactive ligands; 2. vary surface concentrations of each of the many ligands; 3. estimate their concentration thresholds and study its effect on cell response. We are building such model systems by engineering S-layer proteins with potential for precise control of multiple bioactive ligand display.

1.7 S-layers as Molecular Carriers for Protein SAMs

S-layer proteins produce a very high-density array of displayed molecules that retain their underlying regular spacing. We reengineer these surface self-assembling proteins to develop model systems with precise controlled displays of bioactive ligands. In previous studies involving surface chemical modification, the S-layer proteins were first assembled and then conjugated to a single moiety.[77] In contrast, as shown in fig. 1.4, we first build individual bioconjugates of various functionalities tethered by highly hydrophilic poly(ethylene glycol) (PEG) linkers and then assemble sets of S-layer protein conjugate monomers in a modular fashion onto surfaces. The inherent nanostructure of the S-layer dictates the control of bioactive ligand orientation and spacing. As shown in fig. 1.5, the S-layer protein serves as the molecular carrier and the driving force for the formation of protein-based self-assembled

monolayers (SAMs). The size of molecular carrier (headgroup), the S-layer protein, is much larger (ranging from 40 to 200 kDa) than the carriers used in other self-assembly systems (<1 kDa).[68, 69, 70]

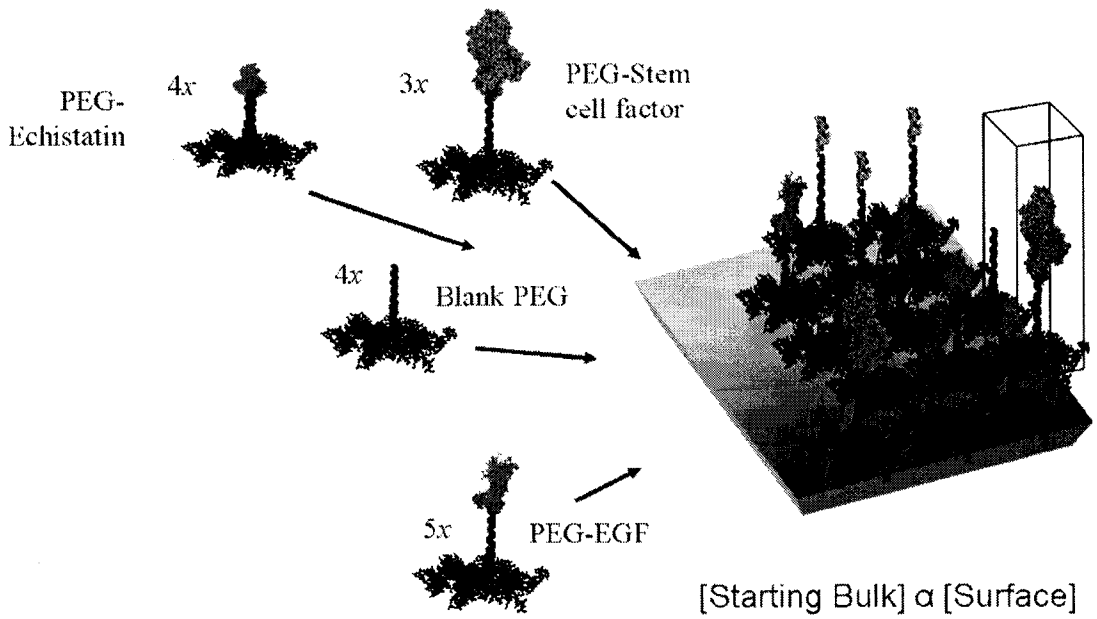

Figure 1.4: Protein Patterning: Modular Self-Assembly

Also, in comparison to these systems, due to the difference in headgroup size, we have attached larger bioactive ligands (3-28 kDa). In addition, we have used longer tethers (2-4 kDa vs 0-1 kDa) and still retained self-assembly. Moreover, phase separation during self-assembly of mixed monomers (disparate sizes) might be suppressed due to the spatial confinement of endgroups within the large protein headgroup regions. In contrast to phase separated monolayers using

gold-thiol systems,[78, 79] our method would display a uniform distribution of dissimilarly sized or functionalized molecules on surfaces with an imposed nanostructure. These self-assembled S-layer protein conjugates would generate stable and structured bioactive surfaces with controlled density and spatial organization of ligands.

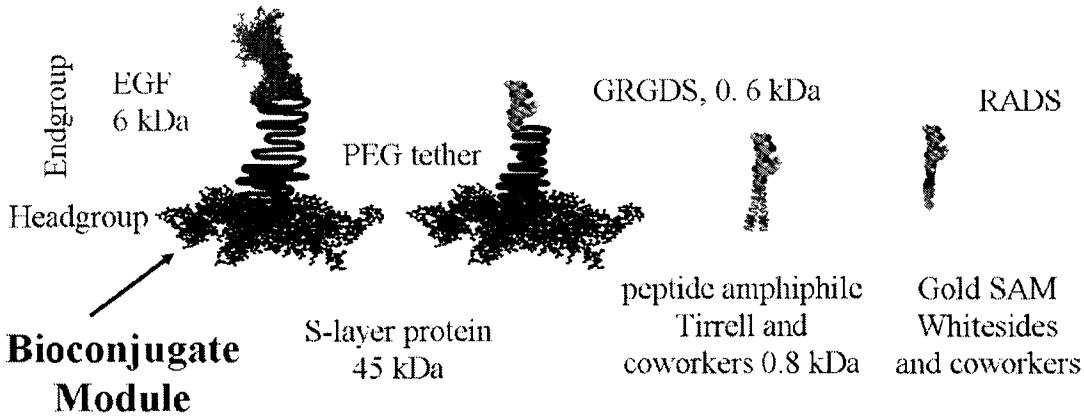

Figure 1.5: S-layer Proteins as Molecular Carriers

1.8 Characteristics of S-layer protein SAMs

The PEG tethers are included to provide passivity from non-specific protein adsorption.[80, 81, 82] Direct force measurements of non-specific and specific protein interactions with PEG tethers have been investigated earlier. [83, 84] Since this system is built upon the nanometer spacing of the S-layer, larger molecules such as polymers are displayed in adjacent lattice sites with imposed separation. This intrinsic

separation between neighboring endgroups would restrain steric hindrance for molecular recognition and further block inter-endgroup interactions that might possibly result in aggregation and loss of functional activity. Consequently, more active and accessible endgroup molecules are placed per unit area. This provides optimized molecular recognition at interfaces and increased miniaturization and complexity of the resulting molecular array.

The self-assembling proteins we use for our studies are derived from the crystalline surface layer of *Lactobacillus brevis* ATCC 8287. *In vitro*, these proteins are known to assemble in 2D crystalline arrays on positively charged surfaces.[85] Exploiting this phenomenon, we conduct assembly experiments on surfaces of arbitrary topology including polymer microspheres, silicon substrates, cation-doped glass slide, and cationic liposomes. We vary the complexity of the display of ligands or desired endgroups by using sets of different bioconjugate modules in various proportions at the beginning of the assembly experiment.

These modules form bioactive surfaces that give rise to an ordered spacing and display of mixture of bioactive ligands in the nanometer range. This will provide a new route to produce evenly distributed displays of adhesion ligands augmented with combinations

of other tethered bioactive ligands such as growth factors. Using this method we hope to further increase the level of simulation of the native extracellular environment and perform quantitative measurements of cellular response. The emerging results could enable systematic investigation of molecular signaling.

Chapter 2: SYNTHESIS & CHARACTERIZATION OF S-LAYER PROTEIN BIOCONJUGATES

S-layers as described earlier, are composed of a single protein or glycoprotein species of molecular weight 40-200 kDa. To utilize these proteins as molecular carriers for protein SAMs (section 1.6), we first have to construct bioconjugate modules. This chapter details the synthesis and characterization of these modules. For our studies, we are using the surface self-assembling proteins of lactic acid bacteria, *Lactobacillus brevis*. We have primarily chosen these bacteria due to its small sized S-layer proteins of 45 kDa. In addition, proteins of molecular size <50 kDa are more conducive for mass spectrometry and solid state NMR studies. Masuda and Kawata have partially characterized the regular array of these S-layer proteins of *Lactobacillus brevis* and have reported its ultrastructure.[86] They have shown with the help of negative staining experiments that one morphological unit of the crystalline array of these S-layer proteins appeared to consist of four spherical subunits, each about 2 nm in diameter. They have reported that the subunits were arranged in a tetragonal pattern about 4.5 nm by 7.0 nm in

dimension. Also, between rows in two directions, there were lattice boundaries at an angle of 75^0. They have also shown that the average spacing between the rows were 10 nm in one direction and 7 nm in another. They have also performed and reported experiments, reassembling the surface layer proteins back onto their cell wall fragments. It has been shown that the subunits possess the information determining their arrangement and are bound to each other by hydrogen bonds in preference to salt bridges.[87] Vidgren and co-workers[88] have sequenced the polymerase chain reaction fragments containing the entire S-layer gene and its regulatory regions. An analysis of the amino acid composition of the S-layer protein deduced from the DNA sequence shows the following:

1. There are large numbers of hydrophobic amino acids
2. There is no cysteine residue,
3. Lots of amino acids with hydroxyl groups are present and
4. Basic amino acids are more in number than acidic amino acids.

The presence of large number of amino acids with hydroxyl groups indicates the likely formation of inter- and/or intramolecular hydrogen bonds. This supports the fact that the S-layer proteins could be disassembled with high concentrations (~ 5-6 M) of salt by breaking

their hydrogen bonds. Subsequently, they can be reassembled onto any arbitrary surface by simply dialyzing out the salt. We isolate these S-layer proteins for our bioconjugation studies and use the purified bioconjugate modules to make model bioactive surfaces.

2.1 Materials and Methods

2.1.1 Growth conditions: *Lactobacillus brevis* ATCC 8287 was obtained from the American Type Culture Collection. The bacteria were grown unstirred in MRS broth[89] (Difco Laboratories, Maryland) at 37°C for 2 days after inoculation with 3% (v/v) 2 day culture. The extraction and purification steps were similar to those performed by Lortal and co-workers.[54]

2.1.2 Scanning Electron Microscopy (SEM): Fixation: Cells were prefixed in 2% glutaraldehyde in 0.1 M cacodylate buffer at 4°C and pH 7.2 for 30 min and post fixed in 1% osmium tetra oxide for 30 min in an ice bath. The cells were filtered on a 0.2 µm polycarbonate filter and washed with distilled water. *Dehydration:* The cells were then sandwiched between two filters and enclosed tightly in a metal cage and were dehydrated in a graded series of 30%, 50%, 75%, 85%, 95%

(two changes) and 100% (two changes) ethanol for 10 min each. For further dehydration the metal cages containing the cells were immersed in amyl acetate, three changes of 10 min each. *Drying:* Critical point drying was done to dry the specimen without ruining the delicate structure. Liquid CO_2 at pressure of 80 bar was flushed in and out of the drying chamber about eight times to remove residual amyl acetate. The cells were slowly allowed to return to room temperature and pressure. *Scanning images:* The cells were then placed on metal stubs and sputter coated with 20 Å of platinum. The samples were incubated at 60°C overnight and subsequently examined under the SEM. Cassettes were replenished with fresh films under complete darkness and loaded into the SEM. Pictures were taken and developed. *Film development:* Under complete darkness, the films was taken out from the cassette and properly placed in film holders. The films were immersed in T-Max 100 developer and agitated gently every 15 seconds for 15 minutes and there after instantly dipped in the stop bath and agitated for 30 seconds. The films were successively dipped in the fixer solution for 10 minutes and then washed with water for half an hour. The films were removed and hung to air dry. *Printing:* Printing was done under safety lights. The image was magnified and printed using a л chart. To obtain the best

contrast, filter #6 was used and exposed for 5 seconds. The prints were then immersed in different solutions taken in trays in a series: in dektol-19 developer diluted 1:1 in water for one minute, in the stop bath for 30 seconds, in the fixer for 4 minutes and finally in water for 5 minutes. The photos were dipped in water containing a few drops of "photo flo" and hung to dry.

2.1.3 Extraction of the S-layer protein: Exponential-phase cells were recovered by centrifugation at 14000 x g for 20 min. The cell pellets were resuspended in distilled water to wash the remaining broth and centrifuged again at 14000 x g for 20 min. After two such wash cycles, 10-15 mg of moist pellet was suspended per ml of 5M Lithium Chloride (LiCl) (Sigma) and incubated for 30 min at 4 C to extract the S-layer protein. The extract was then centrifuged at 14000 x g for 20 min and the supernatant was designated as crude extract.

2.1.4 Purification of the S-layer protein: The crude extract was purified using a XK 50/60 chromatography column (Amersham Biosciences), 5 x 60 cm, with a uniform packing of Sephacryl S200 HR (Sigma) gel, equilibrated with 5M LiCl. The protein was eluted at 30 ml/hr and 1.5 ml

fractions were collected. Prior to injection into the column, the crude extract was concentrated 10 fold using Millipore Ultrafree-15 centrifugal filter device (Sigma) having a cutoff of 30000 Da. The filters were pre-rinsed by spinning at 4000 x g with deionized water (d. H_2O) for ten minutes to remove any residual glycerin from the manufacturing process. Crude S-layer protein was then taken in the filters and spun at 4000 x g to obtain the desired concentration. In some other runs, the protein was first dialyzed overnight against water and the assembled protein was resuspended in 5M LiCl before injection. In a separate experiment to study the difference in peak heights, purification was also performed on the column when equilibrated with 8M LiCl. % purity of protein samples was established using SDS-PAGE.

2.1.5 Protein Quantitation: Protein concentrations were determined using BCA Protein Assay (Pierce)[90, 91] as well as using Coomassie Plus Protein Assay (Pierce).[92, 93] Diluted standards of bovine serum albumin (BSA) were prepared using a 2.0 mg/ml BSA stock.

2.1.5.1 BCA Protein Assay: The BCA working reagent was prepared by mixing 50 parts of reagent A (Sodium carbonate, sodium bicarbonate, bicinchoninic acid and sodium tartrate in 0.1 M sodium

hydroxide) with one part of reagent B (4% cupric sulfate). 0.1 ml of the BSA standards or the protein samples with unknown concentration were added to 2 ml of the working reagent. They were mixed and incubated at 30 C for 30 min. The protein reduces the cupric ion to a cuprous ion which, in turn, reacts with the bicinchoninic acid to generate a purple color. After incubation, the samples were cooled to room temperature and absorbance was measured at 562 nm. A curve was plotted with the average blank corrected absorbance reading for each BSA standard against its concentration. Using this standard curve, the unknown protein concentrations were determined.

2.1.5.2 Coomassie Plus Protein Assay: The advantages of this method as compared to the BCA assay are that the reagent is ready to use (no mixing is required); requires half the amount of protein sample and the incubation period is only 5 min at room temperature. Similar to the above procedure BSA standards were prepared and tested in tandem with protein samples with unknown concentration. Coomassie Plus reagent, stored at 4 C was first brought to room temperature before use. The samples were added to the reagent and incubated at RT for 5 min. Absorbance was measured at 595 nm. Unknown protein concentrations were determined using a standard curve that was

plotted similarly with the average blank corrected absorbance reading for each BSA standard.

2.1.6 Mass Spectrometry: S-layer protein samples and their bioconjugates were analyzed with the help of reverse phase HPLC coupled electrospray ionization mass spectrometer. We analyzed our samples on an LC-MS Agilent Chem Station at the Hunter College of the City University of New York Mass Spectrometry facility. The samples were prepared to possess an average protein content of 10–15 µg in a 10% acetic acid solution. The samples injected into the HPLC-mass spectrometer were either 50 µl or 100 µl and eluted at the rate of 0.5 ml/min with a gradient flow of acetonitrile.

2.1.7 SDS-PAGE of S-layer protein and S-layer protein conjugates: All reagents, gels and instruments were purchased from Bio-Rad Laboratories, Hercules, CA. Both 4-15% and 7.5% Tris-HCl Ready Pre-cast gels were used for analyses. "Running" buffer 25 mM Tris, 192 mM Glycine, 0.1% (w/v) SDS, pH 8.3, was prepared by diluting 10x stock Tris/Glycine/SDS solution with d. H_2O. 2-mercaptoethanol (reducing agent to cleave disulfide bonds and unfold the protein) was added to

the proportion of 5 µl to 95 µl of Lamelli buffer (62.5 mM Tris-HCl pH 6.8, 2% SDS, 25% Glycerol, 0.01% bromophenol blue) to make the "sample" buffer.

After determining protein concentration of each sample that needs to be analyzed, samples were diluted in the "sample" buffer 1:2 and heated at 95 C for 5 minutes. This breaks the secondary structure, reduces and denatures the proteins. The Pre-cast gel was then taken out of its pouch and the comb was carefully removed. The wells were rinsed thoroughly with distilled water. The tape was then cut along the dotted line at the bottom of the gel cassette with a razor blade. The clear tape from the bottom of the gel sandwich was then removed by pulling the tab across the cassette, and the bottom electrode-contact slot exposed. Gel cassette was subsequently inserted into the Ready Gel Cell so that the short plate faces inward toward the notches of the U-shaped gaskets. The procedure was repeated for the second Ready Gel or if only one gel was to be run, the mini cell buffer dam was used. Having the gel cassettes in place against the green gaskets, the Electrode Assembly was slid into the clamping frame. Pressing down on the Electrode Assembly the two cam levers of the clamping frame were closed to form the Inner Chamber. This was to insure proper

sealing of short plate to the notch in the gasket. With the Inner Chamber Assembly lowered into the Mini Tank, the inner chamber was filled with ~125 ml of "running" buffer until the level reached halfway between the tops of the taller and shorter glass plates of the Gel Cassettes. It was important to avoid overfilling the Inner Chamber Assembly which would potentially cause siphoning and loss of buffer resulting in interruption of electrophoresis. ~225 ml of "running" buffer was then added to the Mini Tank or the lower buffer chamber. The samples were consequently loaded into the wells with a pipette using gel loading tips by inserting the tips gently to avoid puncturing the bottom of the well. Loading was done slowly with a steady hand allowing the samples to settle evenly on the bottom of the well. Sample sizes were dependent on well sizes. The Mini Tank was then sealed aligning the color coded banana plugs and jacks. The electrical leads were subsequently inserted into the power supply and a constant 200 volts was applied for ~35 minutes.

After electrophoresis was complete, the power supply was turned off and the electrical leads disconnected. The Inner Chamber was lifted out of the Mini Tank and the "running" buffer was poured before opening the cams to avoid spilling of buffer. Gel cassettes were opened

by hand by carefully separating the 2 plates, starting from one corner. The gel was removed by floating it off the glass plate by inverting the gel and plate under a transfer solution (d. H2O). The gel was gently nudged off one corner of the plate and allowed to roll off into the solution. After washing the gel in d. H_2O for 5 min, thrice, the gel was placed in Bio-Safe Coomassie Blue G-250 stain for 1 hr on a shaker. This stain detects proteins without the use of methanol, acetic acid, or other hazardous agents. It is a ready-to-use, single-reagent protein stain based on a modified Coomassie Blue G-250 stain that produces a linear response allowing quantitative analysis. After staining, the gel was washed in d. H_2O for 30 min to reduce background staining and to increase band intensity. Gel densiotomograms were obtained using a 16 bit Umax flatbed scanner and image processing was done using IgorPro 4.0.

2.1.8 Construction of Bioconjugate Modules: Purified protein suspended in 5M LiCl was dialyzed overnight against water. The assembled proteins were dissolved separately in 50 mM sodium phosphate buffers at pH 6.5 to obtain a final protein concentration of 5-10 mg/ml.

2.1.8.1. Bioconjugation of S-layer Proteins with Fluorophores: The fluorophores used for S-layer protein conjugation reactions were mainly obtained from Molecular Probes and Sigma and are tabulated in Table 1 and shown in Fig 2.1-2.5. To the 5-10 mg of S-layer protein dissolved in 50 mM sodium phosphate buffer at pH 6.5, 20 molar fold excess of fluorophore (dissolved in d. H_2O or dimethylsulfoxide, DMSO for hydrophobic probes) was added. Conjugation experiments were carried out in dark, over ice and overnight on a flask shaker. The reaction was terminated with 150 mM hydroxylamine (Sigma) at pH 7.

Table 1: Fluorescent probes, lipids and tethers used for bioconjugation techniques

Fluorescent Probes and PEG Tethers	Absorption Maximum, nm	Emission Maximum, nm	Molecular Weight, Da
Fluorescein isothiocyanate	494	518	389.4
Tetramethyl rhodamine	555	580	527.53
Cy5 Mono NHS Ester	646	663	792.0
Oregon green	496	524	509.38
BODIPY	558	568	443.23
β-BODIPY PC	508	515	881.93
NBD PC	460	534	882.09
Fluorescein-PEG-NHS	494	518	2000
Fluorescein-PEG-NHS	494	518	5000
Vinylsulfone-PEG-NHS	-	-	3400
Biotin-PEG-CO2-NHS	-	-	3400

Unreacted probes were removed by gel filtration through Sephadex G-25 (Sigma) gravity column that has been equilibrated with 50 mM sodium phosphate, pH 6.5 buffer (The gel was hydrated for an hour and decanted for any floating particles prior to loading). The S-layer protein bioconjugates were analyzed with the help of mass spectrometry to identify their respective yields and also examined under a Nikon Eclipse TE 200 fluorescence microscope.

2.1.8.2 Tethering S-layer proteins (PEGylation): Polyethylene glycol (PEG) tethers (Shearwater Polymers) were conjugated to the S-layer proteins using similar procedures as described above. The PEG compounds were mainly N-hydroxy succinimidyl esters, and water-soluble. Tethers were chosen in the molecular weight range of 2000 to 5000. The reactions were carried out in vials using 10 molar fold excess of PEG molecules and in dark at 4 C. The vials were generally incubated for more than 12 hrs. The reaction was quenched with 150 mM hydroxylamine at pH 7. Unreacted PEG molecules were removed by gel filtration through Sephadex G-50 (Sigma) column that has been equilibrated with 50 mM, pH 6.5 sodium phosphate buffer. The gel was hydrated for 3 hours prior to loading. The yields of bioconjugated S-layer proteins were analyzed with the help of SDS-PAGE.

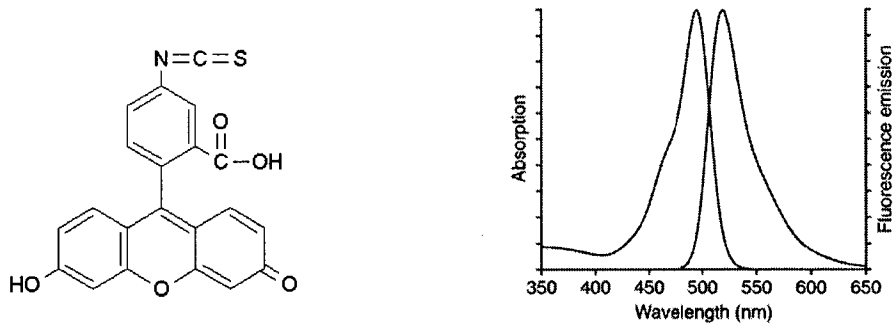

Figure 2.1: Fluorescein isothiocyanate

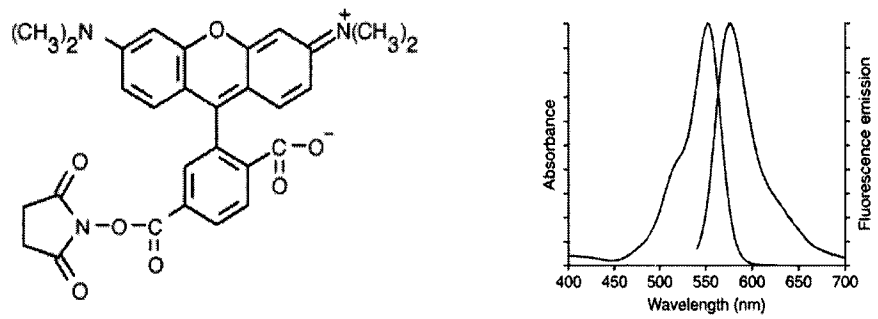

Figure 2.2: 6-carboxytetramethylrhodamine, succinimidyl ester, 546/585

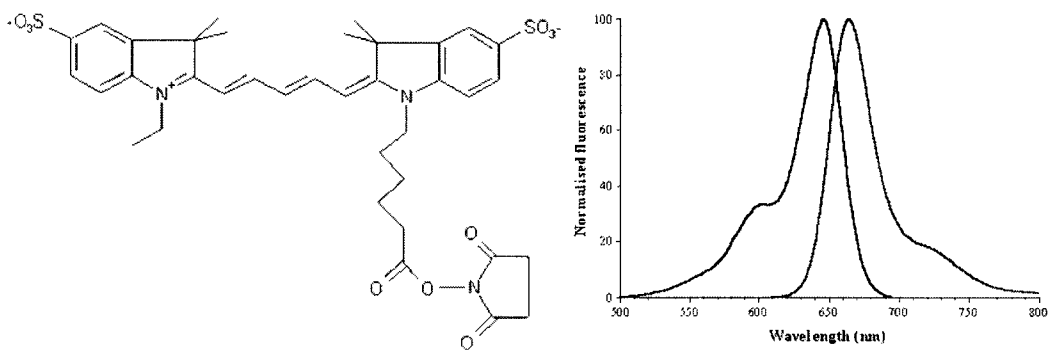

Figure 2.3: Cy5 Mono N-hydroxy succinimidyl ester

2.1.9 Preparation of Biotin-GFP-SS-PEG-SLP: This protocol, illustrated in fig. 2.7, consists of 4 steps. The first step involved the coupling of

Green Fluorescent Protein, (GFP) (Upstate USA, Inc., Lake Placid, NY) MW 28 kDa, with SATA[94] (N-Succinimidyl-S-acetylthioacetate) (Pierce) MW 231.22.

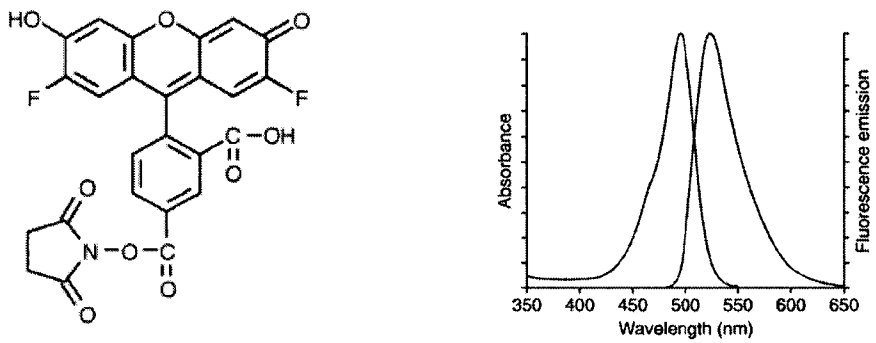

Figure 2.4: Oregon Green® 488 carboxylic acid, succinimidyl ester, 488/524

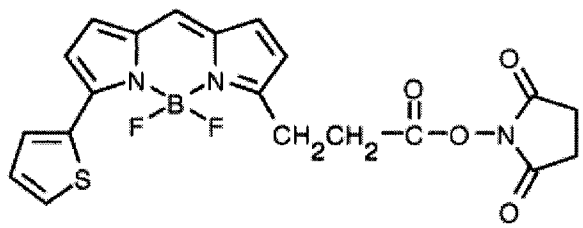

Ex: 558 nm; Em: 568 nm

Figure 2.5: BODIPY: 4,4-difluoro-5-(2-thienyl)-4-bora-3a,4a-diaza- s-indacene-3-propionic acid, succinimidyl ester

Subsequently, the SATA coupled GFP was biotinylated. The third step, PEGylation of the S-layer protein (SLP) with Vinyl Sulfone-PEG_{3400}-N-

Hydroxy Succinimide (VS-PEG_{3400}-NHS or CH_2-CH-SO_2-PEG_{3400}-NHS), was carried out simultaneously. The final step consists of mixing the deprotected bioactive active ligand having the sulfhydryl group (Biotin-GFP-NH-CO-CH_2-SH) with the Vinylsulfone conjugate of the S-layer protein (CH_2-CH-SO_2-PEG_{3400}-SLP) to obtain the final Biotin-GFP-SS-PEG-SLP conjugate.

2.1.9.1 Coupling of GFP with SATA: To begin with, "reaction buffer", 500 ml Sodium Phosphate, 1 mM EDTA pH 7 and "deacetylation buffer", 50 mM Sodium Phosphate, 50 ml 25 mM EDTA, 0.5 M Hydroxylamine.HCl, pH 7 were prepared. Compared to the amount of GFP, 10 molar fold of SATA was dissolved in dimethyl sulfoxide (DMSO). The amount of DMSO was kept less than 5% of total reaction mixture. The SATA DMSO solution was added to GFP and incubated at room temperature for 45 min in dark. The reaction mixture was then diluted 10 fold with the reaction buffer and reduced to its original volume using Millipore Ultrafree-15 centrifugal filter device (10000 Da cut off) to remove excess SATA. Deacetylation buffer was then added to the GFP-SATA product and the solution was incubated for 2 hrs at room temperature in dark. Since hydroxylamine (present in the deactylation buffer) will interfere in the next reaction step, excess

was subsequently removed using similar ultrafiltration methods. The dilution-filtration step was repeated several times for complete removal of residual hydroxylamine.

2.1.9.2 Biotinylation of SATA coupled GFP: Estimating the GFP concentration, 20 molar fold excess of NHS-Biotin was added to the GFP-SATA product. Reaction was conducted in 50 mM sodium phosphate at pH 8 and incubated in dark at room temperature for 2 hours. The product was then recovered using similar dilution-filtration steps as described above.

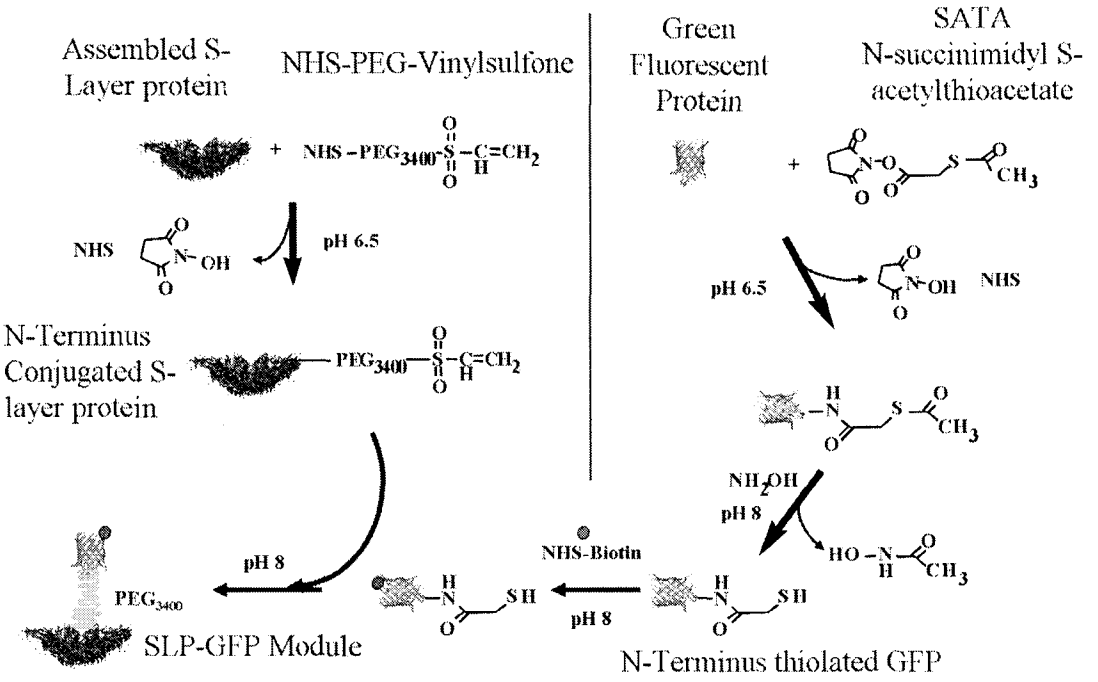

Figure 2.6: Reaction Scheme for Preparation of Biotin-GFP-SS-PEG-SLP

2.1.9.3 Vinyl Sulfone labeling of SLP: This was done using the same procedure as described in section 2.1.8.2.

2.1.9.4 Formation and Purification of Biotin-GFP-S-S-PEG-SLP: Biotin-GFP-SATA and SLP-PEG_{3400}-VS pool were mixed at 1:1 ratio and set for an overnight reaction at 4 C in dark. Gel filtration was performed on Sephadex G-50 column to separate uncoupled products. The first eluted peak was designated our required product Biotin-GFP-S-S-PEG-SLP. The product was further purified using monomeric avidin affinity columns to remove unlabeled S-layer protein.

2.1.10 Affinity Purification of Biotinylated S-layer Bioconjugates: Fig. 2.7 provides a schematic representation of the process. Monomeric avidin resins (Sigma) were packed in glass columns and washed with 50 mM sodium phosphate with 1mg/ml of D (+)-Biotin (Molecular Probes), pH 7 (free biotin buffer) for four column volumes. Subsequently, to displace biotin from exchangeable sites, the column was washed with 8 to 10 column volumes of 100 mM Glycine-HCl at pH 2. Later, the resin was reequilibriated with 50 mM sodium phosphate, 150 mM sodium Chloride at pH 7 (neutral buffer). The binding capacity of monomeric avidin was 30 nmol of biotin per 1 ml resin. Equivalent moles of biotinylated S-layer protein conjugate sample was calculated and injected slowly to saturate

the column. Amount of the injected sample was about 10% volume of column.

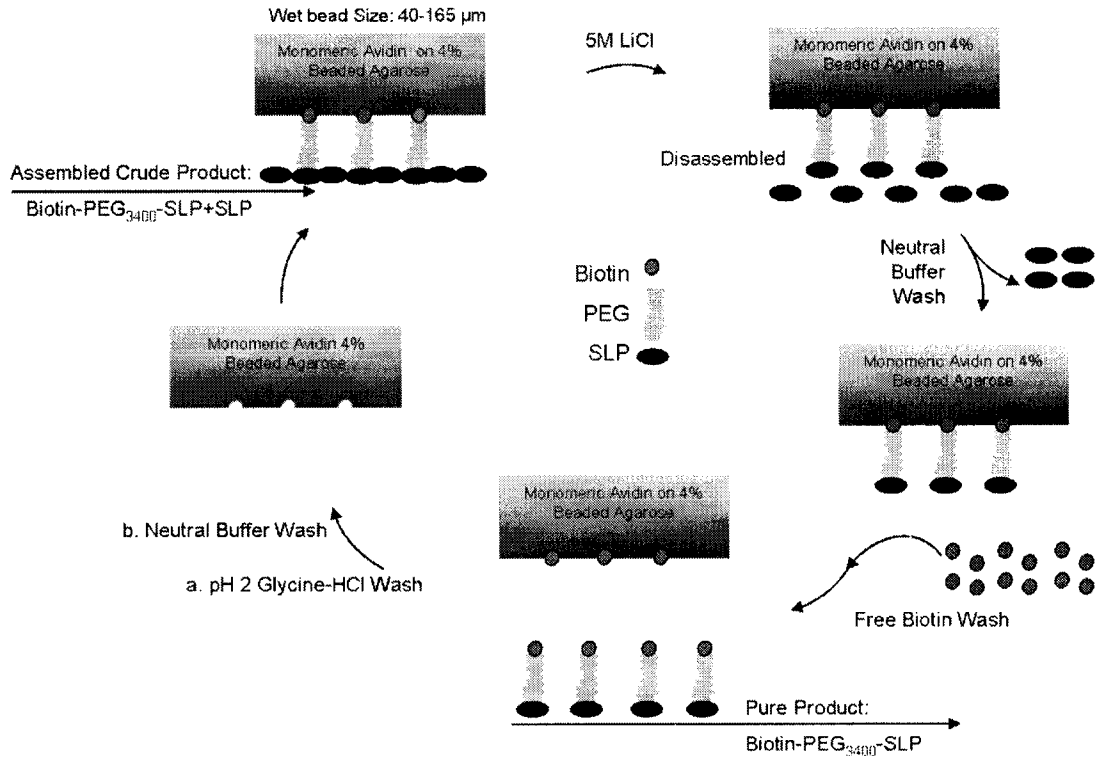

Figure 2.7: Monomeric Avidin Affinity Purification of Biotinylated S-layer Protein

The column was gently agitated after injection to allow complete contact between biotin and avidin and incubated for 1 hr. The column was then filled with 5 M LiCl and agitated mildly to allow disassembly of the non-biotinylated conjugates. After incubating the system in dark for about an hour, the disassembled compounds (non-biotinylated conjugates) were eluted with neutral buffer. For ligands sensitive to 5 M LiCl, neutral

buffer wash for prolonged times allowed disassembly of non-biotinylated conjugates. The column was consequently eluted with free biotin buffer for recovery of column bound biotinylated conjugates. Once the samples were removed, the column was regenerated by washing with 100 mM Glycine-HCl at pH 2 followed by reequilibriating with neutral buffer.

2.1.11 Negative staining: Negative staining with uranyl acetate was done as described by Sleytr and co-workers.[95, 96] 300-mesh Formvar carbon film supported copper grids (Electron Microscopy Sciences) were glow discharged and immediately floated on drops of poly-L-lysine solution (0.1% in d. H_2O) for 15 min. Excess poly-L-lysine was removed by dipping the grids in d. H_2O several times. The grids were floated on drops of Biotin-PEG_{3400}-S-layer protein or Fluorescein-PEG_{2000}-S-layer protein solutions for 30 min, 1hr, 2 hr, 3 hr and overnight in dark. The protein self-assembly solutions were centrifuged for 10 min at 5400 x g prior to use. This step assured that only the clear supernatant containing S-layer proteins that were not assembled into supramolecular structures were used. After incubation, the grids were moved on several drops of d. H_2O. Adsorbed specimens were

chemically fixed by floating the grids on drops of 2.5% glutaraldehyde (Sigma) in 0.1 M sodium cacodylate (Electron Microscopy Sciences) buffer at pH 7.0. The grids were incubated in dark, under the hood, for 30 min and then transferred onto several drops of distilled water. Further, the grids were negatively stained with 1% uranyl acetate for 5 min and then dried with filter paper. The preparations were examined under a Nikon transmission electron microscope at Mount Sinai School of Medicine. The micrographs were taken on Kodak film and later analyzed using NIH Image 1.62.

2.1.12 Protocol for labeling S-Layer Proteins for NMR studies: BioExpress Cell Growth Media Unlabelled, BioExpress Cell Growth Media ^{15}N 96-99%, BioExpress YBN-^{15}N 96-99% and BioExpress MIN-^{13}C 97-98% ^{15}N 96-99% were obtained from Cambridge Isotope Laboratories. Initial batch was conducted with unlabelled BioExpress media to find out the ideal growth conditions of *Lactobacillus brevis*. 15 ml of MRS Broth was autoclaved and injected with frozen culture stock using a 'loop' and incubated at 30 C for 3 days. This culture was used as inoculum. To test growth in BioExpress media, first the 10x stock was diluted with d. H_2O and a mixture of BioExpress media and MRS

Broth at 0%, 25%, 50%, 75% and 100% concentrations were prepared. The culture flasks containing the media were autoclaved, cooled, injected with 2% of inoculum and incubated at 30 C for 3 days. Since growth was observed in all culture media, subsequent cultures in ^{13}C or ^{15}N isotope labeled BioExpress media were conducted with 20% MRS broth and 80% BioExpress media, grown under similar conditions. S-layer proteins were extracted with methods described in section 2.1.3.

2.2 Results and Discussions

2.2.1 Growth, Extraction and Purification of S-layer Proteins: S-layer proteins range in size from 40–200 kDa as stated previously, depending on the species of origin. We chose a smaller *Lactobacillus* variant S-layer protein for these studies to enable simplistic characterization by both mass spectrometry and eventually high-resolution solid state NMR. These *L. brevis* S-layer proteins were obtained in high yield from 5M LiCl extraction of wet cells. The yield was greater than 200 mg per liter of cell culture. Scanning electron microscope images of whole cells

of *L. brevis,* fig. 2.8a, show groups of bacteria where the surface

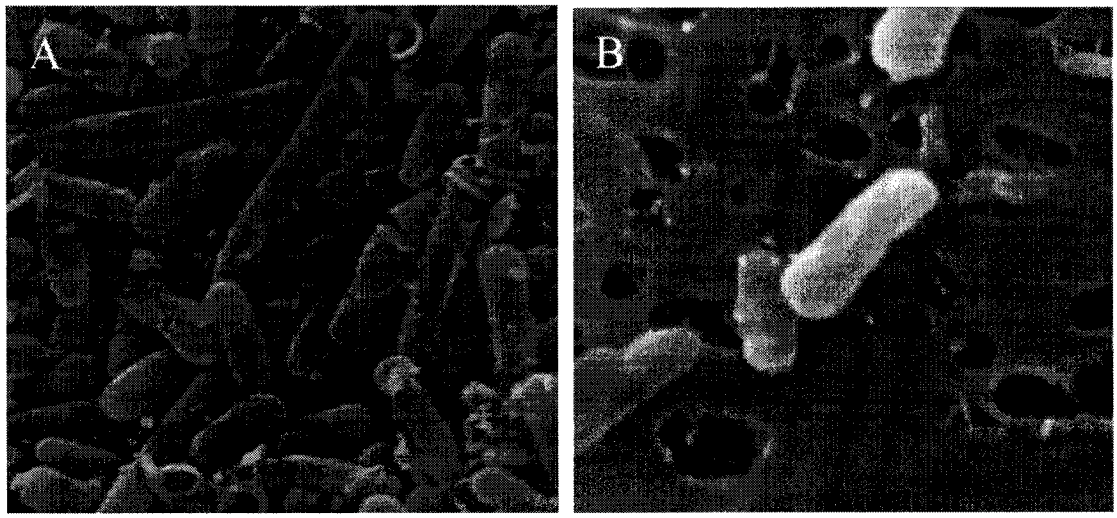

Figure 2.8: SEM of Lactobacillus brevis. A. cells, x 10000 and B. cell, x 20000

layers seemingly appear peeled off partially during proliferation. Higher magnification is needed to observe the surface structure that could not be achieved using a tungsten filament. Later work would be done with the help of LaB_6 filament on the SEM to view whole cells.

The crude extract was purified using two methods, gel permeation chromatography and successive cycles of disassembly/assembly via dialysis. Fig. 2.9 shows a gel permeation

chromatogram of disassembled S-layer proteins, showing one narrow

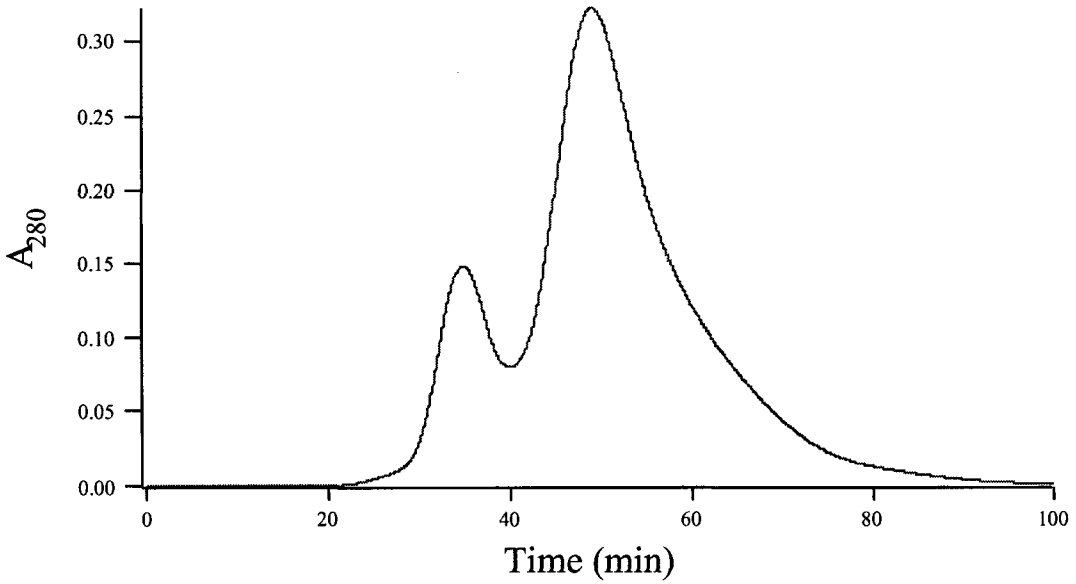

Figure 2.9: Gel Permeation Chromatogram of S-layer Protein on Sephacryl S-200 HR

peak followed by a broad multi-component peak. Fractions pooled from parts of those peaks, were dialyzed against d. H_2O water in a regenerated cellulose membrane with either 10 or 30 kDa MW cutoff and analyzed using Mass spectrometry and SDS-PAGE. Analysis of the fractions shows that both are predominantly S-layer proteins. Our working hypothesis is that the first Gaussian peak at t = 38 min arises from multimers. The initial portion of the second broad peak is the pure S-layer protein. The shoulder and the lagging peak contain lower molecular weight impurities. Experiments conducted with 8M LiCl showed difference in peak heights (data not shown). It was seen that

the 1st peak was smaller in this case. This allows us to deduce that higher concentration of LiCl reduces the amount of multimers in

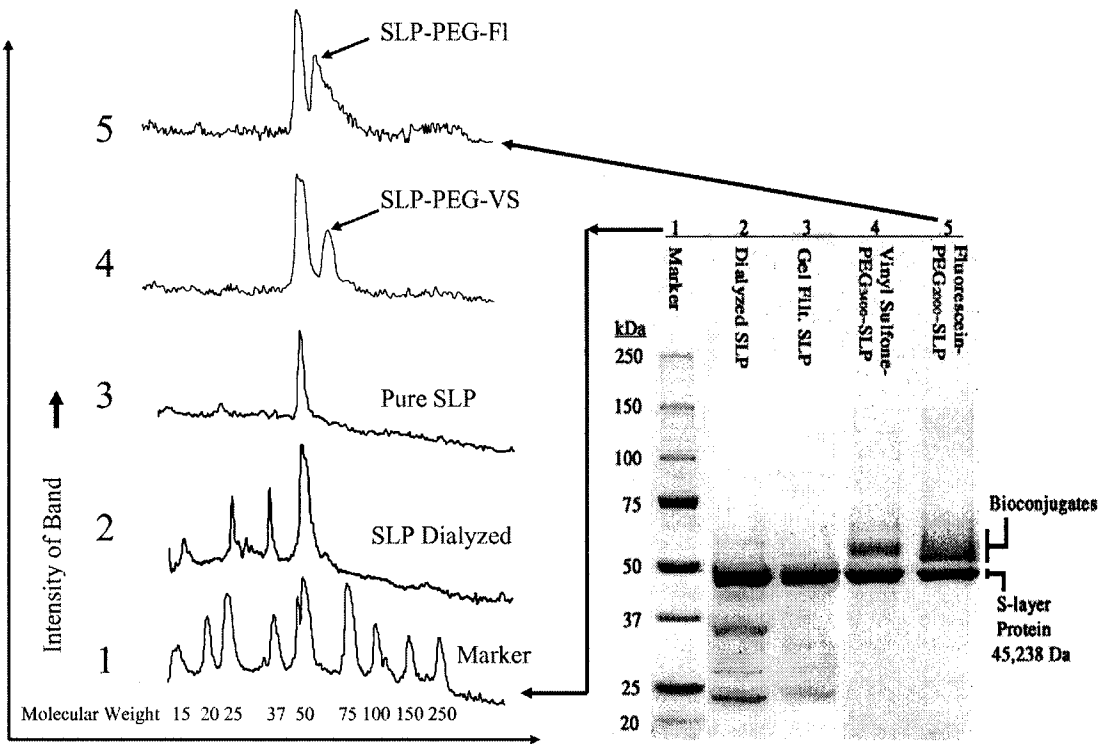

Figure 2.10: SDS-PAGE: Gel scan and Densiotomograms of SLP and SLP conjugates

solution. Dialysis was performed against d. H_2O in Spectra/Por® 7 membranes (Spectrum Laboratories Inc., Rancho Dominguez, CA) with 25 kDa MW cutoff. The assembled S-layer protein was disassembled with 5 M LiCl and dialyzed once again. Fig. 2.10 shows the SDS-PAGE gel of crude and pure SLP and the densiotomograms (intensity profiles using IgorPro 4.0) of individual lanes. It was seen that three main impurities remain with estimated molecular weights of 23, 27, and 35

kDa even after multiple cycles of dialysis. Thus, the S-layer proteins were run through HPLC columns to increase purity to >95%. The densiotomogram of pure S-layer protein is curve 3 corresponding to Lane 3 of the gel in Fig. 2.10.

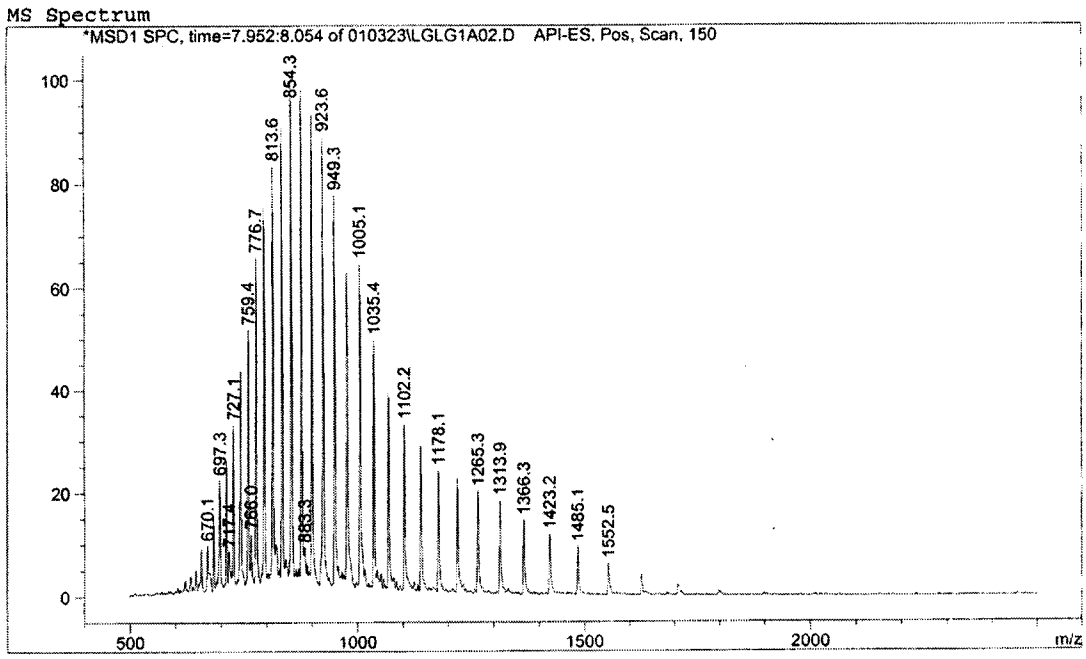

Figure 2.11: ESI Mass Spectrometry: Lactobacillus brevis S-layer Protein

2.2.2 Structural Analyses of *Lactobacillus brevis* S-layer Protein: Mass spectrometry of purified S-layer protein of *Lactobacillus brevis,* fig. 2.11, revealed a molecular mass of 45238 kDa. The molecular mass of the protein corresponds to a 435 residue protein after removal of the 30 residue signal peptide from the 465 residue open reading frame. This

agrees exactly with the amino acid sequence[88] and can be inferred that the sequence is non-edited from the gene and is not glycosylated.

Negative Staining, Fig. 2.12 revealed crystalline pattern of bacterial surface layers. It is evident from the poly-L-Lysine control grids that the stained portions of the protein layer possess a tetragonal nanopatterned structure. In agreement to the work published by Masuda and Kwata,[86] faint crystal lattice boundaries at an angle of 75° can also be seen. More attempts are currently being employed for better resolution. In separate experiments, self-assembly solutions of S-layer proteins were centrifuged at 14000 x g for 20 min and analyzed using Dynamic Light Scattering Particle Analyzer, (Malvern Instruments Ltd, Malvern UK). Results revealed average particle size of 6.12 nm. This could potentially be protein dimers that could be nucleation sites for the formation of assembled structures. On the other hand, it could also hint the existence of dimers in equilibrium with the assembled protein before centrifugation.

Solid State NMR techniques have been employed previously for obtaining 3D structural information of peptides and proteins.[97, 98, 99] Preliminary NMR studies on C^{13} labeled S-layer protein gave narrow C^{13} line widths under magic angle spinning (data not shown). The

encouraging result emphasizes potential for high resolution NMR studies. We are currently using solid state methods for obtaining structural information of S-layer protein from *Lactobacillus brevis*.

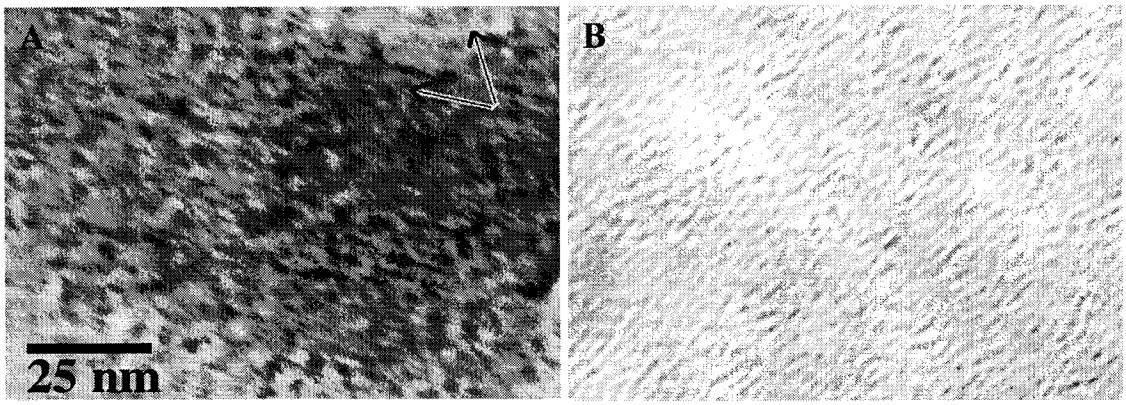

A: S-layer protein self-assembled onto poly-L-Lysine coated grids
B: Poly-L-Lysine coated grids (control)

Figure 2.12: Negative Staining of S-layer Protein with Uranyl Acetate

2.2.3 Secondary Sequence Analyses using Bioinformatics Tools: Studies were also performed using various Bioinformatics tools. Molecular dynamic simulation attempts using MacroModel 7.0 (Schrodinger, Inc., Portland, OR) turned futile. With the total number of atoms of the S-layer protein from L. brevis being over six thousand, the program seized to run. The program worked for fragments of about 1000 atoms. Besides, tools from ExPASy (Expert Protein Analysis System) proteomic server of the Swiss Institute of Bioinformatics were used for the analysis of protein sequence and structure. The protein

has a total of 30 negatively charged residues (Asp + Glu) are and 46 positively charged residues (Arg + Lys) with a theoretical pI of 9.45.

We also attempted to do a simple modeling of the properties such as likely modification sites of the S-Layer protein of Lactobacillus brevis ATCC 8287 based on its primary sequence using Basic Local Alignment Search Tool (BLAST).[100] Post-BLAST analysis was also performed using Position Specific Iterative PSI-BLAST to attempt pairwise homology modeling. The search was conducted on all non-redundant, over 2 million sequences from various databases. High sequence identity was obtained for proteins from three S-layer protein genes from *Lactobacillus brevis* ATCC 14869. These genes were isolated and characterized by Palva and coworkers.[101]

Separate search was conducted with proteins only from the Protein Data Bank (PDB) to obtain 3D structure homology. From our homologous pairs, only cyclodextrin glycosyltransferase[102] (PDB ids: 1CGT through 9CGT) had a good EXPECT, E value of 0.002. It is known that the pairs are accurate only if the E value is less than 0.1.[100] Also, pairwise homology modeling was performed for a large number of random part sequences of the S-layer protein with lengths from 25-120 residues. But no homologous pairs with expectation values less than

0.1 were obtained. The identity of 1CGT to our 465 residue S-layer protein was 24% matching 63 residues to 253 residues with positives and gaps. Considering that pair-wise homology exists between the S-layer protein and 1CGT, the functions of the identical domains were obtained from SCOP[103] classification to acquire more insight. It was evident from viewing the 3D structure of 1CGT and from the part sequences of 1CGT in RasMol that the listed domains were all beta strands. Also, the C-terminal domain had a prealbumin-like fold and belongs to famly of starch-binding domains. Moreover, the region consisting of residues 495-579 had an immunoglobulin like beta sandwich fold and belongs to the immunoglobulin superfamily.

Due to lack of any hits of high identity, it was concluded that presently in the PDB, there isn't any homologous pair or domain structure for the S-layer protein of Lactobacillus brevis ATCC 8287 and thus the attempt to do a modeling of the properties such as likely modification sites was unsuccessful.

Further, we analyzed the S-layer protein using the PredictProtein services for sequence analysis and protein structure prediction at the Columbia University Bioinformatics Center. Results obtained from Profile Network Prediction HeiDelberg (PROFsec[104, 105] and PHDsec[106,

[107]) using multiple sequence alignments are given in Fig. 2.13 and Table 2. It was predicted that ~44% were all beta strands, while 5-8% were helical and the rest loops. Also, with respect to solvent accessibility, almost half of the total residues were predicted to have more than 16% of their surface exposed.

465 Amino Acids H- Helix, E-sheet, " "-loop

```
          ....,....1....,....2....,....3....,....4....,....5....,....6
AA        MQSSLKKSLYLGLAALSFAGVAAVSTTASAKSYATAGAYSTLKTDAATRNVEATGTNALY
PROF_sec     HHHHHHHHHHHHHHHHHHHHHHHHH  HHH       EEEEEEEEEEEE    EEEE
PHD_sec    HHHHHHHHHHHHHHHHHHHEEEEEEEEEE    EEE  EEEE  EEEEEEEEE     EE
          ....,....7....,....8....,....9....,....10.1.,....11.1.,....1
AA        TKPGTVKGAKVVASKATMAKLASSKKSADYFRAYGVKTTNRGSVYYRVVTMDGKYRGYVY
PROF_sec  E         EEEEEHHHHHHH          EEEEEEEE    EEEEEEEE    EEEEEE
PHD_sec   E         EEEEEEHHHHHHH         EEEEEEEE     EEEEEEEE   EEEEEE
          ....,....13.1.,....14.1.,....15.1.,....16.1.,....17.1.,....1
AA        GGKSDTAFAGGIKSAETTTKADMPARTTGFYLTDTSKNTLWTAPKYTQYKASKVSLYGVA
PROF_sec  E    EEEE  EEE EEEEEEEE     EEEEE     EEEE          EEEEEEEE
PHD_sec       EEEEE   EE     EEEEE     EEEE                   EEEEEEEE
          ....,....19.1.,....20.1.,....21.1.,....22.1.,....23.1.,....2
AA        KDTKFTVDQAATKTREGSLYYHVTATNGSGISGWIYAGKGFSTTATGTQVLGGLSTDKSV
PROF_sec    EEEEEEEEEEEEE  EEEEEEEE     EEEEEEEEE EE              EE
PHD_sec     EEEEEEE EEE E  EEEEEEEE      EEEEEEEE               EEE   E
          ....,....25.1.,....26.1.,....27.1.,....28.1.,....29.1.,....3
AA        TATNDNSVKIVYRTTDGTQVGSNTWVTSTDGTKAGSKVSDKAADQTALEAYINANKPSGY
PROF_sec  EEEE    EEEEEE    EEEE  EE                    EEEEEEEE    EE
PHD_sec   EEE     EEEEEE      E                     EEEE    EEEEEEE    E
          ....,....31.1.,....32.1.,....33.1.,....34.1.,....35.1.,....3
AA        TVTNPNAADATYGNTVYATVSQAATSKVALKVSGTPVTTALTTADANDKVAANDTTANGS
PROF_sec  EEE             EEEEEEEE   EEEEE      EEEEEE     EEEEE
PHD_sec   EEE             EEEEEEEE   EEEEE       EEEEE      EEEE
          ....,....37.1.,....38.1.,....39.1.,....40.1.,....41.1.,....4
AA        SVAGSTVYAAGTKLAQLTTDLTGEKGQVVTLTAIDTDLEDATFTGTTTYYSDLGKAYHYT
PROF_sec       EEEE                   EEEEEEEEE     EEEEEEEEEEE  EEEEEE
PHD_sec        EEEEE          E      EEEEEEEEE      EEEEEEEEEEE  EEEEEE
          ....,....43.1.,....44.1.,....45.1.,....46.1.,
AA        YTYNKDSAASSNASTQFGSNVTGTLTATLVMGKSTATANGTTWFN
PROF_sec  E          HHH          EEEEEEEEE  EEE     E
PHD_sec   EE             E     EEEEEEEEEE   EEE
```

Figure 2.13: Secondary Structure Prediction using PHD_sec and PROF_sec

Table 2: Results from PredictProtein: *Lactobacillus brevis* S-layer Protein

Secondary Structure Prediction			
Method, Type	Helix	Beta	Loop
PROF_sec, % in Protein	8.17	44.73	47.1
PHD_sec, % in Protein	5.38	44.52	50.11
Predicted Solvent Accessibility Composition			
Method, Type	Residues exposed with more than 16% of their surface		All other Residues
PROF_sec, % in Protein	55.27		44.73
PHD_sec, % in Protein	49.89		50.11

2.2.4 Reaction Conditions for Bioconjugation of S-layer Proteins: Table 1 and figures 2.1-2.5 lists some of the fluorescent probes conjugated to the S-layer protein. In each case the conjugation was carried out when the protein was in the multimeric assembled state. In this state, the larger multimers in the solid state are in dynamic equilibrium with the soluble monomeric or small multimeric forms of the protein. Fully disassembled or soluble forms of the protein exist only at high concentrations of LiCl or GHCl that are incompatible for bioconjugation reactions. This fact dictates the conjugation reactions be carried out only in the assembled form. An inherent advantage at this state is that reactive sites left exposed when the protein is in the assembled form will most likely lead to conjugates that retain the ability to self-assemble.

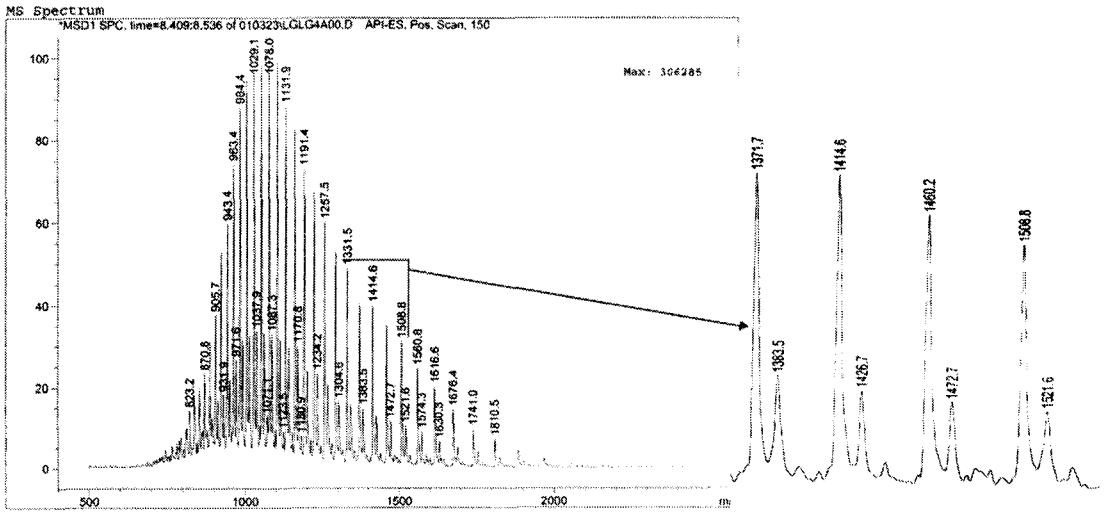

Figure 2.14: S-layer protein-fluorescein isothiocyanate conjugation -RpHPLC-MS

Since the S-layer protein from *Lactobacillus brevis* contains no cysteines but many primary amines, carboxylates and hydroxyls (over 30 each), there exists a challenge to limit multiple labeling when using standard coupling strategies. We have tackled the challenge by using primary amine-reactive N-hydroxy succinimide (NHS) esters as the coupling agent. This species reacts with deprotonated primary amine ($-NH_2$) groups on the protein, such as lysines or the N-terminus of the amino acid. Henderson-Hasselbach equation states that the logarithm of the ratio of protonated to unprotonated forms of a reactive group is the difference between the pKa and pH, i.e., $\log_{10}$ [HA]/[A-] = pKa - pH. In our experiments, we selectively label "only" the N-terminus by

lowering the pH to 6.5. At this pH, the ratio of protonated to unprotonated forms of the ε-amino group of the lysines is 10000 since its pKa is 10.53. Contrastingly, for the N-terminal amine whose pKa is ~8, the ratio is 30. Though the S-layer protein of *Lactobacillus brevis* contains 38 lysines, the ratios at this pH suggest that appreciable amounts of N-terminus α-amino group would remain deprotonated and reactive in comparison to the lysine ε-amino groups.

We investigated the reactivity of the S-layer protein amines at lower pH by employing a number of amine-reactive labels for bioconjugation, ranging from fluorescent probes to polymers. Fig. 2.14 shows mass spectrometric data obtained for fluorescein labeled S-layer protein. Yield of singly labeled S-layer protein was seen to be 33%, presumably at the N-terminus. In the case of Cy5 and BODIPY probes, it was seen that the S-layer protein had more than one attached probe. With Cy5, the bioconjugation reaction yields were respectively 35% and 23% of singly and doubly labeled proteins. In the case of BODIPY, reaction yields were respectively 18% and 14% of singly and doubly labeled proteins. In the more common conjugation set-up where multiple labeling is desired, repeated labeling cycles are carried out to increase the yield. However, in our case this strategy would give

unwanted higher levels of multiple sites labeling that could potentially affect self-assembly. All bioconjugation reactions including biotinylation and PEGylation are influenced by the protein concentration, concentration of reactant probe or tether, pH and the reaction time. Mass spectrometric analysis of series of biotinylation experiments supported the fact that higher biotin concentration (30 molar fold) or higher pH (7.5) or longer times (50 hrs) increases the extent of doubly labeled S-layer proteins. Nevertheless, only low levels of reactive NHS and isothiocyanate groups remained at these long reaction times due to hydrolysis.

Our results with PEG tethered S-layer proteins suggest that, these bioconjugation conditions may not hold for large molecular weight PEG molecules with hydrophobic end groups. In these cases, such as for the Fluorescein-PEG conjugates, the reactants themselves tend to aggregate and form micelles with a hydrophobic (fluorescein) core at higher concentrations. This hypothesis is supported by fig. 2.15 that shows the chromatograms of the PEGylation reactions. In this experiment, S-layer protein solution with concentrations greater than 5 mg/ml was reacted with 20 fold molar excess of PEG tethers. Conjugation reactions were carried out for 3 days in dark on ice with

Fluorescein-PEG_{2000}-NHS, Biotin-PEG_{3400}-NHS and Fluorescein-PEG_{5000}-NHS. The reaction was then stopped with 150 mM hydroxylamine. Subsequently, the reaction mixture was applied to Sephadex G-50 gel to remove excess probe. It can be seen from fig. 2.15 that better separation was achieved for Biotin-PEG tethers. This may be attributed to high concentrations of hydrophobic fluorescein. At these concentrations, Fluorescein-PEG_{2000}- and Fluorescein-PEG_{5000}-tethers might form large aggregates having molecular dimensions comparable to that of the S-layer protein. Thus, they may get eluted along with the proteins in the mobile phase. The third non-fluorescent peak does not possess any hydrophobic fluorescein and thus potentially does not form large aggregates and elutes last. Also, comparing the two fluorescein tethers, it was seen that better separation was achieved for the lower molecular weight PEG (data not shown).

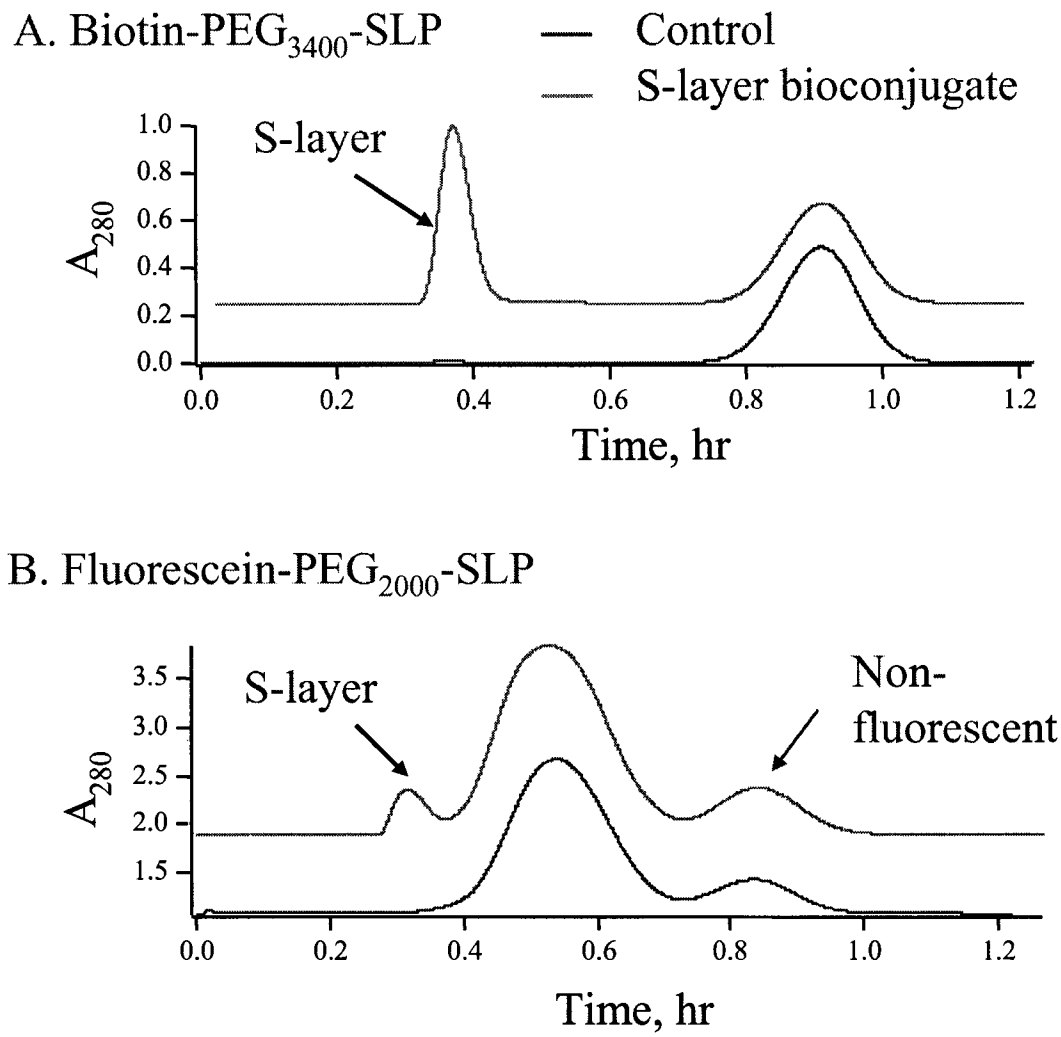

Figure 2.15: Purification of PEG-Tethered Bioconjugates of S-layer Protein

It was thus evident that, to push the conjugation reaction far right, higher pH and longer times but lower concentrations of PEG tethers would be preferred. Apparently, to achieve higher yield of N-terminus

labeled (singly labeled) protein, it was best to do the conjugation reactions with:

1. Assembled S-layer protein concentrations of > 5 mg/ml,
2. 20-fold and 10-fold molar excess reactant of respectively small molecule probes and PEG polymers,
3. 12-24 hour long reactions in dark at 4 C,
4. And at lower pH (6.5) in 50 mM sodium phosphate buffer

The yields of the PEG-tethered SLPs were established using SDS-PAGE and their densiotomograms; refer Fig. 2.10 and Table 3. The trace obtained from the vinyl sulfone-PEG_{3400}-SLP bioconjugate shows the unlabeled protein (first peak) and the two successively smaller area peaks from the bioconjugates. Straightforward peak fitting was done to calculate the yields from the Gaussian like peaks. In the case of the fluorescein-PEG_{2000}-SLP bioconjugate, the peak resulting from the conjugates is more complex due to the fact that the smaller polymer bioconjugate (45 mer vs. 77 mer for the vinyl sulfone-PEG) migrate differently in the gel.[108]

Table 3: Fluorescent Probes and Tethered Bioconjugate Yields

Reactant (<1 kDa) Fluorophores / Probes	Characteristics	Probe to Target Molar Ratio	Yield @ pH 6.5	
			Single Label	Double Label
Fluorescein isothiocyanate	Emission 518 nm (green)	20:1	29%	ND
BODIPY 558/568-succinimidyl ester	Emission 568 nm (red)	20:1	30%	16%
Cy5 succinimidyl ester	Emission 670 nm	20:1	18%	14%
Biotin-NHS	Ligand	20:1	37%	8%
Polymers (<5 kDa)				
Fluorescein-PEG_{2000}-NHS	Surface passivity, Emission 518 nm	10:1	39%	16%
Biotin-PEG_{3400}-NHS	Surface passivity /Ligand	10:1	24%	8%
Vinyl sulfone-PEG_{3400}-NHS	Surface passivity /R-SH coupling	10:1	34%	4%

2.2.5 Purification of Bioconjugate Modules: Table 3 shows different molecules that were conjugated to the S-layer protein and their yields. It can be seen that, yields of singly-labeled bioconjugates ranged 24–39%. Also in most cases, doubly labeled species were obtained, with yields ranging from 4–16%. These multiply-labeled bioconjugates, formed in substantial amounts can be used as bioconjugate modules if they do not affect self-assembly activity. Also, reaction conditions such as multimeric state S-layer protein reactant and low pH (6.5) would result in the presence of conjugated proteins surrounded by unlabeled

protein monomers. This provides an added purification obstacle to separate these bioconjugates.

A logical separation strategy would be to disassemble with 5 M LiCl and purify by size exclusion chromatography. However these high salt concentrations might impair the conjugated target protein or group. Also, we observed poly(ethylene glycol) conjugates precipitate or "salt out" at high LiCl concentrations. We have thus employed monomeric avidin affinity chromatography to achieve high purity S-layer protein bioconjugates. Here, the specific binding of biotin ligands to the protein avidin is exploited to bind the target biotinylated bioconjugate to the column via the formation of a high-affinity ligand-protein complex ($K_D \approx 10^{-15}$ M). The bond formation between avidin and biotin is very rapid and the strongest known noncovalent biological recognition between a protein and a ligand. [109, 110, 111] This bond is unaffected by most organic solvents, extreme pH and other denaturing conditions. But the bonds can be competed with free biotin in solution. We selected monomeric avidin support over tetrameric avidin since the conditions for retrieving the final product were milder and higher yields could be obtained. [112, 113] The working method is shown schematically in Fig. 2.7 and explained in section 2.1.10. It is important to note here that for ligands sensitive to 5

M LiCl, neutral buffer wash for prolonged times allowed disassembly of non-biotinylated conjugates. The assembled, unlabeled proteins in exchange with the soluble form were removed over longer elution times, leaving behind the biotinylated conjugates. In addition, conjugates formed from the PEG labels without biotin, ~20% of the activated PEG reactant, were also removed during this step. The amount of protein eluted can be adjusted by varying the amount loaded to the column and by changing the affinity support bead volume. This protocol thus provides a precise means of controlling the concentration of S-layer bioconjugates used for assembling surfaces in a modular fashion.

Fig. 2.16 shows the densiotomogram of lanes from the SDS-PAGE of Biotin-PEG_{3400}-SLP bioconjugate before and after affinity purification. Comparison of traces shows that there is a significant reduction of ~ 50% of unlabeled SLP after affinity purification. We also obtain higher yields of the multiply biotinylated S-layer proteins since they bind to the monomeric avidin support with higher efficiency. Using this method we envision incorporating parallel columns purifying different sets of bioconjugates and directly applying the purified bioconjugate module eluates for self-assembly experiments.

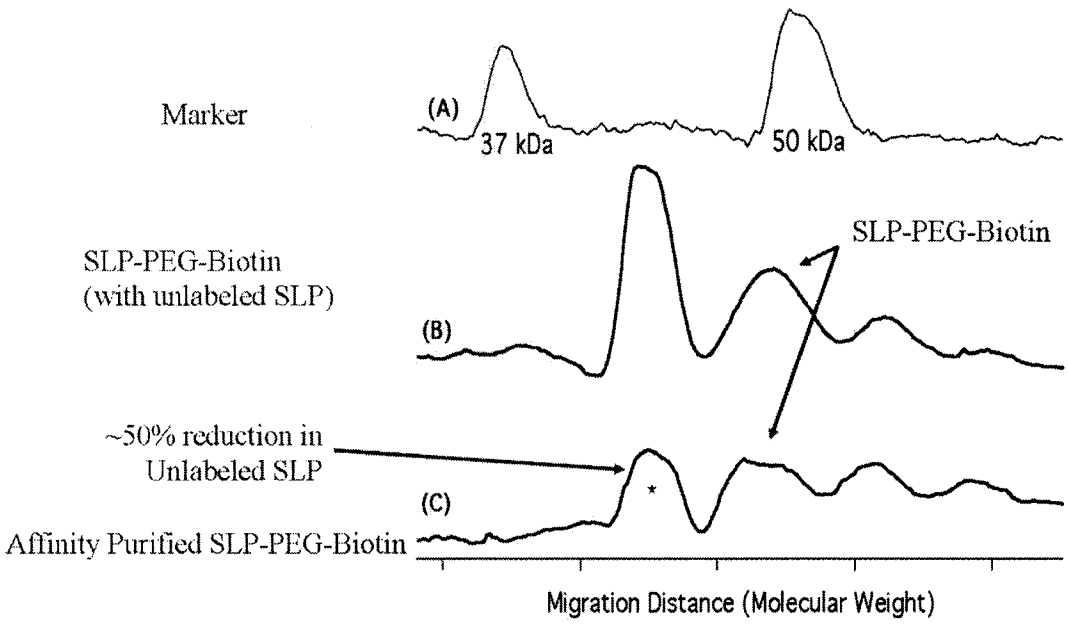

Figure 2.16: Monomeric Avidin Affinity Purified Biotinylated Bioconjugate Modules: Image Profiles of SDS-PAGE gels

2.2.6 Bioconjugation of Bioactive Ligands to S-layer Proteins: The selection of GFP as a ligand was mainly due to its wide applicability and its intrinsic fluorescence.[114, 115, 116] Besides, its molecular size is 28 kDa. This makes GFP a suitable endgroup for an efficiency test of the reaction scheme used for the conjugation of large bioactive ligands to S-layer proteins. As explained in section 2.1.9, we have employed vinyl sulfone-thiol chemistry to conjugate GFP to the S-layer protein. A protected thiol group is introduced with the help of the reactant SATA. Some of the key advantages of using SATA are:

1. The reaction conditions are mild, non-denaturing and specific to primary amines
2. A stable covalent amide linkage is formed from the reaction and the sulfydryl group introduced is protected; it can be stored for long periods of time without degrading the sulfydryl group
3. Deprotection to generate the sulfydryl group is accomplished by mild treatment with hydroxylamine

After forming GFP-SATA, the conjugate was subsequently biotinylated to help affinity purify the bioconjugate module using monomeric avidin affinity chromatography. We wanted to biotinylate one or more of the ε-amino groups of the lysines since we have already labeled the N-terminus with SATA. But the rate of hydrolysis of NHS, which is a competing reaction, is higher at higher pH. So, to compensate, we added excess of reactant (20 molar fold). Also, it helps in driving the reaction forward. But, multiple site biotinylation of GFP or other proteins like growth factors can impair protein function. Thus, we used a pH (8) not very high but more than neutral to successfully label the amino groups and at the same time preserve the protein function.

The yield of the Biotin-GFP-SS-SLP conjugate was expectedly very low due to multiple conjugation steps. Besides, we have used only

minimal quantities (600 µg) of the expensive starting material (1 µg of GFP costs ~$1). Thus our product seemed to be under detectable limits with SDS-PAGE. Although, self-assembly experiments on polymer microspheres showed green fluorescence, we were not able to thrust aside the possibilities of non-specific adsorption of unlabeled GFP.

S-layer protein bioconjugate modules were also made with Zn Protoporphyrin-IX reconstituted sperm whale myoglobin. Myoglobin was used since it was much cheaper as compared to GFP. Thus we would not be limited by the amount of reactant unlike the GFP reaction scheme. Moreover, Zinc Protoporphyrin-IX reconstituted myoglobin absorbs strongly at 462 nm and emits green fluorescence. Reconstitution procedure was followed from work done by previously published procedures.[117] Heme was extracted from the ferric sperm whale myoglobin by first dissolving in 0.01 M HCl (pH 2) at 0 ^{o}C and then mixing with Butanone. The aqueous apoprotein solution was then dialyzed against d. H2O and 50 mM sodium borate buffer (pH 9.2). Zinc protoporphyin-IX dissolved in 0.1 M KOH was then added to the dialyzed solution. The reaction mixture was subsequently centrifuged and purified by gel filtration on Sephadex G-50. Reconstituted myoglobin absorbed strongly at 426 nm but the presence of unreacted

myoglobin masked its presence (data not shown). The reconstituted protein was thus purified further using ultrafiltration procedures and then conjugated to the S-layer protein using the same steps as described in section 2.1.9. The experiments turned out inconclusive due to low yields of multiple reaction steps.

NHS-mediated conjugation reactions were also performed with 1.4 nm size Nanogold® particles (Nanoprobes, Inc., Yaphank, NY). However special considerations were needed for direct viewing of Nanogold® in the EM. 100,000 X magnification with 10 X binoculars were needed for a final magnification of 1,000,000 X. The emission was needed to be full with condenser settings for maximum illumination. The alignment of the microscope also needed to give 0.3 nm resolution. Unfortunately, these high resolution demands were too taxing on our sample and the electron microscope.

Chapter 3: S-LAYER PROTEIN SELF-ASSEMBLY EXPERIMENTS

The previous chapter outlined the *modus operandi* for obtaining pure form of protein and protein bioconjugates for self-assembly studies. This chapter explains the procedures, results and observations of the self-assembly experiments. Experiments were conducted on various substrates, viz., plain glass slides, cation-doped glass slides, copper grids, liposomes, polymer microspheres, silicon chips and crystals. Different microscopic and spectroscopic techniques were used to characterize these self-assembled monolayers. They were namely, confocal microscopy, scanning electron microscopy, transmission electron microscopy with negative staining, FTIR, Total Internal Reflectance Fluorescence (TIRF) and Fluorescence Spectroscopy.

3.1 Materials and Methods

3.1.1 Modular Self-Assembly on Positively Charged Glass Slides: Two sets of fluorescent labeled S-layer protein modules were used in this

experiment. BODIPY-labeled (BODIPY-SLP) and Oregon green labeled (OG-SLP) S-layer protein modules were first spun down at 14000 x g for 30 min. 50 µl of self-assembly suspension consisting of 0:100, 30:70, 50:50, 70:30 and 100:0 (V:V) of OG-SLP:BODIPY-SLP were prepared from the clear supernatant. The suspensions were placed onto sets of pre-cleaned, positively charged glass slides (Erie Scientific Company). The slides were incubated in dark for 30 min and then washed gently with d. H_2O. The adsorbed protein was fixed with 70% glycerol and viewed under a Nikon TE 200 inverted microscope.

3.1.2 Self-Assembly Experiments on Polymer Microspheres: Assembly experiments on polymer microspheres were performed with combinations of Fluorescein-PEG_{2000}-conjugated S-layer protein (Fluorescein-PEG_{2000}-SLP) and Biotin-PEG_{2000}-conjugated S-layer protein (Biotin-PEG_{3400}-SLP). A solution containing 250 µl each of disassembled Fluorescein-PEG_{2000}-SLP and Biotin-PEG_{3400}-SLP were mixed together at different concentrations and spun down at 14000 x g for 20 min. The self-assembly suspension was added to sets of microcentrifuge tubes containing few microliters of 6 µm NH_2-terminated polystyrene microspheres (Polysciences, Inc. Warrington, PA)

microspheres. The tubes were incubated for 30 min at room temperature in dark. After 30 min, the microspheres were centrifuged for 5 min at 100 x g to induce settling. The suspension was decanted and washed thrice with water by refilling, sedimentation and decanting procedures. After the washes, the adsorbed protein was cross-linked with 200 µl of 10 mM amine-reactive homobifunctional Bis(sulfo succinimidyl) suberate (BS^3, NHS-O_2C-$(CH_2)_6$-CO_2-NHS, 572.43 MW, 11.4 Å, Pierce) in 50 mM sodium phosphate at pH 8 buffer. The tubes were incubated at room temperature in dark for 30 min. Subsequently the reaction was quenched with 150 mM hydroxylamine and was given similar washes with d. H_2O. To test the ligand display of S-layer protein conjugates that are assembled on the microspheres, red fluorescent (488/605) NeutrAvidin® coated TransFluoSpheres® 100 nm polystyrene nanospheres (Molecular Probes) were used. The fluorescent nanospheres were first sonicated for 5 min in Block Aid solution (Molecular Probes) to minimize non-specific adsorption of proteins. The tubes with protein adsorbed microspheres were injected with 50 µl of the nanospheres and incubated for 30 min in dark at room temperature. Subsequently, the solutions were given a thorough wash with d. H_2O water.

3.1.3 Confocal Microscopy: Samples were viewed under a Leica TCS-SP four channel confocal microscope at the Mt. Sinai School of Medicine, using excitation at 488 nm for fluorescein and 568 nm for the TransFluoSpheres® fluorescent nanospheres. The transmitted light channel was used to position the imaging plane at the center of the microsphere. For examining samples on silicon chips, the chips were first mounted on glass slides using double sided Scotch tapes. The side having the protein layers was kept facing outward. One drop (~25 µl) of VectaShield mounting medium was added to all the chips and cover slips were placed. The ends of the cover slip were sealed with one-sided Scotch tape or nail polish. The specimens were then examined under the confocal microscope.

3.1.4 Scanning Electron Microscopy (SEM) of Polymer Microspheres: Samples for scanning electron microscopy were dried, sputter-coated with gold, and observed with a JEOL 35 scanning electron microscope at the Mt. Sinai School of Medicine. Image analysis, including fluorescence emission intensity profiling, was accomplished with IgorPro 4.0 and NIH Image 1.63.

3.1.5 Self-Assembly Experiments on Silicon Chips and Silicon Crystals and Fourier Transform Infrared (FT-IR) Spectroscopy: Silicon chips and crystals were cleaned by first sonicating for 30 min in a solution of conc. Sulfuric acid and Nochromix powder (Godax Laboratories, Inc., Takoma Park, MD). The acid was discarded and rinsed thoroughly with d. H2O. The substrates (chips/crystals) were subsequently sonicated in d. H2O for 30 min and stored in fresh d. H2O. With the crystals, the substrates were first cleaned in Plasma Cleaner/Sterilizer PDC-32G (Harrick Scientific Corporation, Ossining, NY) prior to acid cleaning. The cleaned chips and crystals were then coated with either 3-aminopropyltrimethoxysilane (APS) or p-aminophenyltrimethoxysilane (APhMS) SAMs. This was achieved by incubating the substrates in either 1 mM APS solution in toluene or 1 mM APhMS solution in chloroform for times ranging from 10 min, 1 hr to overnight. Subsequently the substrates were rinsed several times with the solvent (toluene or chloroform) and dried with nitrogen. Contact angles were measured at random at many points using NRL Contact Angle Goniometer (Rame-hart, Inc., Mountain Lakes, NJ) to verify extent of coating. Initially self-assembly experiments were carried out on these

surface modified NH_2-terminated substrates by just squirting the spun down S-layer protein suspensions and incubating overnight. Following which, the substrates were gently washed with d. H_2O, air-dried and viewed under Bio-Rad FTS 175 FT-IR Spectrometer equipped with a LN_2-cooled MCT (Mercury-Cadmium-Tellurium) detector. The spectrometer was first filled with liquid nitrogen in the coolant chamber. The substrates were then fitted in the appropriate holders for performing either surface reflection on the chips or Attenuated Total Reflectance (ATR) on the crystals. The IR beam was subsequently focused on the substrates by adjusting the mirrors for maximum signal. An interferogram was then recorded where the signal was measured as a function of the optical path difference between the fixed and the movable mirrors. From this interferogram the spectrum was calculated as a function of wavelength by applying a Fourier Transform algorithm.

For large-scale parallel self-assembly experiments on silicon chips, a Teflon trough 1x3x30 inch was machined with thirty 1 mm circular wells. The wells had volume of 300 µl with a slot on top to accommodate 8x15 mm chips. To start with, APhMS SAM coated chips were placed in the slots on the Teflon slab. 300 µl of the appropriate protein self-assembly solution filtered through a 0.2 µm syringe filter

was injected through the gap into the troughs on the Teflon slab. All solutions were centrifuged for 20 min at 14000 x g prior to injection into the troughs. The chips were incubated for 12 hrs or overnight at RT in a hydrated chamber. The self-assembly solution was subsequently slowly pipetted out and refilled with 300 µl of cross-linker solution (BS^3 in 50 mM sodium phosphate at pH 8). The cross-linking was carried out for 1 hr at RT and then was pippetted out. 300 µl of stop reagent, 150 mM hydroxylamine solution, pH 7 was then injected to quench the reaction. The stop reagent was then pipetted out after 15 min and the wells were injected with 300 µl d. H2O. The water was pipetted out and 300 µl of d. H_2O was injected for a second washing step. The chips were then injected with 300 µl of 40 nm Neutravidin labeled red (580/605 nm) nanosphere solution and incubated for 30 min at RT. Prior to injection; the nanospheres were sonicated for 5 min in "Block Aid" solution. The nanosphere solution was consequently replaced with d. H_2O and the chips were given 2 more washings. The chips were then air dried and viewed under confocal microscope and AFM.

3.1.6 Atomic Force Microscopy (AFM): A Nanoscope IIIa scanning probe microscope (Digital Instruments, Inc., Santa Barbara, CA) was

used for structural studies of self-assembled S-layer protein bioconjugate modules. The substrates were prepared by the procedure described in section 3.1.5 for large scale self-assembly experiments and mounted on metal discs using double-sided Scotch tape. The measurements were carried out in contact mode with oxide sharpened silicon nitride probes (NP-S, Veeco Instruments, Inc., Woodbury, NY) having 4 levers per probe. The nominal tip radius of curvature was 5-40nm and spring constants range from 0.58 to 0.06 N/m.

3.1.7 Fluorescent Labeling of Lipids and Preparation of Liposomes: Cationic liposomes were prepared by a procedure similar to that described by Mader and co-workers.[118] Phosphatidylcholine (PC) lipids (Avanti Polar Lipids) and other fluorescent lipids were dissolved separately in 8 ml vials with chloroform and evaporated to a dry film at room temperature under vacuum. Lyophilized lipids were stored at –20 C. To prepare fluorescent labeled liposomes, PC lipids, β-BODIPY-PC lipids (Molecular Probes) and NBD-PC lipids (Avanti Polar Lipids), Fig. 3.1-3.3, were first dissolved separately in chloroform and mixed together such that the molar ratio of PC lipids to fluorescent labeled PC lipids was maintained at 400:1. They were then desiccated under

vacuum in dark for 1 hour to form a dry film. The lipid was subsequently re-hydrated using a buffer that consisted of 50 mM Sodium Chloride and 100 mM Tris adjusted to pH 7. Unilamellar vesicles were prepared by extrusion through a polycarbonate membrane (Millipore) of 1 μm size using a mini-extruder (Avanti Polar Lipids). Experiments were then conducted in cuvettes to investigate the assembly process of S-layer proteins onto the liposomes.

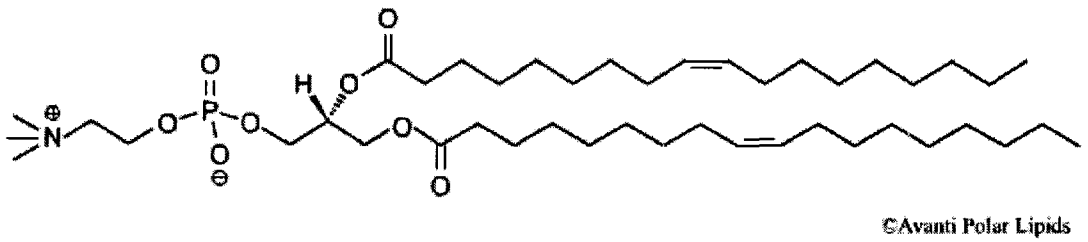

Figure 3.1: PC: 1, 2-Dioleoyl-sn-Glycero-3-Phosphocholine, MW: 786.13

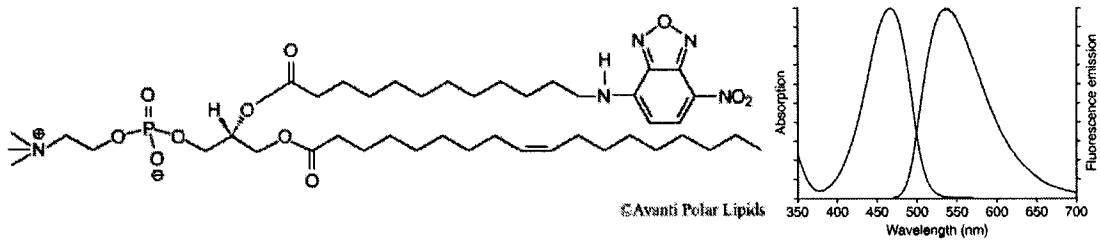

Figure 3.2: NBD PC: 1-Oleoyl-2-[12-[(7-nitro-2-1,3-benzoxadiazol-4-yl)amino]dodecanoyl]-sn-Glycero-3-Phosphocholine

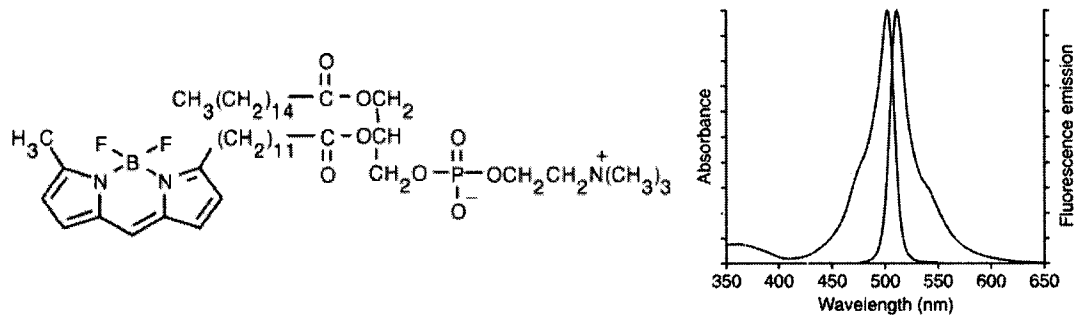

Figure 3.3: β-BODIPY: 2-(4,4-difluoro-5-methyl-4-bora-3a,4a-diaza-s-indacene- 3-dodecanoyl)-1-hexadecanoyl-sn-glycero-3-phosphocholine

3.1.8 Total Internal Reflectance Fluorescence (TIRF) Measurements:

We first tested our cell with simple fluorescent labeled slides. For this purpose, microscopic slides coated with aminoalkylsilane (Sigma) were incubated with 0.5 ml of fluorescent dye solutions in dark for 30 min. The slides were thoroughly washed and then examined on an inverted microscope. Pulsed dye laser beam deflected through a dove prism was incident on the back of the glass slide. The objective was focused through the liquid reservoir on to the surface of the glass slide. Further,

similar to the experiments performed on microspheres; self-assembling suspension modules of Fluorescein-PEG_{2000}-SLP and Biotin-PEG_{3400}-SLP were also used. The suspension was injected into the reservoir underneath a positively charged surface slide and incubated for half hour. The self-assembling suspension was then replaced with solution of red fluorescent neutravidin labeled nanospheres. After a step of washing with d. H_2O, TRES was recorded.

3.2 Results and Discussions

3.2.1 Modular self-assembly on positively charged glass slides: The Nikon TE 200 inverted microscope employs an epi-illuminating system where, the exciting light (mercury lamp or dye laser), on its way to the specimen, is reflected into the back aperture of the microscope objective by a dichromatic beam-splitting (dichroic) mirror. The objective first serves as a condenser and then captures the light emitted by the fluorescently labeled protein adsorbed on the surface. The captured light passes thorough the dichroic mirror to the eyepiece or camera. The mirror is designed to transmit only light of longer wavelengths, typically the emission light (exciting light is of higher energy and shorter wavelengths). Epi-fluorescence micrographs, fig. 3.4, were taken using

a Nikon Coolpix 990 digital camera. The pictures, showing a featureless colorful surface, depict the evenly inter-dispersed homogeneous monolayers of self-assembled S-layer proteins of the same glass slide (50:50 suspensions) with different emission filters. The micrographs, demonstrate the fact that N-terminus labeled S-layer proteins, irrespective of their attached probes, self-assemble in a modular fashion. For further proof of the concept, time-resolved emission spectra (TRES) were taken for sets of glass slides at different excitation wavelengths. Shown in fig. 3.5 are the fluorescence emission spectra of samples assembled (on cation-doped glass slides) with two different starting concentrations of Oregon green-S-layer and BODIPY-S-Layer bioconjugates (50:50 and 25:75 V:V ratios). The spectra were obtained at two excitation wavelengths, 460 nm (Oregon green) and 550 nm (BODIPY). Although the spectra were not corrected for differences in quantum yields, lifetime differences or other effects, we still see a trend

where the module concentration on the monolayer surface is dependent

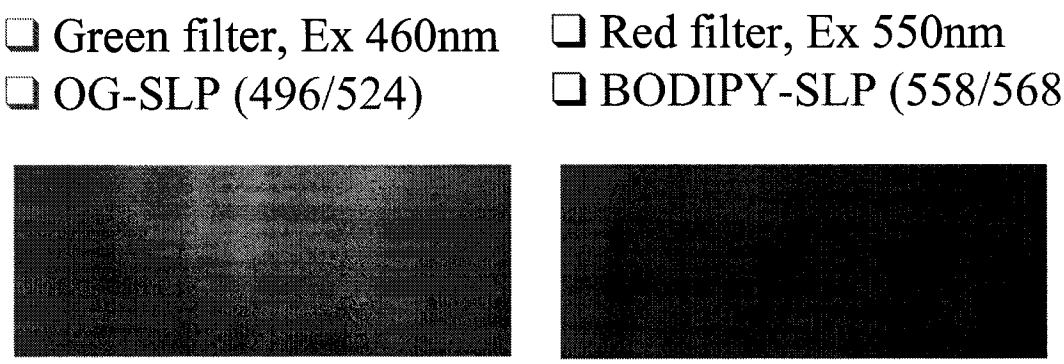

Figure 3.4: Modular Self-Assembly on Positively Charged Glass Slides: Epi-Fluorescence Micrographs of Mixed S-layer Protein Conjugates

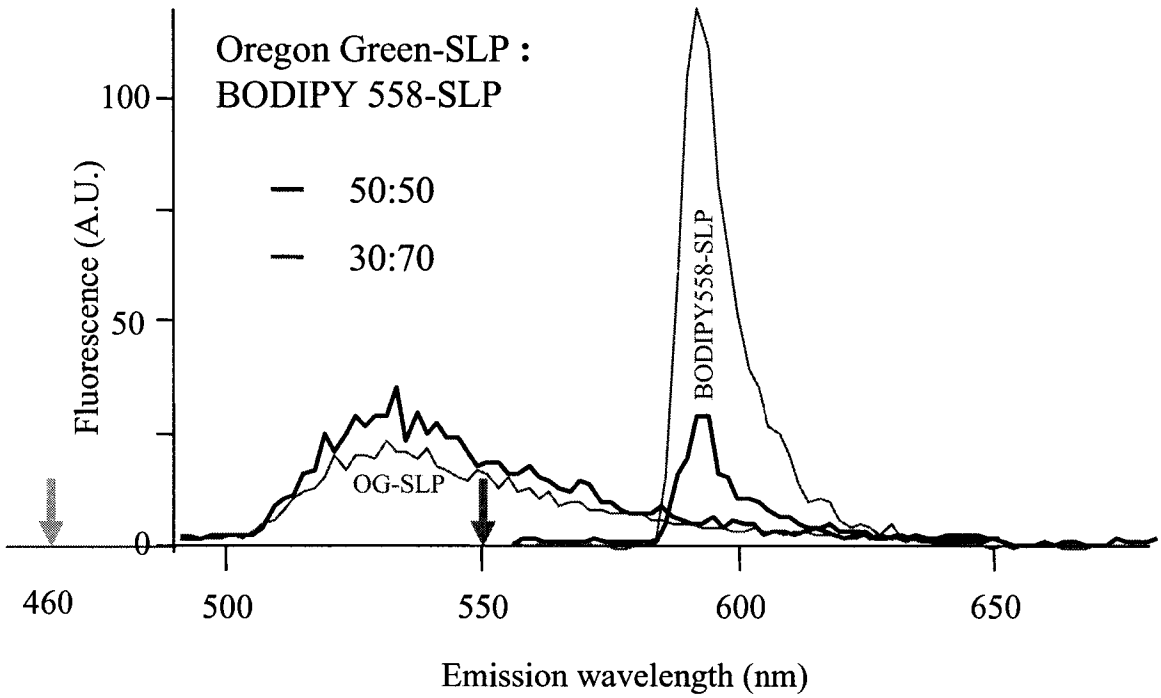

Figure 3.5: Modular Self-Assembly on Positively Charged Glass Slides: Time Resolved Emission Spectra of OG-SLP and BODIPY558-SLP conjugates

on the starting module concentration. We have found that when the assembly was performed properly, the emission intensity was uniform, as expected from a monolayer (as shown). To compare results from other assembled monolayers, we self-assembled tetramethyl rhodamine molecules onto aminoalkylsilane-coated glass slides and measured emission intensities (data not shown). The fluorescence intensities at various positions were comparable to the emission intensities obtained from the S-layer protein conjugates.

3.2.2 Bioconjugate Modules Assembled onto Polymer Microspheres: We have conducted assembly experiments using 6 μm amine-terminated polystyrene microspheres as the assembly substrate. Fig. 3.6A displays a confocal image of the S-layer-PEG_{2000}-Fluorescein bioconjugate assembled onto one of these microspheres, taken as 2D XY slice through the center. The light area exhibited symmetrically around the particle in the converted grayscale image corresponds to the emission of green fluorescence (518 nm). Fig. 3.6B shows the fluorescence emission intensity profile taken through the center of the image. The profile underscores the annular distribution of fluorescence intensity at the microsphere surface arising from the assembled

conjugate. Also, fluorescence intensity profiles obtained from other angles relative to horizontal gave similar results. Within the resolution of this image, it is directly evident that the fluorescence was emitted evenly over the microsphere surface. It is important to note here that excess NHS-PEG_{2000}-Fluorescein used for the conjugation reaction was removed by gel filtration before using the S-layer-PEG_{2000}-Fluorescein conjugate for self-assembly experiments. Moreover, the highly hydrophilic PEG polymer retards any non-specific adsorption of free PEG_{2000}-Fluorescein onto the microsphere surface. This confocal image is consistent with complete coverage of the microsphere surface with a layer of S-layer proteins and S-layer-PEG_{2000}-Fluorescein bioconjugates.

To examine surface display capabilities of our S-layer bioconjugates we have employed Biotin-PEG_{3400} tethered S-layer protein that were detected using 100 nm Neutravidin coated fluorescent spheres (nanospheres). These nanospheres selectively bind to the modularly assembled biotins that are displayed at the surface. Fig. 3.7 shows the results obtained from the self-assembly of avidin-affinity purified S-layer-PEG_{3400}-Biotin conjugates onto the microspheres. Fig. 3.8A was obtained from the average of confocal images taken as 2D

slices in the XY plane, detecting the red fluorescence emission of the nanospheres. This can be seen as dots in grayscale. This image presents the localization of 100 nm nanospheres over the surface of 6 μm microsphere. Since the nanospheres appear evenly distributed, it is evident that the PEGylated and unlabeled S-layer proteins are not phase separated (i.e., not assembled in separate domains). Fig. 3.7B shows the image line profile taken through a section of the image as indicated. The peaks correspond to the fluorescent nanospheres.

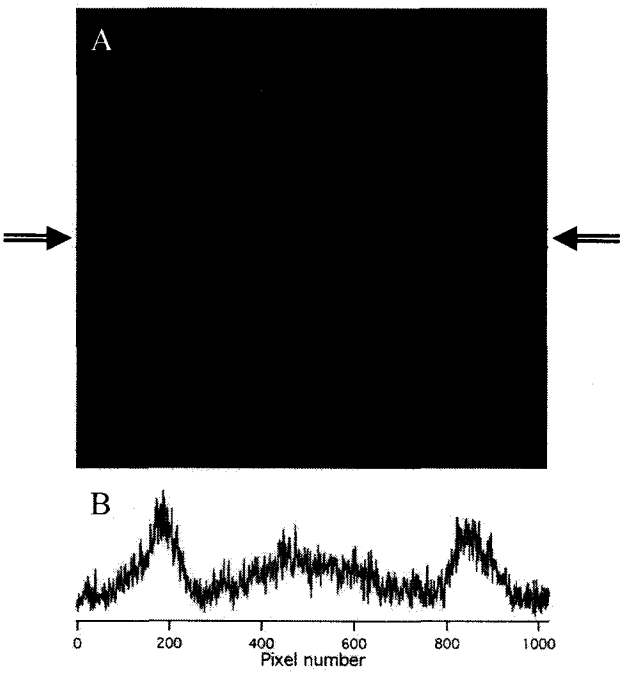

Figure 3.6: Image of S-layer-PEG_{2000}-Fluorescein bioconjugates Assembled onto Microspheres

Fig. 3.6A: Confocal Image; Fig. 3.6B: Fluorescence emission intensity profile taken through the center of the image

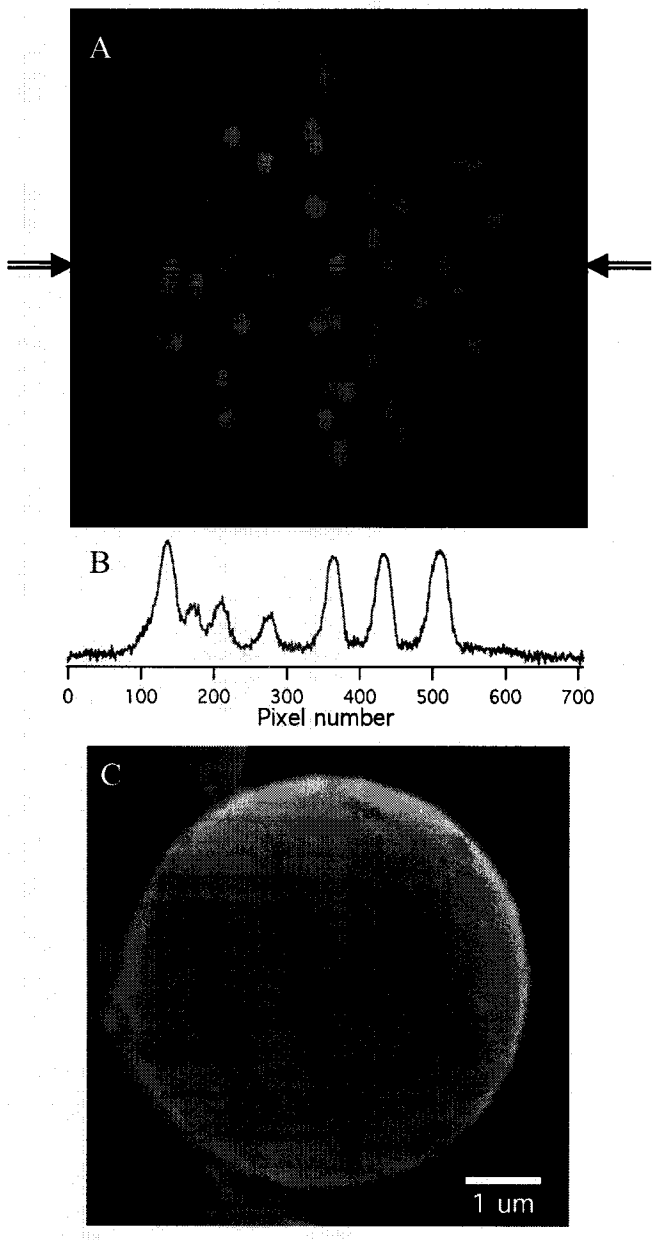

Figure 3.7: Images of Self-Assembled Affinity Purified S-layer-PEG_{3400}-Biotin Conjugates onto Microspheres

Fig. 3.7A: Average as 2D slices in the XY plane, detecting the red fluorescence emission of the nanospheres. This can be seen as dots in grayscale. Fig. 3.7B: Image

line profile taken through a section of the image as indicated. Fig. 3.7C: SEM image of microspheres with self-assembled avidin-affinity purified S-layer-PEG_{3400}-Biotin

Also, no peak in fluorescence emission intensity is seen at the microsphere edges. Often, in epi-fluorescence images emitted light of these highly fluorescent nanospheres scatters and produces additional intensity peaks. In fact, this was also absent. To further study the surface features of microspheres with assembled Biotin-PEG_{3400}-S-layer bioconjugates, scanning electron micrographs (SEM) were obtained from the same samples. The microspheres were first sputter-coated with a thin layer of gold atoms prior to examination. Fig. 3.7C shows the SEM image of microspheres with self-assembled avidin-affinity purified S-layer-PEG_{3400}-Biotin. Faint yet clear bump-like features arising from the nanospheres bound to surface-displayed biotin was seen over the predominantly smooth microsphere surface. At this resolution (>50 nm) it appeared that the microspheres were completely covered with an even monolayer of assembled S-layer bioconjugates with no evidence for multiple layers.

Next, we performed modular self-assembly of S-layer-PEG_{3400}-Biotin and S-layer-PEG_{2000}-Fluorescein conjugates onto these microspheres. Fig. 3.8A shows a converted grayscale confocal

microscopy image that was averaged from multiple 2D confocal XY planes. It shows both the green (fluorescein) and red (nanosphere) fluorescence emissions. The gray dots correspond to the nanospheres while the background fluorescence intensity distributed around the rim of the microsphere relates to the fluorescein conjugates. This was emphasized by the emission intensity profile, fig. 3.8B showing features from the nanosphere as sharp peaks bounded by smaller peaks on each side at the edge of the microsphere. In contrast to Fig 3.6B, as this image was an average over multiple 2D confocal slices over the whole microsphere, the fluorescein emission intensity line profile was also substantial in the middle of the microsphere. It was apparent from the inspection of fig. 3.8 that the modular self-assembly resulted in homogeneous coverage of three-dimensional polystyrene microspheres. Also, no evidence of phase separation was seen. The attachment of nanospheres to the biotin sites, suggest that the ligands are displayed properly irrespective of the difference in tether lengths of the two conjugates. Furthermore, the sparse coverage may have occurred due to this difference in tether lengths (77 mer PEG in S-layer-PEG_{3400}-Biotin vs. 45 mer PEG in S-layer-PEG_{2000}-Fluorescein). Differences in tether lengths (proportional to Flory radius, $R_F=3.5*N^{0.6}$,

where N is the number of monomer units) introduce differences in module sizes. The Flory radius of the 77 mer and 45 mer tethers are respectively 4.75 nm and 3.5 nm. [119, 120] This affects their diffusion rates in solution and consequently the assembly kinetics of the modules, i.e., smaller modules (S-layer-PEG_{2000}-Fluorescein) might assemble faster. Studies involving other disparate endgroups are in progress. Also, in contrast to monolayers obtained using dissimilar lengths of thiolated endgroups on gold,[78, 79] no phase separation was observed. Clearly, affinity purification of all S-layer protein bioconjugates has to be performed when we desire an ideal surface without sparse coverage. The data presented above confirms the ability of our method to produce homogeneous mixed SAMs on surfaces using modular self-assembly approach with no phase separation.

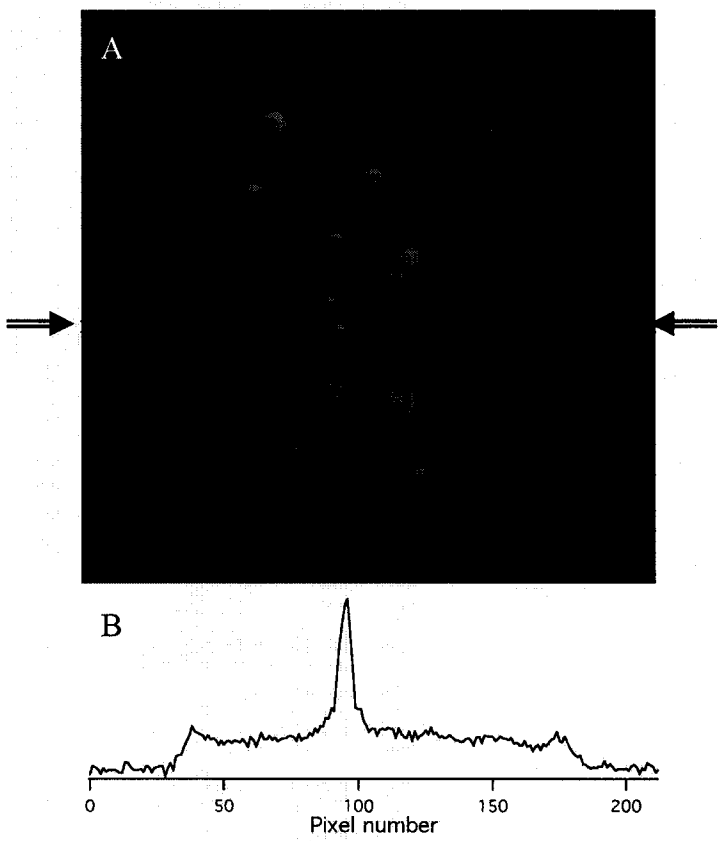

Figure 3.8: Modular Self-Assembly of S-layer-PEG_{3400}-Biotin and S-layer-PEG_{2000}-Fluorescein conjugates onto Microspheres.

Fig. 3.8A Converted grayscale confocal microscopy image that was averaged from multiple 2D confocal XY planes. The gray dots correspond to the nanospheres while the background fluorescence intensity distributed around the rim of the microsphere relates to the fluorescein conjugates. Fig. 3.8B is the emission intensity profile showing features from the nanosphere as sharp peaks bounded by smaller peaks on each side at the edge of the microsphere

Further, we wanted to investigate the relationship between starting conjugate concentration (bulk concentration) and surface conjugate display (surface concentration) by varying the self-assembly conditions. This was achieved by conducting self-assembly experiments with different ratios of S-layer-PEG_{3400}-Biotin and S-layer-PEG_{2000}-Fluorescein bioconjugate modules in the bulk. The difference in surface displays was established by determining the average number of nanospheres bound per microsphere using epi-fluorescence microscopy. Fig. 3.9 shows comparative results of average surface coverage obtained from seven samples. In each sample set, 20 microspheres were examined to obtain the average. In the controls that did not contain biotin (Lane 1-3), nonspecific adsorption of nanospheres was observed at low levels. Specifically for the S-Layer-PEG_{2000}-Fluorescein sample (Lane 3), the PEG endgroup gave rise to significant suppression of this non-specific adsorption of nanospheres. Moreover, from lanes 3 to 7, it was observed that increasing the ratio of starting S-layer-PEG_{3400}-Biotin to S-layer-PEG_{2000}-Fluorescein bioconjugate modules translated to an increasing trend in the number of surface nanospheres. This was due to the formation of greater number of

avidin-biotin complexes by the nanospheres with increase in the amount of displayed biotin.

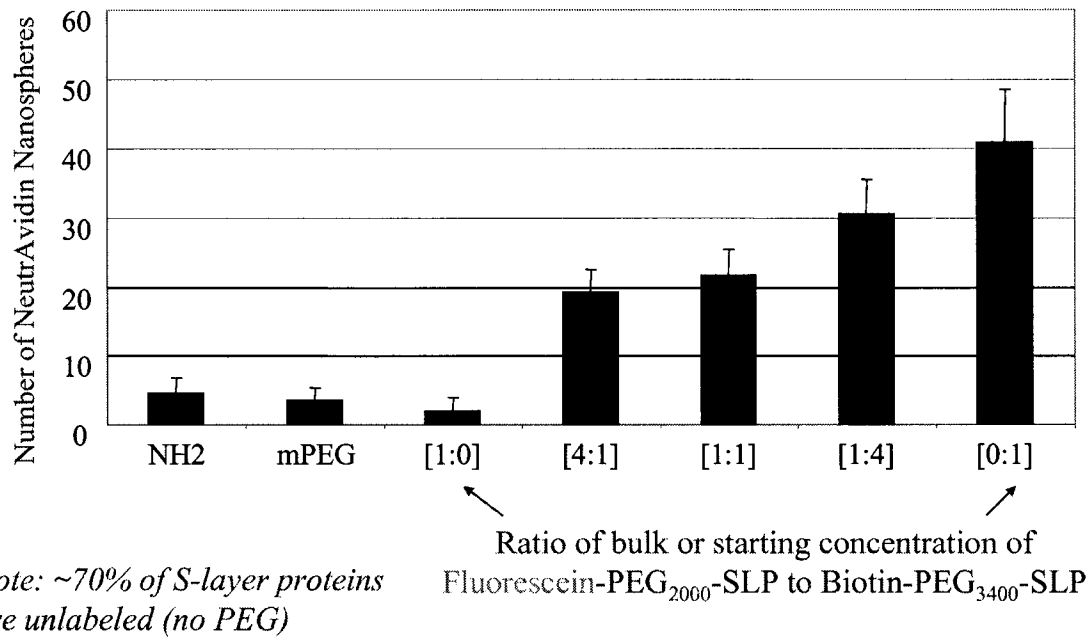

Figure 3.9: Surface Display of Bioconjugates Based on Starting (Bulk) Module Concentrations of S-layer-PEG_{3400}-Biotin and S-layer-PEG_{2000}-Fluorescein

In these samples, the levels of nanosphere coverage obtained from S-layer-PEG_{3400}-Biotin conjugates were approximately only 1-5% of total coverage based on surface geometry arguments. This was probably due the presence of unlabeled S-layer protein monomers. Since these monomers were present at appreciably higher concentrations, they would tend to dominate the assembly process. Furthermore, due to their smaller size they might potentially have faster

assembly kinetics than the larger polymer conjugates. We are currently conducting the assembly experiments using high purity S-layer bioconjugates to investigate these kinetic effects and fully exploit our methodology. However, from the above observations, an important trend is apparent; the surface density of displayed biotin can be manipulated by changing the starting concentration of S-layer-PEG_{3400}-Biotin conjugates. The implication of this trend is that, we could dictate the amount of ligand (Biotin) displayed by tailoring the initial starting module (S-layer-PEG_{3400}-Biotin) concentration. The ligand or endgroup can be varied in size due to the larger molecular carrier or headgroup size (S-layer protein). The functionality of the ligand (adhesion peptides to growth factors) could also be varied. Mixtures of known concentrations of these S-layer headgroup tethered ligands could also be self-assembled to form uniform bioactive surfaces with a controlled display of endgroups. We could thus direct the composition and functionality of the surfaces. This technique thus offers a new route for the formation of surfaces that contain homogeneous displays of mixtures of molecular functionalities (adhesion peptides and growth factors).

3.2.3 Self-Assembly on Silicon Supports: Fourier Transform Infrared Spectroscopy (FTIR) characterization of protein structure has been performed in both aqueous and non-aqueous environments.[121] FTIR techniques can also be used for more detailed studies of the molecular composition of the assembled surfaces. We could quantify the monolayers at the molecular level since the peaks are an added sum of individual groups. In our case, we perform FTIR on air-dried protein samples assembled onto silicon chips for detailed studies of their molecular composition. We used both external reflection and Attenuated Total Reflectance (ATR) techniques for examining our samples. With the ATR technique, the infrared beam samples the surface by internal reflection of the light. The infrared light penetrates the surface via the evanescent field and samples the molecule of interest on the surface. Higher spectral resolution and higher intensity gains are achievable with this technique. But we preferred the external reflection mode since its detection range was wider.

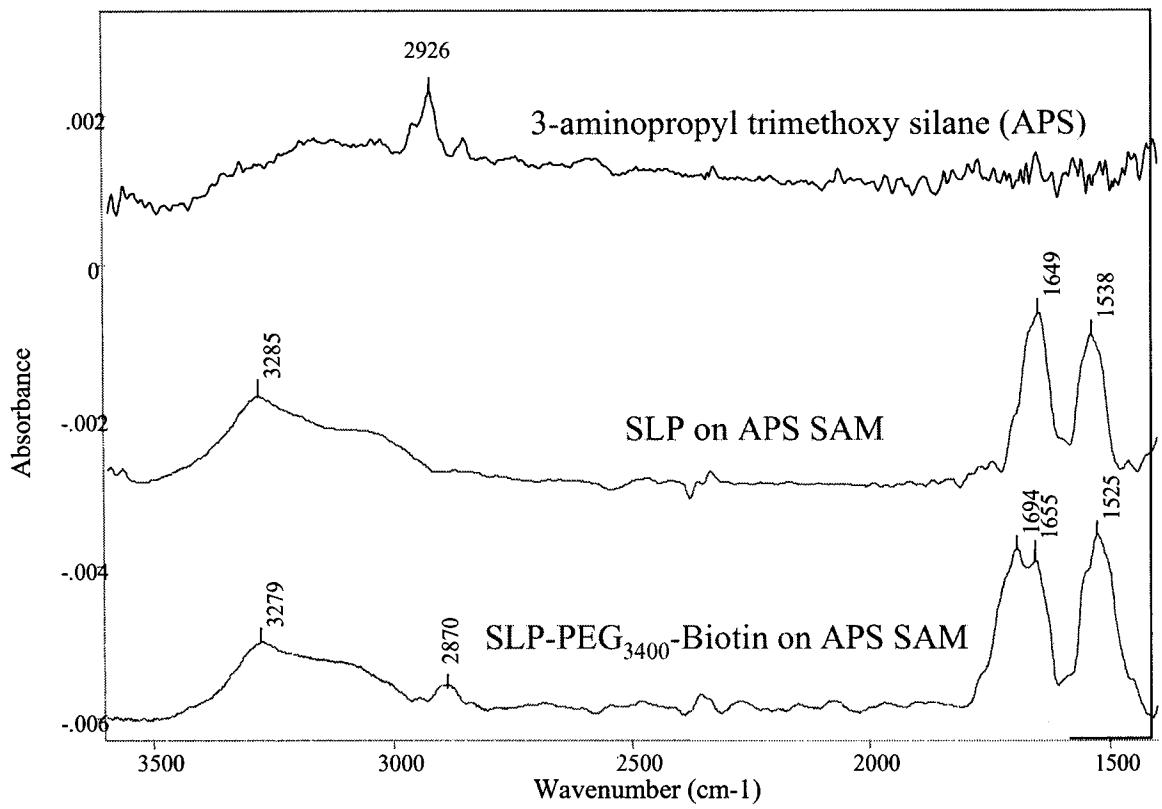

Figure 3.10: FT-IR Spectra of Self-Assembled Monolayers of S-layer Protein and S-layer Protein Conjugates on APS coated Silicon Chips (External Reflection)

The FTIR data in fig. 3.10 shows external reflection spectra of the control, APS coated silicon chips and samples, S-layer protein and S-layer-PEG_{3400}-Biotin conjugates on APS coated chips. The band at 2926 cm^{-1} corresponds to the CH_2 vibrations of APS. The other spectra were obtained with this chip as reference. In both the S-layer spectra, characteristic solid state bands of alpha amino acids can be seen at 3390-3260 cm^{-1} (NH) and 1565-1508 cm^{-1} (CNH). Absorption of amides

in the protein at 1695-1630 cm^{-1} due to their C=O stretching can also be seen. The symmetric stretching band of OCH_2 of the PEG in the third sample can be seen at 2870 cm^{-1}. Strong CH_2-O-CH_2 bands of PEG at 1140-1085 cm^{-1} were not viewed due to our detection range. More experiments are needed to be performed to obtain detailed signatures of the S-layer protein and their conjugates.

AFM has been used by many researchers to obtain high resolution images of biological samples and their surface topology. [122, 123, 124, 125] Engel's group has used AFM for conformational changes of the HPI layer of *Deinococcus radiodurans*.[126, 127] Sleytr and coworkers have recently used AFM to image self-assembly and recrystallization of S-layers of *Bacillus sphaericus* in real time on silicon supports.[128] A brief description of the instrumentation and operation of the AFM is given in section 5.4. In our work, we have used AFM in contact mode to image air-dried, cross-linked, S-layer protein conjugates self-assembled onto silane modified silicon supports. The topographical and friction AFM images, fig. 3.11, indicated silicon chips covered with homogeneous layers of the combination of S-layer-PEG_{3400}-Biotin and S-layer-PEG_{2000}-Fluorescein conjugates. The displayed biotin in this case was detected with 40 nm nanospheres that can be seen clearly in

the image. The radius of curvature of the tip was 5-40 nm as specified by the manufacturer. This surely limits our spatial resolution. More experiments are in progress to study the crystalline underlying nanostructure in other modes.

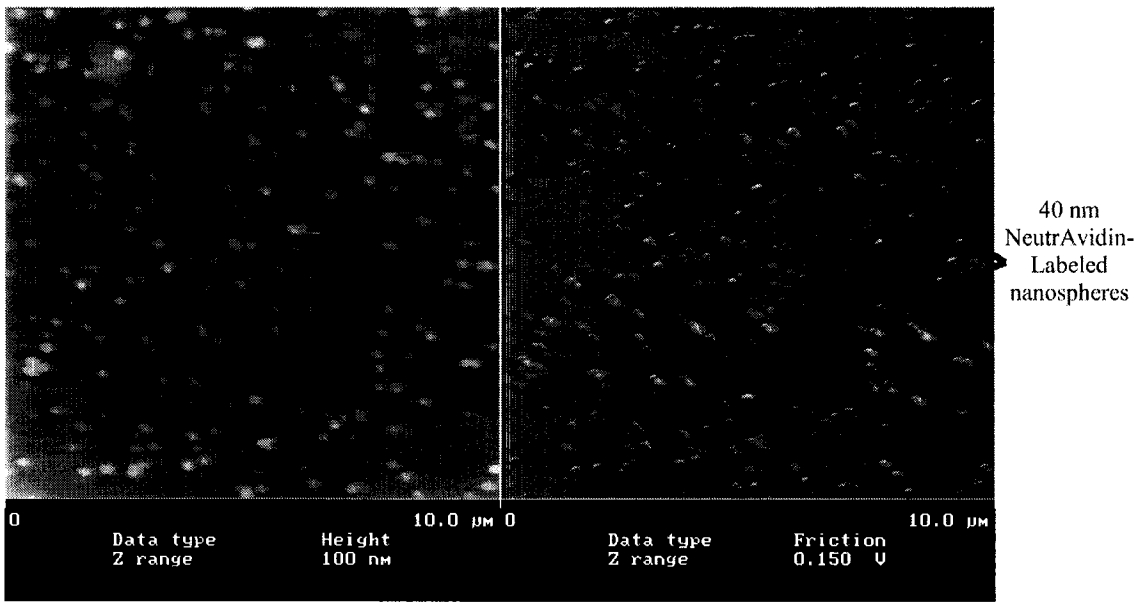

Figure 3.11: AFM Images of Self-Assembled S-layer-PEG_{3400}-Biotin and S-layer-PEG_{2000}-Fluorescein conjugates onto APhMS coated Silicon chips

Confocal microscopy studies on silicon chips with mixed monolayers of S-layer-PEG_{3400}-Biotin, S-layer-PEG_{2000}-Fluorescein and S-layer-Cy5 conjugates were conducted on Zeiss LSM 510 META instrument. The images as shown in fig. 3.12 revealed uniform homogeneous layers of all 3 components. The same homogeneity was observed all over the chips. It is worthy of noting here that modules with disparate lengths of PEG (77mer, 45mer and no PEG) were used for self-assembly. In a

related study pertaining to phase behavior of mixed alkanethiol SAMs on Au(111), it was observed that a chain length difference of 3 atoms led to phase separation.[129] In contrast, S-layer protein monomers attached to a variety of sizes of ligands self-assemble without any visible phase separation. This critical result provides a proof for possibility of obtaining uniform layers of multiple S-layer conjugate modules when coupled with various bioactive ligands.

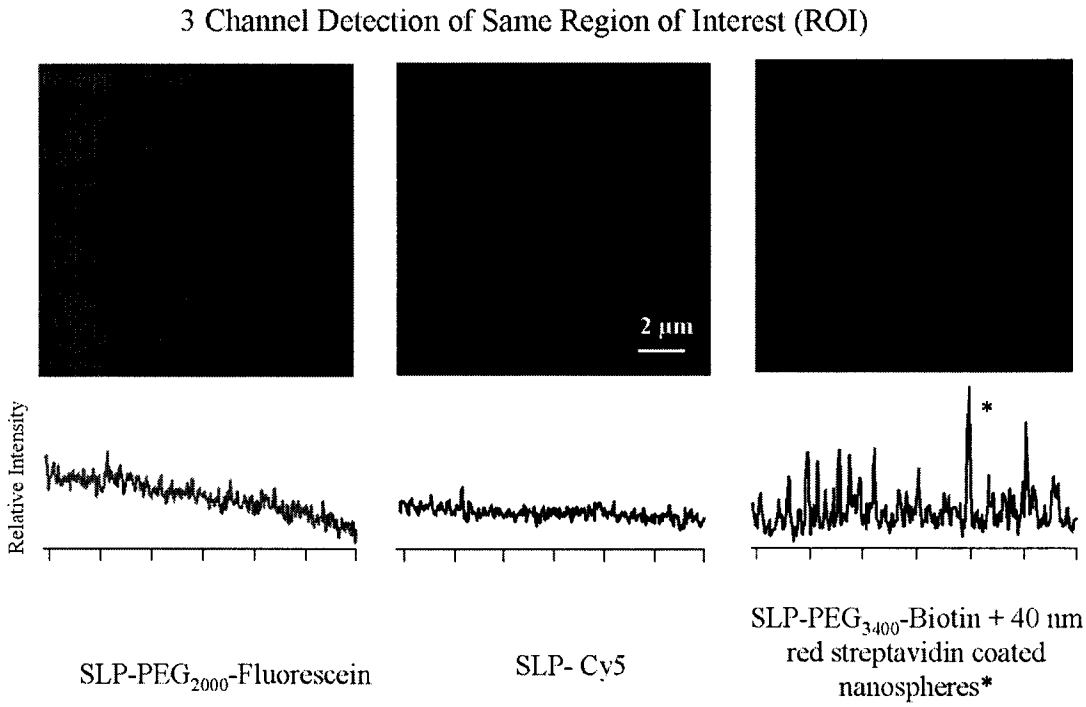

Figure 3.12: Confocal Images of Mixed Monolayers of Three Bioconjugate Modules S-layer-PEG_{3400}-Biotin, S-layer-PEG_{2000}-Fluorescein and S-layer-Cy5 Modules Self-Assembled Simultaneously on APhMS Coated Silicon Chips. Images were obtained

at the same pf region of interest. Biotin was detected with red fluorescent streptavidin coated 40 nm nanospheres.

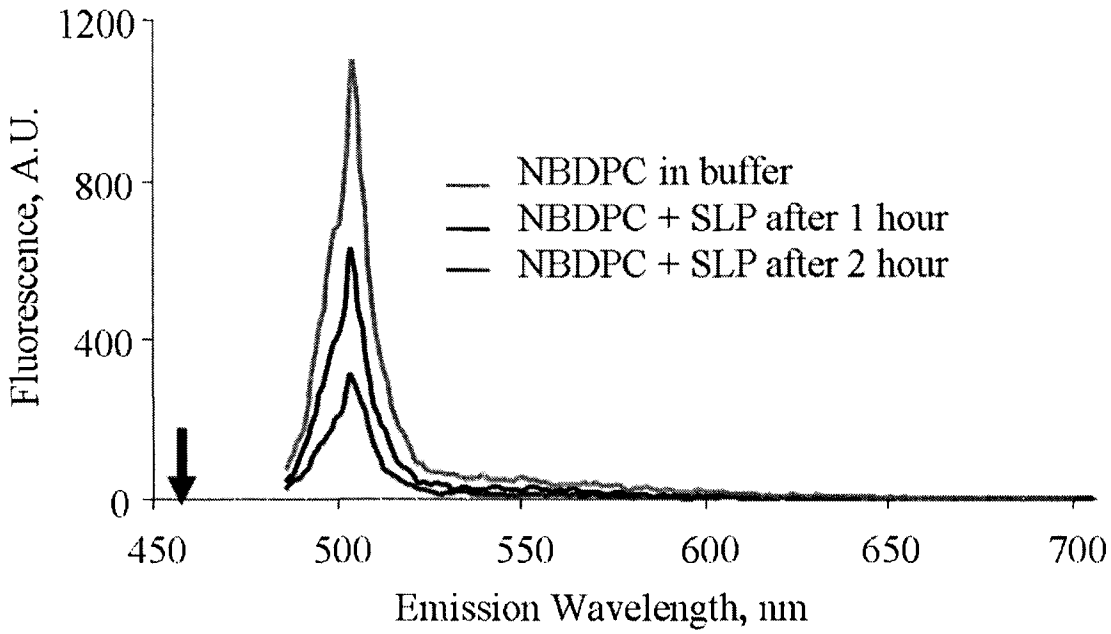

Figure 3.13: TRES: Self-Assembly of S-layer Protein on NBD PC Liposomes

3.2.4 Assembly Experiments on Cationic Liposomes: S-layer stabilized liposomes have been proposed for use as vehicles for drug-targeting and drug-delivery systems, immune and gene therapy, and for the construction of biomimetic viruses. [130, 131] Specifically, the use of S-layers to increase stability of lipid bilayers is of great interest to us. [132, 133] Sleytr and coworkers have studied the interaction of these S-layers with lipid bilayers in liposomes by measuring the elastic properties

using ultrasound velocity and density measurements.[134] They have shown evidence that the S-layer proteins soften or condense the lipid bilayers with changes in temperature. In another related research, it has been shown by the same group that the S-layers have a stabilizing effect on liposomes towards thermal and mechanical stresses.[135] In pursuit of model systems, we performed a simple study on the effect of our self-assembling S-layer proteins on fluorescently labeled cationic liposomes. We thus took 2 ml of NBD-PC (fig. 3.liposome solution (NBD-PC doped PC liposomes) in a cuvette and excited at 460 nm to record TRES, fig. 3.13. The solution was then injected with a suspension of disassembled S-layer protein, at a molar ratio estimated to completely cover the surfaces of the liposomes in the cuvette. The self-assembly process was observed over 2 hours taking TRES at regular intervals. As the self-assembly proceeded there was a marked decrease in the fluorescence emission intensity. This might presumably be due to perturbation in the environment of NBD caused by S-layer protein-probe interactions. This is supported by the fact that NBD present in the tail (lower acyl chain) of the PC lipids "loops back" to the head group region and prefer the lipid-water interface.[136, 137] In fact, it has been shown that NBD groups of acyl chain labeled C_{12} PC (NBD-

PC) and headgroup-labeled phosphatidylethanolamine (NBD-PE) are both located at the polar region and behave similarly.[138, 139] More detailed analysis are needed to be performed with different probes to investigate further in this regard.

3.2.5 Total Internal Reflectance Fluorescence (TIRF): When a light beam passes through two different media having different refractive indices, the light beam propagating in the medium with higher refractive index will get totally reflected at the boundary between the medium with lower refractive index (fig. 3.14). This would happen when the angle of incidence equals or exceeds a critical angle. However, a wave enters the second medium that exponentially decays within 200 nm. This wave is often called the evanescent wave. This wave can thus only excite those fluorophores that are within few nanometers from the surface or only those at the interface. This particular technique can be used to measure the adsorption-desorption kinetics and surface diffusion rates of proteins at the interface. We have performed preliminary experiments with our homemade TIRF cell which was machined similar to that described by Burmeister and co-workers.[140] Analogous to the experiments performed on microspheres, self-assembling suspension

modules of Fluorescein-PEG_{2000}-SLP and Biotin-PEG_{3400}-SLP were used to test self-assembly kinetics on the surface of a positively charged glass slide. The TRES of the nanospheres that were tightly bound to the Biotin-PEG-SLP adsorbed on the inner surface is shown in fig. 3.15. In concurrence with the microsphere studies, we were able to show that bioconjugated S-layer protein can be used for the modular display of ligands at interfaces.

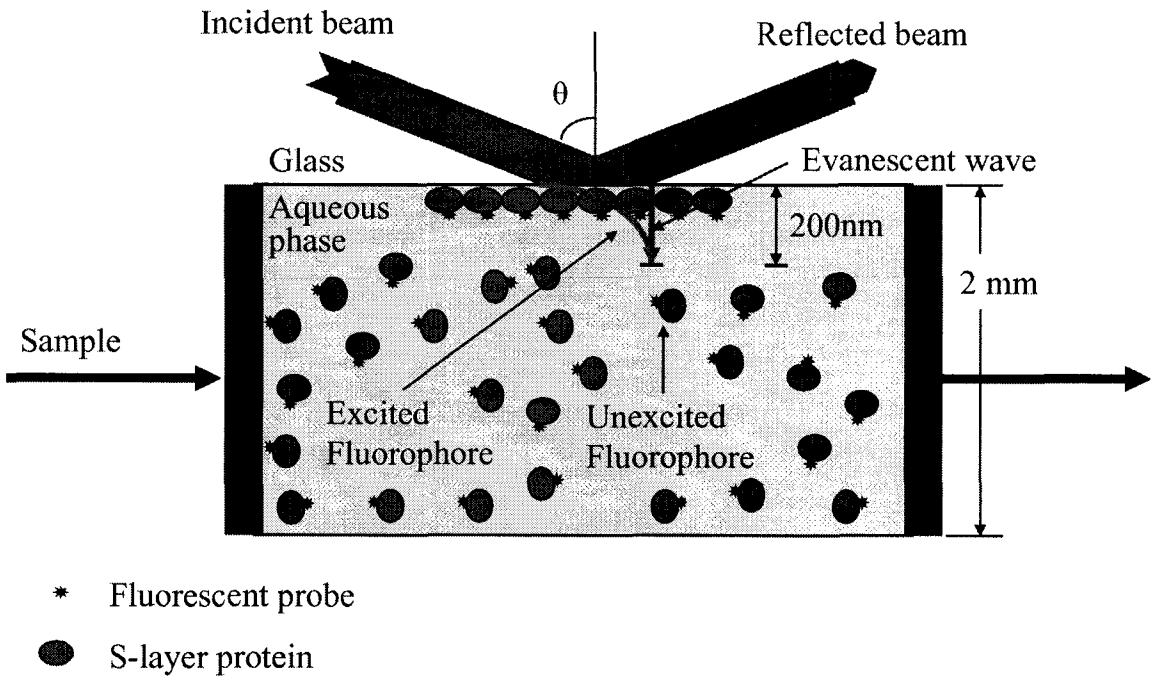

Figure 3.14: Total Internal reflectance fluorescence: TIRF Phenomena

These preliminary results are from the static cases of pre-assembled surfaces. The sensitivity was too low and the spectra were signal averaged for noise. To attempt measurement of assembly in real

time, the experiment has to be conducted for longer times since the self-assembly kinetics are slow.

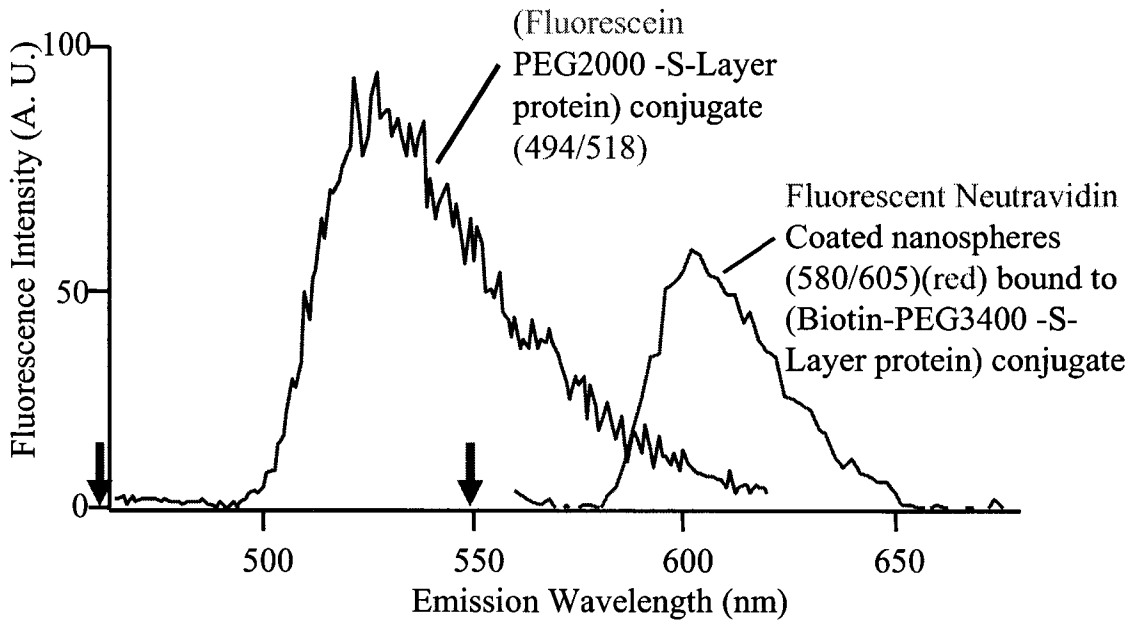

Figure 3.15: TIRF: S-layer-PEG_{3400}-Biotin and S-layer-PEG_{2000}-Fluorescein Conjugates on Positively Charged Glass Slides.

Chapter 4: FUTURE DIRECTIONS

S-layer proteins were successfully purified using successive cycles of assembly/disassembly followed by gel permeation chromatography to obtain plentiful starting material for the conjugation reactions. Though at low yields, SDS-PAGE and Mass Spectrometry results revealed that mainly singly-labeled proteins were obtained with reactions at pH 6.5. Monomeric Avidin Affinity chromatography of biotinylted S-layer protein conjugates provided a novel route to obtain high purity monomers with less unlabeled protein. This method can also be scaled up and be used to precisely control surface assembly conditions.

The bioconjugation reactions demonstrated that selective N-terminal labeling of S-layer proteins was achieved through NHS-mediated reactions. Assembly of S-layer proteins was preserved even after N-terminal labeling. We obtained modular self-assembly of conjugated S-layer proteins onto surfaces of arbitrary topology, namely, cation-doped glass slides, liposomes, polymer microspheres and silicon chips. Modular self-assembly of polyethylene glycol tethered

bioconjugate modules of different sizes and types were also achieved. It was also evident from the epi-fluorescence micrographs, confocal images and SEM that we obtained homogeneous distribution of bioconjugate modules with no detectable phase separation. In addition, our studies with S-layer-PEG_{3400}-Biotin conjugates showed that we were able to assemble modular surfaces capable of ligand display. A reduction in non-specific binding of nanospheres onto microspheres assembled with non-biotin PEG tethered S-layer bioconjugates was also observed. Further, with this approach we have shown that the surface densities of mixed S-layer bioconjugate modules can be controlled by changing the relative bulk concentrations of the self-assembly suspensions.

Apparently, these mixed monolayers would retain the underlying native nanostructure of the S-layer array, thus, dictating the spacing of the functional endgroups. Besides, in comparison with current technologies utilizing polymers and nanoparticles for forming SAMs, our headgroup protein size is substantially larger than most functional endgroups. Also, the self-assembled S-layer structures are probably highly stable and energetically favored due to the protein-protein and protein-substrate interactions. Thus, our method provides a novel route

for the display of intact proteins with large functionalized molecules at interfaces; presenting notable innovation in SAM technology. These molecularly engineered surfaces can also be exploited as a tool to test cell responses and to manufacture "Protein Chips".

One can construct modules that retain both self-assembly and bioactivity of ligated proteins with the bioconjugation methodology explained in section 2.1.9. Other reaction schemes such as maleimide mediated or carboxylate mediated routes could also be used. The conjugation of molecules of different functions and sizes to the S-layer proteins can also be investigated. Specific molecules (functions in nature) that are of interest are given below with increasing sizes:

- GRGDS of fibronectin (adhesion peptide),
- YKKIIKKL (heparin-binding),
- PHSRN (adhesion and synergy)
- Echistatin, RGD-containing integrin inhibitor protein, 5.4 kDa (adhesion),
- Epidermal growth factors (EGF), 6 kDa (signaling),
- Stem cell factor (c-kit), 18.5 kDa (signaling),
- Antibodies (antigen specific)
- Single stranded DNA (nucleotide)

- 2-Mercaptoethanol, as a blank (non-adsorbing).

Specifically, an S-layer protein 2D array conjugated to single stranded DNA molecules would complement the capabilities of DNA microarrays. The strands would also be confined to the crystallographic unit dimensions of the S-layer nanostructure.

To minimize nonspecific protein adsorption some sets of the Vinylsulfone-PEG_{3400}-SLP can be coupled with 2-mercaptoethanol to form "blank" modules. Bifunctional poly ethyleneglycol linkers could be used as tethers in the conjugation process. An important aspect of using these PEG linkers is that, the blank PEG molecules could also reduce non-specific adsorption of proteins in the areas between the displayed bioactive ligands.

Assembly experiments using these bioconjugate modules could be conducted on polymer microspheres and silicon substrates. Quantification of these modularly self-assembled surfaces could be done by incorporating fluorescent probes and examining them under Confocal Microscopy and XPS. The adsorption-desorption kinetics of the self-assembly process and the surface diffusion rates of proteins at any given planar surface could also be measured using TIRF. The influence of molecular tether length and conjugated biomolecular size

on self-assembly can also be examined using these techniques. Griffith and co-workers have compared the biomaterials surface properties made with the help of star and linear polyethylene oxide tethers.[141] Similarly, larger linear PEG molecules can be used for making bioactive surfaces and investigated.

Fluorescence Resonance Energy Transfer (FRET) microscopy can be used to obtain temporal and spatial information about the binding and interactions between S-layer proteins monomers and also between the S-layer and lipid bilayers. The principle of FRET underlies in the fact that proximity of donor and acceptor fluorophores results in irradiative transfer of the donor excitation energy to the acceptor molecules. A potential donor-acceptor combination could be Oregon green-tetramethyl rhodamine. Detailed spatial information can be obtained by incorporating fluorescent probes separately in the tail or head group of lipid bilayers along with self-assembled, fluorescent labeled or tethered S-layer protein.

Freeze fracturing and negative staining experiments can also be performed to obtain an image of the structure of assembled surfaces. Also, Atomic Force Microscopy (AFM) can be employed to learn topographical data of the assembled monolayers. AFM in tapping mode

or in contact mode under liquid would also enable us to analyze the S-layer nanostructure in greater detail. Fourier Transform Infrared Spectroscopy (FTIR) techniques as described in section 3.1.5 can also be used for more detailed studies of the molecular composition of the assembled surfaces. We could quantify the monolayers at the molecular level since the peaks are an added sum of individual groups. Ellipsometry can be used to determine the monolayer thickness and also test conditions and threshold for formation of multilayers. Dynamic light scattering can be used to analyze monomer size prior to self-assembly experiments and also for obtaining assembly kinetics in solution.

Chapter 5: APPENDIX

5.1 Principles of Fluorescence

Fluorescence is the property of some atoms and molecules to absorb light of a particular wavelength and emit light with lower energy at longer wavelengths. Absorption of energy by fluorescent molecules occurs in different orbitals between a number of closely spaced vibrational and rotational excited states. The Jablonski diagram, fig. 5.1a, explains the different energy levels involved in the above phenomena. Internal conversion is the relaxation from the excited state to the lowest excited singlet state where energy is thermally lost to the environment due to the collisions of the excited state probe with solvent molecules. Subsequent relaxation of the molecule to the ground state with an emission of a photon is referred to as fluorescence. The time the molecule dwells at the lowest excited singlet state is called the fluorescence lifetime and is in the order of 1 nanosecond. In time resolved fluorescence, fig. 5.1b, fluorescence emitted from the probe is measured after a delay time when the background fluorescence or autofluorescence has already completely decayed.

A. Jablonski diagram

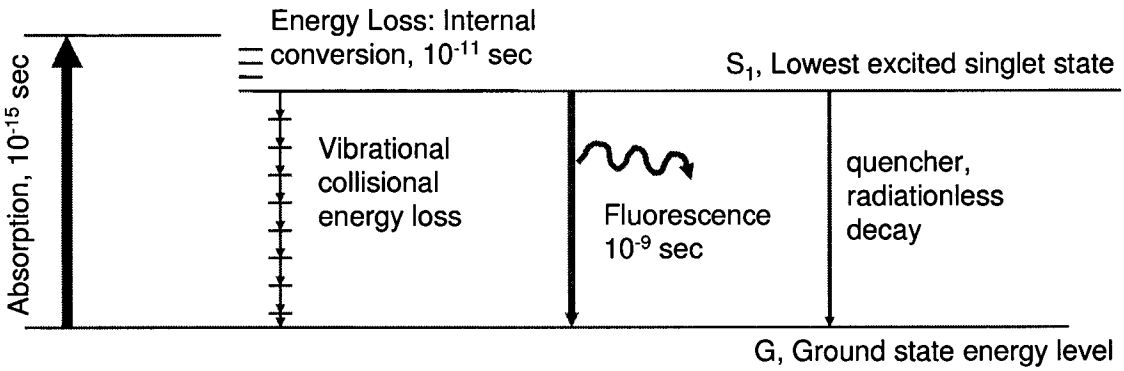

B. Principles of time resolved fluorescence

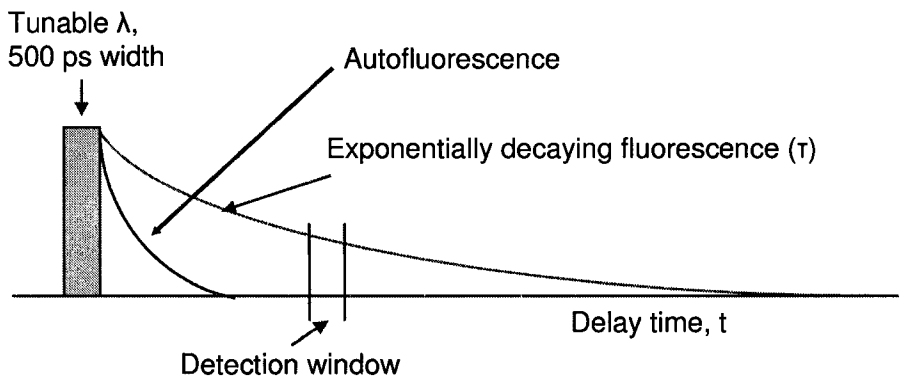

Figure 5.1: Fluorescence Basics

Fluorescence Resonance Energy Transfer (FRET) microscopy can be used to obtain temporal and spatial information about the binding and interactions of proteins and lipids. The principle of FRET underlies in the fact that proximity of donor and acceptor fluorophores results in irradiative transfer of the donor excitation energy to the

acceptor molecules. This phenomena result in the decrease of donor emission intensity while increasing the acceptor emission intensity. Energy transfer occurs over a distance of 1 to 10 nm that provides information to the molecular scale beyond the resolution of the microscope. The lifetimes of the donor probe in the presence and absence of the acceptor can also be measured. The concentration of the donor and acceptor needs to be tightly controlled during FRET studies. Donor and acceptor chosen for study should be such that there is relatively little direct excitation of the acceptor at the excitation maxima of the donor.

5.2 Principles of Mass Spectrometry

A mass spectrometer is an instrument that produces ions and separates them in the gas phase according to their mass-to-charge ratio (m/z). Electrospray Ionization (ESI) Mass Spectrometry (MS) involves an ionization technique that produces charged molecules in the gas phase. In the ESI source design, the sample is ejected through a capillary tip that induces electrostatic dispersion causing a spray of droplets. A heated bath of nitrogen aids the droplets to undergo declustering, losing solvent molecules. Desolvation of the droplets

increases the charge density on the droplet surfaces and causes a Coulombic explosion, leading to individual ions. Ions are formed at atmospheric pressure and enter a cone shaped orifice, which acts as a first vacuum stage where they undergo free jet expansion. Subsequently, a skimmer samples the ions and guides them to the mass spectrometer. For macromolecules, each ion entering the mass spectrometer usually has a high number of charges. This distribution of ions permits the calculation of the molecular mass of the original sample from any two neighboring ions. The measurement of the charge state distribution of large molecules is not always easy or reproducible since it varies with pH, solvents or salts, partial denaturation of the protein or breaking disulfide bonds.[142] In ESI-MS, partial denaturation of proteins is observed from the increase in the number of charges and m/z shifts to a lower value. [143, 144] This process presumably involves the breaking of ionic bridges within the protein and also on the ability of basic groups to retain a charge.[145]

5.3 Principles of Gel Filtration

The method of gel filtration chromatography or as it is also called as gel exclusion or gel permeation or molecular sieve chromatography,

exploits the physical property of molecular size to achieve separation. The stationary phase consists of inert particles that contain small pores of a controlled size. A solution containing solutes of various molecular sizes are passed through the column under the influence of continuous solvent flow. Larger solute molecules are limited to the space between the beads since they cannot enter the pores of the gel beads. Therefore, they are not slowed in their progress through the column and elute rapidly in a single zone. Small molecules that are capable of diffusing in and out of the pores are delayed in their journey through the column bed. As a result, the order of elution of the various solute molecules is directly dependent on their molecular dimensions.

5.4 Principles of Atomic Force Microscopy

Atomic Force Microscopy (AFM) is widely used in various fields of research to study the surface properties of various materials. AFM measures attractive or repulsive forces between a probe or "tip" and the surface of a sample at nano Newton scales.[146] Tips are typically made of silicon nitride or silicon oxide. The measuring element consists of a microcantilever that supports tips of atomic dimensions. The tips are raster scanned over the surface using a peizo-electric scanner. The

contour of the surface leads to motions in the cantilever. These deflections are sensed by a laser beam reflected on the top of the cantilever and detected by position sensitive photodiode. An image is generated using this signal which correlates to the topography of the sample. Feedback from the photodiode signal enables the instrument to maintain the tip at constant force or at constant height over the sample. The size and geometry of the probe (radius of curvature) and the sample geometry generally limits the resolution.

There are generally 3 modes in AFM imaging: contact mode, non-contact mode and tapping mode. In the contact mode, the probe is essentially dragged across the sample surface. The cantilever remains bent constantly during scanning. This bending denotes a displacement of the probe tip in relative to the straight cantilever. The applied normal force for this bending motion is the product of the displacement and the spring constant of the cantilever. Using the feedback from the photodiode, with change in topography, the tip is maintained at a position to produce constant deflection. Low spring constant (< 1 N/m) probes minimize the amount of applied force used for scanning. Nevertheless, the lateral forces created by the dragging motion of the probe tip across the sample result in high contact stresses that can

potentially damage the sample and the tip. Contact mode can also be performed under a liquid, which requires lower contact forces.

In non-contact mode the tip oscillates close to the sample surface.[147] The resonance frequency and amplitude of the oscillating probe is influenced by attractive van der Waals forces between the tip and the surface. These types of forces are much smaller compared to the repulsive forces encountered in contact mode. Thus cantilevers possess higher spring constants (20-100 N/m) and are driven at smaller amplitudes to increase sensitivity. Besides, the lateral resolution is limited by the tip-sample separation and is generally lower compared to other modes.

In tapping mode, the cantilever oscillates close to its resonance frequency, as in non-contact mode. The tip makes contact with the sample only for a small fraction in its oscillation cycle. Tapping mode is preferred for soft surfaces, as the resolution is similar to contact mode while the lateral forces on the sample are lower and less damaging.

Chapter 6: REFERENCES

[1] Hubbell JA. Biomaterials in tissue engineering. Biotechnology (NY). 1995 Jun; 13(6):565-76

[2] Akiyama SK. Integrins in cell adhesion and signaling. Hum Cell. 1996 Sep; 9(3):181-6

[3] Clark EA, Brugge JS. Integrins and signal transduction pathways: the road taken. Science. 1995 Apr 14; 268(5208):233-9

[4] Guan JL, Chen HC. Signal transduction in cell-matrix interactions. Int Rev Cytol. 1996; 168:81-121

[5] Griffith LG. Polymeric Biomaterials. Acta mater. 2000; 48:263-277

[6] Griffith LG, Grodzinsky AJ. Advances in biomedical engineering. JAMA. 2001 Feb 7; 285(5):556-61

[7] Christenson L, Mikos AG, Gibbons DF, Picciolo GL. Biomaterials for tissue engineering: summary. Tissue Eng. 1997 Spring; 3(1):71-6

[8] Hubbell JA. Bioactive Biomaterials. Curr Opin Biotechnol. 1999 Apr; 10(2):123-9

[9] Sleytr UB, Bayley H, Sara M, Breitwieser A, Kupcu S, Mader C, Weigert S, Unger FM, Messner P, Jahn-Schmid B, Schuster B, Pum D,

Douglas K, Clark NA, Moore JT, Winningham TA, Levy S, Frithsen I, Pankovc J, Beale P, Gillis HP, Choutov DA, Martin KP. Applications of S-layers. FEMS Microbiol Rev. 1997 Jun; 20(1-2):151-75

[10] Schuster B, Pum D, Braha O, Bayley H, Sleytr UB. Self-assembled alpha-hemolysin pores in an S-layer-supported lipid bilayer. Biochim Biophys Acta. 1998 Mar 13; 1370(2):280-8

[11] Shenton W, Pum D, Sleytr UB, Mann S. Synthesis of cadmium sulphide superlattices using self-assembled bacterial S-layers. Nature. 1997; 389:585-7

[12] Pum D, Sleytr UB. Large scale reconstitution of crystalline S-layer proteins at the air-water interface and on lipid films. Thin Solid Films. 1994; 244:882-886

[13] Wetzer B, Pfandler A, Györvary E, Pum D, Lösche M, Sleytr UB. S-layer reconstitution at phospholipid monolayers. Langmuir. 1998; 14:6899-6906

[14] Diederich A, Sponer C, Pum D, Sleytr B, Lösche M. Reciprocal influence between the protein and lipid components of a lipid-protein membrane model. Coll. Surfaces B 1996; 6:335-346

[15] Wagner ML, Tamm LK. Tethered polymer-supported planar lipid bilayers for reconstitution of integral membrane proteins: silane-

polyethyleneglycol-lipid as a cushion and covalent linker. Biophys J. 2000 Sep; 79(3):1400-14

[16] Knoll W, Frank CW, Heibel C, Naumann R, Offenhausser A, Ruhe J, Schmidt EK, Shen WW, Sinner A. Functional tethered lipid bilayers. J Biotechnol. 2000 Sep; 74(3):137-58

[17] Radler U, Mack J, Persike N, Jung G, Tampe R. Design of supported membranes tethered via metal-affinity ligand-receptor pairs. Biophys J. 2000 Dec; 79(6):3144-52

[18] Naumann CA, Prucker O, Lehmann T, Ruhe J, Knoll W, Frank CW. The polymer-supported phospholipid bilayer: tethering as a new approach to substrate-membrane stabilization. Biomacromolecules. 2002 Jan-Feb; 3(1):27-35

[19] Sinner EK, Knoll W. Functional tethered membranes. Curr Opin Chem Biol. 2001 Dec; 5(6):705-11

[20] Sára M, Sleytr UB. Biotechnology and biomimetic with crystalline bacterial cell surface layers (S-layers). Micron. 1996; 27:141-156

[21] Sleytr UB, Sara M. Bacterial and archaeal S-layer proteins: structure-function relationships and their biotechnological applications. Trends Biotechnol. 1997 Jan; 15(1):20-6

[22] Pum, D., Sleytr, U.B. The application of bacterial S-layers in molecular nanotechnology. Trends in Biotechnology 1999; 17:8-12

[23] Sleytr UB, Pum D, Sara M. Advances in S-layer nanotechnology and biomimetics. Adv Biophys. 1997; 34:71-9

[24] Pum, D., Stangl, G., Sponer, C., Fallmann, W., Sleytr, U.B. Deep Ultraviolet patterning of monolayers of crystalline S-layer protein on silicon surfaces. Colloids and Surfaces B: Biointerfaces 1996; 8:157-162

[25] Breitwieser A, Mader C, Schocher I, Hoffmann-Sommergruber K, Aberer W, Scheiner O, Sleytr UB, Sara M. A novel dipstick developed for rapid Bet v 1-specific IgE detection: recombinant allergen immobilized via a monoclonal antibody to crystalline bacterial cell-surface layers. Allergy 1998 Aug; 53(8): 786-93

[26] Schuster KC, Mayer H, Kieweg R, Hampel W, Sara M. A synthetic medium for continuous culture of the S-layer carrying Bacillus stearothermophilus PV72 and studies on the influence of growth conditions on cell wall properties. Biotechnol. Bioeng. 1995; 48:66-77

[27] Neubauer A, Pum D, Sleytr UB. Fiber-optic glucose biosensor using enzyme membranes with 2-D crystalline structure. Biosensors & Bioelec. 1996; 11(3): 317-325,

[28] Jahn-Schmid B, Graninger M, Glozik M, Kupcu S, Ebner C, Unger FM, Sleytr UB, Messner P. Immunoreactivity of allergen (Bet v 1) conjugated to crystalline bacterial cell surface layers (S-layers). Immunotechnology. 1996 Jun; 2(2):103-13

[29] Moll D, Huber C, Schlegel B, Pum D, Sleytr UB, Sara M. S-layer-streptavidin fusion proteins as template for nanopatterned molecular arrays. Proc Natl Acad Sci U S A. 2002 Nov 12; 99(23):14646-51

[30] Pleschberger M, Neubauer A, Egelseer EM, Weigert S, Lindner B, Sleytr UB, Muyldermans S, Sara M. Generation of a functional monomolecular protein lattice consisting of an s-layer fusion protein comprising the variable domain of a camel heavy chain antibody. Bioconjug Chem. 2003 Mar-Apr; 14(2):440-8

[31] Breitwieser A, Egelseer EM, Moll D, Ilk N, Hotzy C, Bohle B, Ebner C, Sleytr UB, Sara M. A recombinant bacterial cell surface (S-layer)-major birch pollen allergen-fusion protein (rSbsC/Bet v1) maintains the ability to self-assemble into regularly structured monomolecular lattices and the functionality of the allergen. Protein Eng. 2002 Mar; 15(3):243-9

[32] Ilk N, Vollenkle C, Egelseer EM, Breitwieser A, Sleytr UB, Sara M. Molecular characterization of the S-layer gene, sbpA, of Bacillus sphaericus CCM 2177 and production of a functional S-layer fusion

protein with the ability to recrystallize in a defined orientation while presenting the fused allergen. Appl Environ Microbiol. 2002 Jul; 68(7):3251-60

[33] Buckmire FL, Murray RG. Studies on the cell wall of Spirillum serpens. II. Chemical characterization of the outer structured layer. Can J Microbiol. 1973 Jan; 19(1):59-66

[34] Howard L, Tipper DJ. A polypeptide bacteriophage receptor: modified cell wall protein subunits in bacteriophage-resistant mutants of Bacillus sphaericus strain P-1. J Bacteriol. 1973 Mar; 113(3):1491-504

[35] Egelseer E, Schocher I, Sara M, Sleytr UB. The S-layer from Bacillus stearothermophilus DSM 2358 functions as an adhesion site for a high-molecular-weight amylase. J Bacteriol. 1995 Mar; 177(6):1444-51

[36] Egelseer EM, Schocher I, Sleytr UB, Sara M. Evidence that an N-terminal S-layer protein fragment triggers the release of a cell-associated high-molecular-weight amylase in Bacillus stearothermophilus ATCC 12980. J Bacteriol. 1996 Oct; 178(19):5602-9

[37] Beveridge TJ, Pouwels PH, Sara M, Kotiranta A, Lounatmaa K, Kari K, Kerosuo E, Haapasalo M, Egelseer EM, Schocher I, Sleytr UB, Morelli L, Callegari ML, Nomellini JF, Bingle WH, Smit J, Leibovitz E, Lemaire M, Miras I, Salamitou S, Beguin P, Ohayon H, Gounon P,

Matuschek M, Koval SF. Functions of S-layers. FEMS Microbiol Rev. 1997 Jun; 20(1-2):99-149

[38] Weigert S, Sára M. Ultrafiltration membranes prepared from crystalline bacterial cell surface layers as model systems for studying the influence of surface properties on protein adsorption. J. Membr. Sci. 1996; 121:185-196

[39] Sara M, Sleytr UB. Molecular sieving through S layers of Bacillus stearothermophilus strains. J Bacteriol. 1987 Sep; 169(9):4092-8

[40] Engelhardt H, Peters J. Structural research on surface layers - A focus on stability, surface layer homology domains, and surface layer-cell wall interactions. J. Struct. Biol. 1998; 124:276-302

[41]Sleytr UB, Sara M, Messner P, Pum D. Two-dimensional protein crystals (S-layers): Fundamentals and Applications. J. of Cellular Biochem 1994; 56:171-176

[42] Sleytr UB, Beveridge T. Bacterial S-layers. Trends in Microb. 1999 Jun; 7:253-60

[43] Beveridge TJ. Bacterial S-layers. Curr. Opin Struct Biol. 1994; 4:204-12

[44] Sara M, Sleytr UB. Crystalline bacterial cell surface layers (S-layers): from cell structure to biomimetics. Prog Biophys Mol Biol. 1996; 65(1-2): 83-111

[45] Sleytr UB, Messner P. Crystalline surface layers on bacteria. Ann Rev Microbiol. 1983; 37:311-39

[46] Lupas A, Engelhardt H, Peters J, Santarius U, Volker S, Baumeister W. Domain structure of the Acetogenium kivui surface layer revealed by electron crystallography and sequence analysis. J. Bacteriol. 1994; 176:1224-33

[47] Engel AM, Cejka Z, Lupas A, Lottspeich F, Baumeister W. Isolation and cloning of Omp-alpha, a coiled-coil protein spanning the periplasmic space of the ancestral eubacterium Thermotoga maritime. EMBO J. 1992; 11:4369-78

[48] Woodcock CL, Engelhardt H, Baumeister W. The tetragonal surface layer of Clostridium aceticum: three-dimensional structure and comparison with the hexagonal layer of Clostridium thermohydrosulfuricum. Eur J Cell Biol. 1986 Dec;42(2):211-7

[49] Bingle WH, Engelhardt H, Page WJ, Baumeister W. Three-dimensional structure of the regular tetragonal surface layer of Azotobacter vinelandii. J Bacteriol. 1987 Nov; 169(11):5008-15

[50] Pum D, Sara M, Sleytr UB. Structure, surface charge, and self-assembly of the S-layer lattice from Bacillus coagulans E38-66. J Bacteriol. 1989 Oct; 171(10):5296-303

[51] Jing H, Takagi J, Liu JH, Lindgren S, Zhang RG, Joachimiak A, Wang JH, Springer TA. Archaeal surface layer proteins contain beta propeller, PKD, and beta helix domains and are related to metazoan cell surface proteins. Structure (Camb). 2002 Oct; 10(10):1453-64

[52] Scheuring S, Stahlberg H, Chami M, Houssin C, Rigaud JL, Engel A. Charting and unzipping the surface layer of Corynebacterium glutamicum with the atomic force microscope. Mol Microbiol. 2002 May; 44(3):675-84

[53] Messner P, Allmaier G, Schaffer C, Wugeditsch T, Lortal S, Konig H, Niemetz R, Dorner M. Biochemistry of S-layers. FEMS Microbiol Rev. 1997 Jun; 20(1-2):25-46

[54] Lortal S, Heijenoort JV, Gruber K, Sleytr UB. S-Layer of Lactobacillus helveticus ATCC 12046: isolation, chemical characterization and re-formation after extraction with lithium chloride. J. Gen. Microbiol. 1992; 138:611-618

[55] Peters J, Nitsch M, Kuhlmorgen B, Golbik R, Lupas A, Kellermann J, Engelhardt H, Pfander JP, Muller S, Goldie K, et al. Tetrabrachion: a

filamentous archaebacterial surface protein assembly of unusual structure and extreme stability. J Mol Biol. 1995 Jan 27; 245(4):385-401

[56] Beveridge TJ, Sterward M, Doyle RJ, Sprott GD. Unusual stability of the Methanospirillum hungatei sheath. J. Bacteriol. 1985; 162:728-37

[57] Sara M, Sleytr UB. S-Layer proteins. J Bacteriol 2000 Feb; 182(4):859-68

[58] Sleytr UB, Messner P. Crystalline surface layers in procaryotes. J Bacteriol. 1988 Jul; 170(7):2891-7

[59] Gebb C, Clark JM, Hirtenstein MD, Lindgren G, Lindskog U, Lundgren B, Vretblad P. Alternative surfaces for microcarrier culture of animal cells. Dev Biol Stand. 1981; 50:93-102

[60] Hirtenstein MD, Clark JM, Gebb C. A comparison of various laboratory scale culture configurations for microcarrier culture of animal cells. Dev Biol Stand. 1981; 50:73-80

[61] Kao WJ, Liu Y. Utilizing biomimetic oligopeptides to probe fibronectin-integrin binding and signaling in regulating macrophage function in vitro and in vivo. Front Biosci. 2001 Aug 1; 6:D992-9.

[62] Kao WJ, Lee D, Schense JC, Hubbell JA. Fibronectin modulates macrophage adhesion and FBGC formation: the role of RGD, PHSRN, and PRRARV domains. J Biomed Mater Res. 2001 Apr; 55(1):79-88.

[63] Sakiyama SE, Schense JC, Hubbell JA. Incorporation of heparin-binding peptides into fibrin gels enhances neurite extension: an example of designer matrices in tissue engineering. FASEB J. 1999 Dec; 13(15):2214-24.

[64] Mann BK, Tsai AT, Scott-Burden T, West JL. Modification of surfaces with cell adhesion peptides alters extracellular matrix deposition. Biomaterials 1999 Dec; 20(23-24):2281-6

[65] Patel N, Padera R, Sanders GH, Cannizzaro SM, Davies MC, Langer R, Roberts CJ, Tendler SJ, Williams PM, Shakesheff KM. Spatially controlled cell engineering on biodegradable polymer surfaces. FASEB J. 1998 Nov; 12(14):1447-54

[66] Maheshwari G, Brown G, Lauffenburger DA, Wells A, Griffith LG. Cell adhesion and motility depend on nanoscale RGD clustering. J Cell Sci. 2000 May; 113 (Pt 10):1677-86.

[67] Sofia S, McCarthy MB, Gronowicz G, Kaplan DL. Functionalized silk-based biomaterials for bone formation. J Biomed Mater Res. 2001 Jan; 54(1):139-48

[68] Zhang S, Yan L, Altman M, Lassle M, Nugent H, Frankel F, Lauffenburger DA, Whitesides GM, Rich A. Biological surface

engineering: a simple system for cell pattern formation. Biomaterials. 1999 Jul; 20(13):1213-20

[69] Fields GB, Lauer JL, Dori Y, Forns P, Yu YC, Tirrell M. Protein-like molecular architecture: biomaterial applications for inducing cellular receptor binding and signal transduction. Biopolymers. 1998; 47(2):143-51

[70] Pakalns T, Haverstick KL, Fields GB, McCarthy JB, Mooradian DL, Tirrell M. Cellular recognition of synthetic peptide amphiphiles in self-assembled monolayer films. Biomaterials. 1999; 20(23-24): 2265-79

[71] Griffith LG, Lopina S. Microdistribution of substratum-bound ligands affects cell function: hepatocyte spreading on PEO-tethered galactose. Biomaterials. 1998 Jun; 19(11-12):979-86

[72] Mann BK, Schmedlen RH, West JL. Tethered-TGF-beta increases extracellular matrix production of vascular smooth muscle cells. Biomaterials. 2001 Mar; 22(5):439-44

[73] Haller MF, Saltzman WM. Nerve growth factor delivery systems. J Control Release. 1998 Apr 30; 53(1-3):1-6

[74] Lu L, Stamatas GN, Mikos AG. Controlled release of transforming growth factor beta1 from biodegradable polymer microparticles. J Biomed Mater Res. 2000 Jun 5; 50(3):440-51

[75] Elisseeff J, McIntosh W, Fu K, Blunk BT, Langer R. Controlled-release of IGF-I and TGF-beta1 in a photopolymerizing hydrogel for cartilage tissue engineering. J Orthop Res. 2001 Nov; 19(6):1098-104.

[76] Santos EM, Radin S, Ducheyne P. Sol-gel derived carrier for the controlled release of proteins. Biomaterials 1999 Sep; 20(18):1695-700

[77] Mader C, Kupcu S, Sleytr UB, Sara M. S-layer-coated liposomes as a versatile system for entrapping and binding target molecules. Biochim Biophys Acta. 2000 Jan 15; 1463(1):142-50

[78] Tamada K, Hara M, Sasabe H, Knoll W. Surface Phase Behavior of n-Alkanethiol Self-Assembled Monolayers Adsorbed on Au(111): An Atomic Force Microscope Study. Langmuir. 1997; 13(6):1558-1566

[79] Folkers JP, Laibinis PE, Whitesides GM, Deutch J. Phase-Behavior of 2-Component Self-Assembled Monolayers of Alkanethiolates on Gold. J. Phys. Chem. 1994; 98(2):563-571

[80] Herrwerth S, Eck W, Reinhardt S, Grunze M. Factors that determine the protein resistance of oligoether self-assembled monolayers - internal hydrophilicity, terminal hydrophilicity, and lateral packing density. J Am Chem Soc. 2003 Aug; 125(31):9359-66

[81] Prime KL, Whitesides GM. Self-assembled organic monolayers: model systems for studying adsorption of proteins at surfaces. Science. 1991 May; 252(5010):1164-7

[82] Prime KL, Whitesides GM. Adsorption of proteins onto surfaces containing end-attached oligo(ethylene oxide): A model system using self-assembled monolayers. J. Am. Chem. Soc. 1993; 115:10714–10721

[83] Leckband DE, Schmitt FJ, Israelachvili JN, Knoll W. Direct force measurements of specific and nonspecific protein interactions. Biochemistry. 1994 Apr 19; 33(15):4611-24

[84] Sheth SR, Leckband D. Measurements of attractive forces between proteins and end-grafted poly(ethylene glycol) chains. Proc Natl Acad Sci U S A. 1997 Aug 5; 94(16):8399-404

[85] Wetzer, B. Pfandler, A., Györvary, E., Pum, D., Lösche, M., Sleytr, U.B. S-layer reconstitution at phospholipid monolayers. Langmuir 1998; 14:6899-6906

[86] Masuda K, Kawata T. Ultrastructure and partial characterization of a regular array in the cell wall of Lactobacillus brevis. Microbiol Immunol. 1979; 23(10):941-53

[87] Masuda K, Kawata T. Reassembly of the regularly arranged subunits in the cell wall of Lactobacillus brevis and their reattachment to cell walls. Microbiol Immunol. 1980; 24(4):299-308

[88] Vidgren G, Palva I, Pakkanen R, Lounatmaa K, Palva A. S-layer protein gene of Lactobacillus brevis: cloning by polymerase chain reaction and determination of the nucleotide sequence. J Bacteriol 1992 Nov; 174(22):7419-27

[89] DeMan JC, Rogosa M, Sharpe ME. A medium for the cultivation of lactobacilli. J. Appl. Bacteriol. 1960; 23:130

[90] Smith PK, Krohn RI, Hermanson GT, Mallia AK, Gartner FH, Provenzano MD, Fujimoto EK, Goeke NM, Olson BJ, Klenk DC. Measurement of protein using bicinchoninic acid. Anal Biochem. 1985 Oct; 150(1):76-85

[91] Wiechelman KJ, Braun RD, Fitzpatrick JD. Investigation of the bicinchoninic acid protein assay: identification of the groups responsible for color formation. Anal Biochem. 1988 Nov 15; 175(1):231-7

[92] Bradford MM. A rapid and sensitive method for the quantitation of microgram quantities of protein utilizing the principle of protein-dye binding. Anal Biochem. 1976 May 7; 72:248-54

[93] Glover BP, McHenry CS. The DNA polymerase III holoenzyme: an asymmetric dimeric replicative complex with leading and lagging strand polymerases. Cell. 2001 Jun 29; 105(7):925-34

[94] Duncan RJ, Weston PD, Wrigglesworth R. A new reagent which may be used to introduce sulfhydryl groups into proteins, and its use in the preparation of conjugates for immunoassay. Anal Biochem. 1983 Jul 1; 132(1):68-73

[95] Messner P, Hollaus F, Sleytr UB. Paracrystalline cell wall surface layers of different Bacillus stearothermophilus strains. International J Sys Bacteriology 1984; 34:202-210

[96] Pum D, Sara M, Sleytr UB. Structure, surface charge, and self-assembly of the S-layer lattice from Bacillus coagulans E38-66. J Bacteriol. 1989 Oct; 171(10):5296-303

[97] Fu R, Cross TA. Solid-state nuclear magnetic resonance investigation of protein and polypeptide structure. Annu Rev Biophys Biomol Struct. 1999; 28:235-68

[98] Hafner S, Spiess HW. Advanced solid-state NMR spectroscopy of strongly dipolar coupled spins under fast magic angle spinning. Concepts in Magnetic Resonance. 1998; 10(1):99-128

[99] Tycko R. Solid-state nuclear magnetic resonance techniques for structural studies of amyloid fibrils. Methods Enzymol. 2001; 339:390-413

[100] Altschul, Stephen F, Thomas L. Madden, Alejandro A. Schäffer, Jinghui Zhang, Zheng Zhang, Webb Miller, and David J. Lipman, Gapped BLAST and PSI-BLAST: a new generation of protein database search programs, Nucleic Acids Res. 1997; 25:3389-3402

[101] Jakava-Viljanen M, Avall-Jaaskelainen S, Messner P, Sleytr UB, Palva A. Isolation of Three New Surface Layer Protein Genes (slp) from Lactobacillus brevis ATCC 14869 and Characterization of the Change in Their Expression under Aerated and Anaerobic Conditions. J. Bacteriol. 2002; 184 (24):6786-6795

[102] Klein C, Schulz GE. Structure of cyclodextrin glycosyltransferase refined at 2.0 A resolution. J Mol Biol 1991 Feb 20; 217(4):737-50

[103] Murzin AG, Brenner SE, Hubbard T, Chothia C. SCOP: a structural classification of proteins database for the investigation of sequences and structures. J. Mol. Biol. 1995; 247:536-540

[104] Rost B, Fariselli P, Casadio R. Topology prediction for helical transmembrane proteins at 86% accuracy. Prot Science 1996; 7:1704-1718

[105] Rost B, Sander C. Prediction of protein secondary structure at better than 70% accuracy. J Mol Biol. 1993; 232:584-599

[106] Rost B. PHD: predicting one-dimensional protein structure by profile-based neural networks. Methods in Enzymology 1996; 266:525-539

[107] Rost B, Sander C. Conservation and prediction of solvent accessibility in protein families. Proteins.1994; 20:216-226

[108] Dhara D, Chatterji PR. Electrophoretic Transport of Poly(ethylene glycol) Chains through Poly(acrylamide) Gel, J. Phys. Chem. B 1999, 103, 8458-8461

[109] Stayton PS, Freitag S, Klumb LA, Chilkoti A, Chu V, Penzotti JE, To R, Hyre D, Le Trong I, Lybrand TP, Stenkamp RE. Streptavidin-biotin binding energetics. Biomol Eng. 1999 Dec 31; 16(1-4):39-44

[110] Wong JY, Kuhl TL, Israelachvili JN, Mullah N, Zalipsky S. Direct measurement of a tethered ligand-receptor interaction potential. Science. 1997 Feb 7; 275(5301):820-2

[111] Wong J, Chilkoti A, Moy VT. Direct force measurements of the streptavidin-biotin interaction. Biomol Eng. 1999 Dec 31; 16(1-4):45-55

[112] Wilchek M, Bayer EA. Introduction to avidin-biotin technology. Methods Enzymol. 1990; 184:5-13

[113] Green NM. Avidin. Adv Protein Chem. 1975; 29:85-133

[114] Prasher DC, Eckenrode VK, Ward WW, Prendergast FG, Cormier MJ. Primary structure of the Aequorea victoria green-fluorescent protein. Gene. 1992 Feb 15; 111(2):229-33

[115] Chalfie M, Tu Y, Euskirchen G, Ward WW, Prasher DC. Green fluorescent protein as a marker for gene expression. Science. 1994 Feb 11; 263(5148):802-5

[116] Prasher DC. Using GFP to see the light. Trends Genet. 1995 Aug; 11(8):320-3

[117] Tew D, Ortiz de Montellano PR. The Myoglobin Protein Radical. J. Biol. Chem. 1988 Nov; 263(33):17880-86

[118] Mader C, Kupcu S, Sara M, Sleytr UB. Stabilizing effect of an S-layer on liposomes towards thermal or mechanical stress. Biochim Biophys Acta. 1999 Apr 14; 1418(1):106-16

[119] Jeppesen C, Wong JY, Kuhl TL, Israelachvili JN, Mullah N, Zalipsky S, Marques CM. Impact of polymer tether length on multiple ligand-receptor bond formation. Science. 2001 Jul 20; 293(5529):465-8

[120] Kiessling V, Tamm LK. Measuring Distances in Supported Bilayers by Fluorescence Interference-Contrast Microscopy: Polymer Supports and SNARE Proteins. Biophys. J., 2003 Jan 1; 84(1): 408-418

[121] Haris PI, Severcan F. FTIR spectroscopic characterization of protein structure in aqueous and non-aqueous media. J. Mol. Catalysis B: Enzymatic. 1999; 7:207-221

[122] Hansma HG, Bezanilla M, Zenhausern F, Adrian M, Sinsheimer RL. Atomic force microscopy of DNA in aqueous solutions. Nucleic Acids Res. 1993 Feb 11; 21(3):505-12

[123] Hansma HG. Varieties of imaging with scanning probe microscopes. Proc Natl Acad Sci U S A. 1999 Dec 21; 96(26):14678-80

[124] Engel A, Schoenenberger CA, Muller DJ. High resolution imaging of native biological sample surfaces using scanning probe microscopy. Curr Opin Struct Biol. 1997 Apr; 7(2):279-84

[125] Muller DJ, Schoenenberger CA, Schabert F, Engel A. Structural changes in native membrane proteins monitored at subnanometer resolution with the atomic force microscope: a review. J Struct Biol. 1997 Jul; 119(2):149-57

[126] Muller DJ, Baumeister W, Engel A. Conformational change of the hexagonally packed intermediate layer of Deinococcus radiodurans monitored by atomic force microscopy. J Bacteriol. 1996 Jun; 178(11):3025-30

[127] Muller DJ, Baumeister W, Engel A. Controlled unzipping of a bacterial surface layer with atomic force microscopy. Proc Natl Acad Sci U S A. 1999 Nov 9; 96(23):13170-4

[128] Gyorvary ES, Stein O, Pum D, Sleytr UB. Self-assembly and recrystallization of bacterial S-layer proteins at silicon supports imaged in real time by atomic force microscopy. J Microsc. 2003 Dec; 212(Pt 3):300-6

[129] Shevade AV, Zhou J, Zin MT, Jiang S. Phase Behavior of Mixed Self-Assembled Monolayers of Alkanethiols on Au(111): A Configurational-Bias Monte Carlo Simulation Study. Langmuir 2001; 17(24):7566-7572

[130] Kupcu S, Sara M, Sleytr UB. Liposomes coated with crystalline bacterial cell surface protein (S-layer) as immobilization structures for macromolecules. Biochim. Biophys. Acta 1995; 1235:263-269

[131] Mader C, Küpcü S, Sleytr UB, Sara M. S-layer coated liposomes as a versatile system for entrapping and binding target molecules. Biochim. Biophys. Acta. 2000; 1463:142-150

[132] Schuster B, Sleytr UB. S-layer-supported lipid membranes. J Biotechnol. 2000 Sep;74(3):233-54

[133] Wetzer B, Pum D, Sleytr UB. S-layer stabilized solid support lipid bilayers. J Struct Biol. 1997 Jul;119(2):123-8

[134] Hianik T, Küpcü S, Sleytr UB, Rybár P, Krivánek R, Kaatze U. Interaction of crystalline bacterial cell surface proteins with lipid bilayers in liposomes. A sound velocity study. Colloids and Surfaces A. 1999; 147:331-9

[135] Mader C, Küpcü S, Sara M, Sleytr UB. Stabilizing effect of an S-layer on liposomes towards thermal or mechanical stress. Biochim. Biophys. Acta. 1999; 1418:106-116

[136] Huster D, Muller P, Arnold K, Herrmann A. Dynamics of membrane penetration of the fluorescent 7-nitrobenz-2-oxa-1,3-diazol-4-yl (NBD) group attached to an acyl chain of phosphatidylcholine. Biophys J. 2001 Feb; 80(2):822-31

[137] Chattopadhyay A, London E. Parallax method for direct measurement of membrane penetration depth utilizing fluorescence quenching by spin-labeled phospholipids. Biochemistry. 1987 Jan 13; 26(1):39-45

[138] Chattopadhyay A. Chemistry and biology of N-(7-nitrobenz-2-oxa-1,3-diazol-4-yl)-labeled lipids: fluorescent probes of biological and model membranes. Chem Phys Lipids. 1990 Mar; 53(1):1-15

[139] Chattopadhyay A, London E. Spectroscopic and ionization properties of N-(7-nitrobenz-2-oxa-1,3-diazol-4-yl)-labeled lipids in model membranes. Biochim Biophys Acta. 1988 Feb 8; 938(1):24-34

[140] Burmeister JS, Olivier LA, Reichert WM, Truskey GA. Application of total internal reflection fluorescence microscopy to study cell adhesion to biomaterials. Biomaterials. 1998 Mar; 19(4-5):307-25

[141] Irvine DJ, Mayes AM, Satija SK, Barker JG, Sofia-Allgor SJ, Griffith LG. Comparison of tethered star and linear poly(ethylene oxide) for control of biomaterials surface properties. J Biomed Mater Res. 1998 Jun 5; 40(3):498-509

[142] Niessen WM. Advances in instrumentation in liquid chromatography-mass spectrometry and related liquid-introduction techniques. J Chromatogr A. 1998 Jan 23; 794(1-2):407-35

[143] Miranker AD. Protein complexes and analysis of their assembly by mass spectrometry. Curr Opin Struct Biol. 2000 Oct; 10(5): 601-6

[144] Miranker AD. Mass spectrometry of proteins of known mass. Proc Natl Acad Sci U S A. 2000 Dec 19; 97(26):14025-7

[145] Veenstra TD. Electrospray ionization mass spectrometry: a promising new technique in the study of protein/DNA noncovalent complexes. Biochem Biophys Res Commun. 1999 Apr 2; 257(1):1-5

[146] Binnig G, Quate CF, Gerber C. Atomic Force Microscope. Phys. Rev. Lett. 1986 Mar 3; 56(9):930-933

[147] Martin Y, Williams CC, Wickramasinghe HK. Atomic force microscope–force mapping and profiling on a sub 100-Å scale. J. Appl. Phys. 1987 May 15; 61(10):4723